UNIVERSIDADE FEDERAL FLUMINENSE

PROGRAMA DE PÓS-GRADUAÇÃO EM DINÂMICA DOS OCEANOS E DA TERRA

LARA DE PAULA CUNHA HERCOLANO

GEOCHEMICAL CONTROLS ON ORGANIC MATTER ACCUMULATION IN PRE-SALT LACUSTRINE SOURCE ROCKS: EVIDENCE FROM THE CAMPOS AND SANTOS BASINS, BRAZIL

NITERÓI

2026

LARA DE PAULA CUNHA HERCOLANO

GEOCHEMICAL CONTROLS ON ORGANIC MATTER ACCUMULATION IN PRE-SALT LACUSTRINE SOURCE ROCKS: EVIDENCE FROM THE CAMPOS AND SANTOS BASINS, BRAZIL

Thesis submitted to the Graduate Program in Dynamics of Oceans and Earth at Universidade Federal Fluminense, as a partial requirement for the degree of Doctor in Geology and Geophysics.

Advisor: Profa. Dra. Ana Luiza Spadano Albuquerque

NITERÓI

2026

Ficha catalográfica automática - SDC/BIG
Gerada com informações fornecidas pelo autor

H539c Hercolano, Lara de Paula Cunha
Controles geoquímicos sobre o acúmulo de matéria orgânica em rochas geradoras lacustres do pré-sal : Evidências das bacias de Campos e Santos - Brasil / Lara de Paula Cunha Hercolano. - 2026.
95 p.: il.

Orientador: Ana Luiza Spadano Albuquerque.
Tese (doutorado)-Universidade Federal Fluminense, Instituto de Geociências, Niterói, 2026.

1. Geoquímica. 2. Rochas geradoras. 3. Matéria orgânica. 4. Pré-sal. 5. Produção intelectual. I. Albuquerque, Ana Luiza Spadano, orientadora. II. Universidade Federal Fluminense. Instituto de Geociências. III. Título.

CDD - XXX

Bibliotecário responsável: Debora do Nascimento - CRB7/6368

LARA DE PAULA CUNHA HERCOLANO

GEOCHEMICAL CONTROLS ON ORGANIC MATTER ACCUMULATION IN PRE-SALT LACUSTRINE SOURCE ROCKS: EVIDENCE FROM THE CAMPOS AND SANTOS BASINS, BRAZIL

Thesis submitted to the Graduate Program in Dynamics of Oceans and Earth at Universidade Federal Fluminense, as a partial requirement for the degree of Doctor in Geology and Geophysics.

Approved on 23 / March / 2026.

EXAMINATION COMMITTEE

_____

Profa. Dra. Ana Luiza Spadano Albuquerque (Chair – Advisor)

Universidade Federal Fluminense – UFF

_____

Prof. Dr. Arthur Ayres Neto

Universidade Federal Fluminense – UFF

Prof. Dr. Igor Martins Venancio Padilha de Oliveira
Universidade Federal Fluminense – UFF

Dr. André Luiz Durante Spigolon
Centro de Pesquisas da PETROBRAS – CENPES

Prof. Dr. Victor Ribeiro Carreira
Universidade Federal do Acre – UFAC

Profa. Dra. Renata Marins Alvim Gama
Universidade do Estado do Rio de Janeiro – UERJ

Agradecimentos

Agradeço à minha orientadora Ana, pela oportunidade de integrar o projeto, pela gentileza de sempre e pela confiança de que eu faria um bom trabalho.

Aos colegas do PR4, especialmente ao Victor Carreira, pela disponibilidade em sempre ajudar e pela amizade que ficou. Aos amigos da salinha, pelos cafés, pela companhia no almoço jogando conversa fora e por tornarem os dias mais leves. Aos técnicos do LOOP, pela boa vontade e ajuda com as amostras, especialmente por serem amostras bem desafiadoras.

À Petrobras, pelo apoio financeiro que tornou esta pesquisa possível.

À minha família, pelo apoio incondicional, mesmo sem saber o que raios eu faço. Especialmente à minha mãe Tânia, aos meus avós Antônio e Nora, ao meu tio Higor e Ben. E à Brunna e Helena, meus grandes amores, meus lugares no mundo, onde tenho a sensação de que no final tudo fica bem.

À Karyna, por tanto apoio, por me acalmar nos momentos de grande ansiedade e por ser sempre a minha maior incentivadora.

Aos amigos que torceram por mim, especialmente Suzana, que sempre se emociona com as minhas conquistas.

E, por fim, dedico também a mim, por nunca ter desistido.

"Eu me organizando posso desorganizar,
eu desorganizando posso me organizar."

***Chico Science**, Da Lama ao Caos*

RESUMO

As rochas geradoras lacustres pré-sal no Brasil representam alguns dos sistemas petrolíferos mais prolíficos do mundo, porém a compreensão comparativa dos controles sobre a preservação da matéria orgânica entre diferentes bacias permanece limitada. Esta tese investigou os controles geoquímicos sobre a acumulação e preservação da matéria orgânica em formações lacustres do Cretáceo Inferior das bacias de Campos e Santos por meio de dois estudos complementares. O primeiro estudo (Hercolano et al., no prelo, *Marine and Petroleum Geology*) apresenta uma análise geoquímica e mineralógica comparativa do Folhelho Jiquiá de ambas as bacias, utilizando dados de DRX, FRX e Rock-Eval 7S de 50 amostras em quatro poços, revelando arquiteturas deposicionais contrastantes: a Bacia de Santos desenvolveu-se como um sistema predominantemente carbonático (74,6 ± 10,7% de carbonatos totais) com valores de COT consistentemente mais elevados (5,1 ± 1,1%), enquanto a Bacia de Campos representa um sistema misto carbonático-siliciclástico (38,3 ± 13,0% de carbonatos) com conteúdos de COT mais variáveis e inferiores (3,1 ± 1,3%). A análise de componentes principais identificou três controles principais: produtividade primária, diluição terrígena e estabilidade da estratificação. O segundo estudo amplia a cobertura espacial dentro da Bacia de Campos, integrando 80 amostras de oito poços distribuídos ao longo de uma transecta paleobatimétrica proximal-distal, combinando pirólise Rock-Eval, combustão LECO e análise elementar por FRX. O Carbono Orgânico Total varia de 0,5% a 7,5% (média de 2,7%), com querogênio Tipo I–II (Índice de Hidrogênio de até 779 mg HC/g COT) indicando excelente potencial gerador de óleo. Foi identificado um modelo de dupla diluição no qual tanto o excesso de carbonato quanto os siliciclásticos podem diluir a matéria orgânica, com a relação Ca-COT invertendo-se ao longo do gradiente paleobatimétrico. O vanádio emerge como o proxy redox mais robusto ($\rho = +0,76$), enquanto as concentrações de Mn indicam que a estabilidade redox controla a qualidade do querogênio. O modelo hierárquico proposto organiza os controles em três níveis — formação estratigráfica, posição paleobatimétrica e condições redox — fornecendo um arcabouço preditivo para a avaliação de rochas geradoras em sistemas lacustres pré-sal.

Palavras-chave: Pré-sal. Rochas geradoras lacustres. Preservação de matéria orgânica. Modelo de dupla diluição. Proxies redox. Bacia de Campos. Bacia de Santos. Grupo Lagoa Feia. Quimioestratigrafia.

ABSTRACT

Pre-salt lacustrine source rocks in Brazil represent some of the world's most prolific petroleum systems, yet comparative understanding of organic matter preservation controls across different basins remains limited. This thesis investigated the geochemical controls on organic matter accumulation and preservation in Lower Cretaceous lacustrine formations from the Campos and Santos basins through two complementary studies. The first study (Hercolano et al., in press, Marine and Petroleum Geology) presents a comparative geochemical and mineralogical analysis of the Jiquiá Shale from both basins, using XRD, XRF, and Rock-Eval 7S data from 50 samples across four wells, revealing contrasting depositional architectures: Santos Basin developed as a predominantly carbonate-dominated system (74.6 ± 10.7% total carbonates) with consistently higher TOC values (5.1 ± 1.1%), while Campos Basin represents a mixed carbonate-siliciclastic system (38.3 ± 13.0% carbonates) with more variable and lower TOC contents (3.1 ± 1.3%). Principal component analysis identified three key controls: primary productivity, terrigenous dilution, and stratification stability. The second study expands the spatial coverage within the Campos Basin, integrating 80 samples from eight wells distributed along a proximal-to-distal paleobathymetric transect, combining Rock-Eval pyrolysis, LECO combustion, and XRF elemental analysis. Total Organic Carbon ranges from 0.5% to 7.5% (mean 2.7%), with Type I–II kerogen (Hydrogen Index up to 779 mg HC/g TOC) indicating excellent oil-prone potential. A dual dilution model was identified in which both carbonate excess and siliciclastics can dilute organic matter, with the Ca-TOC relationship inverting along the paleobathymetric gradient. Vanadium emerges as the most robust redox proxy ($\rho = +0.76$), while Mn concentrations indicate that redox stability controls kerogen quality. The proposed hierarchical model organizes controls into three levels — stratigraphic formation, paleobathymetric position, and redox conditions — providing a predictive framework for source rock assessment in lacustrine pre-salt systems.

Keywords: Pre-salt. Lacustrine source rocks. Organic matter preservation. Dual dilution model. Redox proxies. Campos Basin. Santos Basin. Lagoa Feia Group. Chemostratigraphy

Table of Contents

CHAPTER 1: INTRODUCTION

Lacustrine rift basins rank among the most prolific settings for the development of petroleum source rocks, hosting some of the highest-quality oil-prone kerogens known in the geological record (Katz, 1995, 2001; Bohacs et al., 2000). Compared to marine systems, lacustrine basins are smaller in scale but exhibit more pronounced lateral and vertical heterogeneity, heightened sensitivity to regional environmental changes, and distinctive biological communities (Soreghan and Cohen, 1996). Notably, their high carbon burial efficiency, often exceeding that of marine systems, makes them especially relevant for understanding organic matter preservation processes (Kelts, 1988). Individual hydrocarbon accumulations derived from lacustrine source rocks can exceed billions of barrels (Katz, 2001).

The Brazilian pre-salt petroleum system constitutes a prime example of hydrocarbon accumulation derived from lacustrine sources. Lower Cretaceous rift basin deposits form the source rock intervals that charge pre-salt carbonate reservoirs, which currently account for over 78% of national petroleum production, exceeding 2.3 million barrels per day (ANP, 2025). These deposits are associated with ancient lacustrine systems strongly influenced by climatic, tectonic, and hydrological variations during the Barremian–Aptian rift phase of the South Atlantic opening (Mello et al., 1988; Guardado et al., 2000; Glenn and Kelts, 1991). The Campos and Santos basins, located along the southeastern Brazilian continental margin, exemplify such systems: their shared tectono-stratigraphic evolution during the rift stage enabled the accumulation of thick organically rich lacustrine shale sequences during the Lower Cretaceous (Cainelli and Mohriak, 1999; Chang et al., 1992).

The Campos Basin, bounded to the north by the Vitória High and to the south by the Cabo Frio High, encompasses an area of approximately 100,000 km² (Winter et al., 2007). Its tectono-stratigraphic evolution is organized into three supersequences: Rift, Post-Rift (transitional), and Drift (Dias et al., 1990; Winter et al., 2007). The Lagoa Feia Group, originally defined by Schaller (1973) as the Lagoa Feia Formation and later elevated to group status by Winter et al. (2007), constitutes the main pre-salt petroleum system of the basin, comprising non-marine to transitional sequences deposited in a predominantly lacustrine environment during the Barremian–Aptian. This group includes three main formations: the Atafona Formation (Buracica Stage, Barremian), characterized by terrigenous-dominated deposition; the Coqueiros Formation (Jiquiá Stage, Lower Aptian), recording bioclastic carbonate sedimentation during the late rift phase; and the Macabu Formation (Alagoas Stage, middle to upper Aptian), representing the post-rift transitional phase with microbial carbonates (Winter et al., 2007; De Jesus and Vilela, 2023; Bertani and Carozzi, 1985).

The Santos Basin, the largest sedimentary basin in Brazil (~350,000 km²), shares a similar tectonic history with the Campos Basin, also comprising the Rift, Post-Rift, and Drift supersequences (Moreira et al., 2007; Pereira and Feijó, 1994). The chronostratigraphically analogous units in the Santos Basin — the Piçarras and Itapema formations — were deposited during the same Jiquiá Stage and offer a valuable framework for comparative analysis of controls on organic matter preservation in basins with different depositional architectures (Winter et al., 2007; Barra et al., 2021; Penteado et al., 2024).

The fundamental controls on organic enrichment in lacustrine systems have been extensively debated. Katz (2001) identified three primary factors determining source rock potential and quality: primary productivity level, organic preservation potential, and sedimentation rate, which controls dilution of preserved organic matter. Pedersen and Calvert (1990) argued that productivity, rather than anoxia itself, is the primary control on the formation of organic carbon-rich sediments, while Demaison and Moore (1980) emphasized the role of anoxic environments in source rock genesis. Tyson (2001) demonstrated through modeling that sedimentation rate and dilution interact nonlinearly with preservation to determine final TOC values, with dilution emerging as the dominant control at high sedimentation rates regardless of oxygen conditions.

Traditional interpretations of carbonate-dominated lacustrine systems have emphasized carbonate dilution as the main mechanism limiting organic carbon accumulation (Kelts, 1988; Harris et al., 2004). However, recent studies have demonstrated that terrigenous input can equally dilute organic matter. Behar et al. (2021) documented terrigenous dilution by coastal rivers in the Congo Basin, and Liang et al. (2020) observed similar patterns in Chinese rift basins. The interaction between these two dilution mechanisms — carbonate and siliciclastic — and their dependence on paleobathymetric position remains poorly understood, especially in mixed carbonate-siliciclastic systems such as those of the Brazilian pre-salt. Ricken (1993) conceptualized sedimentation as a three-component system (organic carbon, carbonate, non-carbonate), providing a framework for understanding how compositional balance affects organic enrichment.

Beyond dilution effects, organic matter preservation is fundamentally controlled by redox conditions at the water-sediment interface (Demaison and Moore, 1980; Tyson, 1995). Trace element proxies, particularly vanadium, nickel, and molybdenum, have been widely employed to reconstruct paleoredox conditions in ancient sediments (Tribovillard et al., 2006; Algeo and Maynard, 2008). Vanadium concentrations exceeding average values of oxic sediments serve as indicators of low-oxygen and anoxic conditions (Tribovillard et al., 2006; Morford and Emerson, 1999). Manganese concentration provides additional information on redox stability through the "Mn-shuttle" mechanism (Calvert and Pedersen, 1996). The stability of anoxic conditions, rather than merely their presence, appears to determine final source rock quality (Harris et al., 2004).

In lacustrine environments, water column stratification plays a critical role in establishing and maintaining bottom-water anoxia necessary for organic matter preservation. Two main stratification mechanisms operate in rift lakes: chemical stratification, driven by evaporitic concentration and salinity gradients, and thermal stratification, resulting from reduced freshwater input and surface warming (Kelts, 1988; Talbot, 1988). Meromictic conditions in deep, oligo- to hypersaline lakes commonly lead to very high preservation potential, as observed in modern East African lakes such as Tanganyika and Kivu (Talbot, 1988; Katz, 2001).

The integration of chemostratigraphic data has become increasingly relevant for understanding depositional and diagenetic controls on source rock quality. Whole-rock geochemistry and mineralogical profiles have emerged as powerful tools for enhancing stratigraphic resolution (Hildred et al., 2010; Ratcliffe et al., 2010; Craigie, 2015, 2016). XRF elemental analysis

provides high-resolution datasets enabling detailed assessment of paleoenvironmental conditions, including redox state, terrigenous input, and carbonate productivity (Chan et al., 2022; Tribovillard et al., 2006).

Despite the economic importance of Brazilian pre-salt source rocks, several fundamental questions remain unresolved. First, the relative importance and interaction between carbonate versus siliciclastic dilution in controlling TOC distribution across different paleobathymetric positions is poorly constrained. Second, the comparative understanding of controls on organic matter preservation between the Santos and Campos basins remains limited. Third, the hierarchy of controls and their spatial variability along proximal-distal transects have not been systematically evaluated.

This thesis addresses these gaps through an integrated geochemical investigation of Lower Cretaceous lacustrine source rocks from the Campos and Santos basins. The work is structured as an article-based thesis, with each study presented in chapter format. Chapter 2 is currently in press at Marine and Petroleum Geology, and Chapter 3 is in the final stages of preparation and submission. Methodological details are presented within each chapter. The first study presents a comparative geochemical and mineralogical analysis of the Jiquiá Shale from both basins, using XRD, XRF, and Rock-Eval 7S data from 50 samples across four wells (BCBR-1, BCBR-2, BCBR-3, and BSBR-1). This study establishes the contrasting depositional architectures between the basins, demonstrating that differences in organic enrichment reflect variations in stratification stability and dilution intensity, rather than fundamentally different redox states.

The second study expands the spatial coverage within the Campos Basin, integrating 80 samples from eight wells (BCBR-1, BCBR-3, and BCBR-5 through BCBR-10) distributed along a proximal-to-distal paleobathymetric transect. Combining Rock-Eval pyrolysis, LECO combustion, and XRF elemental analysis, this study characterizes the complete Lagoa Feia Group (Atafona, Coqueiros, and Macabu formations) and evaluates how dilution mechanisms, redox conditions, and stratigraphic context interact to control organic matter accumulation.

Together, these two studies provide a comprehensive multi-scale framework for understanding organic matter accumulation in pre-salt lacustrine source rocks, with contributions that include: (1) the first systematic comparison of chronostratigraphically analogous Middle Aptian lacustrine source rocks between the Santos and Campos basins; (2) a dual dilution model with formation-specific calibrations; (3) validated trace element proxies for paleoredox reconstruction in carbonate lacustrine systems; and (4) a predictive hierarchical model for source rock quality with implications for analogous rift basins worldwide.

CHAPTER 2

Geochemical and mineralogical controls on organic matter preservation in Lower Cretaceous pre-salt lacustrine systems (Jiquiá Shale):

A comparative study of Santos and Campos basins, Brazil

Marine Geoscience and Energy Resources

Volume 189, July 2026, 207733

DOI: 10.1016/j.marger.2026.207733

Geochemical and mineralogical controls on organic matter preservation in Lower Cretaceous pre-salt lacustrine systems (Jiquiá Shale): A comparative study of Santos and Campos basins, Brazil

Lara de Paula Cunha Hercolano[1], Rut Díaz[2], Igor Martins Venancio[2], Manuel Moreira-Ramírez[2], Gabriel de Alemar Barberes[1], André Luiz Durante Spigolon[3], Ana Luiza Spadano Albuquerque[1]*

[1] Programa de Pós-Graduação em Dinâmica dos Oceanos e da Terra, Universidade Federal Fluminense, Niterói, 24210346, Brazil
[2] Programa de Geociências (Geoquímica), Universidade Federal Fluminense, Niterói 24020141, Brazil
[3] Centro de Pesquisas da PETROBRAS, Rio de Janeiro, RJ, Brazil

*Corresponding author: Programa de Pós Graduação em Dinâmica dos Oceanos e da Terra, Universidade Federal Fluminense, Niterói, 24210346, Brazil. E-mail address: larapch@id.uff.br (L. P. C. Hercolano).

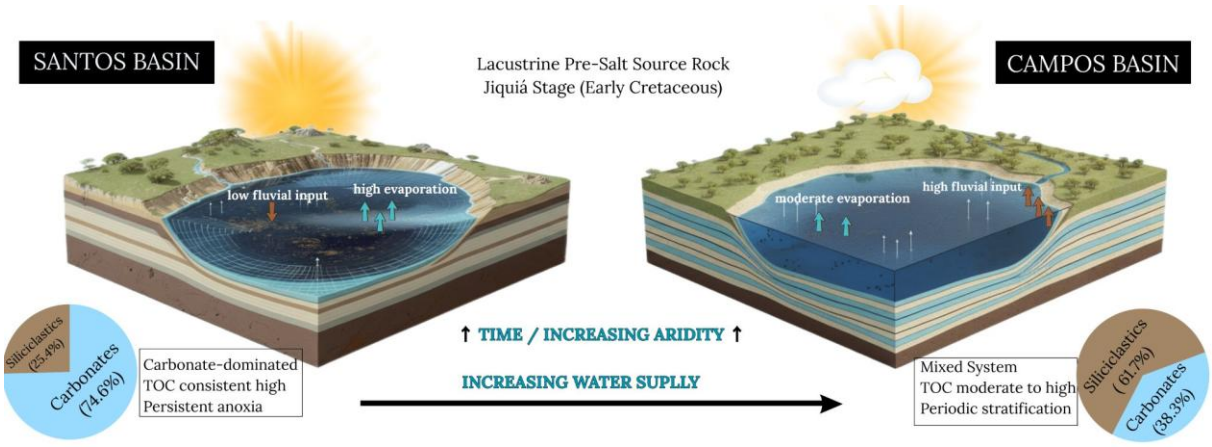

Abstract

Pre-salt lacustrine source rocks in Brazil represent some of the world's most prolific petroleum systems, yet comparative understanding of organic matter preservation controls across different basins remains limited. This study presents an integrated geochemical and mineralogical analysis of Lower Cretaceous lacustrine formations from the Santos and Campos basins using XRD, XRF, and Rock-Eval 7S data from 50 samples across four wells. Despite established chronostratigraphic correlation within the Jiquiá Stage (biozonas NRT-008/009 to NRT-010), results reveal contrasting depositional architectures: Santos Basin developed as a predominantly carbonate-dominated system (74.6 ± 10.7% total carbonates) with consistently higher TOC values (5.1 ± 1.1%), while Campos Basin represents a mixed carbonate-siliciclastic system (38.3 ± 13.0% carbonates) with more variable and lower TOC contents (3.1 ± 1.3%). Both basins developed under predominantly anoxic bottom-water conditions, as evidenced by TOC values that classify both systems as excellent source rocks. Santos Basin developed stable chemical stratification driven by evaporative concentration, maintaining persistent anoxia, while Campos Basin relied more heavily on thermal stratification and experienced episodic

terrigenous input during humid climatic pulses. The difference in organic enrichment reflects variations in stratification stability and dilution intensity rather than fundamentally different redox states. Principal component analysis (71.5% variance explained) identifies three key preservation controls operating within anoxic systems: (1) primary productivity and nutrient availability; (2) terrigenous dilution, showing systematic inverse relationships with organic matter accumulation; and (3) stratification stability, with Santos Basin's chemical stratification proving more resistant to disruption than Campos Basin's thermal stratification. Optimal preservation occurs in moderate carbonate environments (45-65%), while extreme calcite concentrations (>70%) dilute organic matter through sedimentary dilution. Rock-Eval 7S analysis reveals significant methodological limitations in carbonate-rich samples, where matrix interference systematically reduces pyritic sulfur signal recovery by up to 95%. These findings advance understanding of Brazilian pre-salt lacustrine source rock controls and provide insights for petroleum system modeling in analogous carbonate-dominated lacustrine sequences worldwide.

Keywords: Pre-salt petroleum systems; Lacustrine source rocks; Santos Basin; Campos Basin; Organic geochemistry; Brazil offshore

1. Introduction

Lacustrine source rocks contribute significantly to global petroleum systems, with Brazil standing as a prime example where Early Cretaceous rift basin deposits form pre-salt carbonate reservoirs that currently account for over 78% of national oil production, exceeding 2.3 million barrels daily (ANP, 2025). These deposits are associated with ancient lacustrine systems strongly influenced by climatic, tectonic, and hydrological variations (Glenn & Kelts, 1991). Compared to marine systems, lacustrine basins are smaller in scale, yet exhibit sharper lateral and vertical heterogeneity, enhanced sensitivity to regional environmental shifts, and distinctive biological communities (Soreghan & Cohen, 1996). Notably, their high carbon burial efficiency, often exceeding that of marine systems, makes them especially relevant in the context of organic matter preservation (Kelts, 1988). In this regard, the Campos and Santos basins exemplify such systems: their shared tectonic-stratigraphic evolution during the rift stage enabled the accumulation of substantial organic-rich lacustrine shale sequences during the Lower Cretaceous. These source rocks, deposited during the Jiquiá Stage (Middle Aptian; biozones NRT-008/009 to NRT-010) with main generative potential concentrated in biozone OS-1000, are considered chronostratigraphically analogous, offering a valuable framework for comparative analysis (Mello et al., 1988; Guardado et al., 2000; Moreira et al., 2007; Barra et al., 2021; Penteado et al., 2024).

Recent studies have advanced our understanding of the environmental controls over the deposition of thick Lower Cretaceous lacustrine carbonates in Brazilian pre-salt basins (Alvarenga et al., 2016; Pietzsch et al., 2020; Barra et al., 2021; Zuo et al., 2022). Among the pre-salt units, the Coqueiros Formation has received particular attention due to its economic relevance as a carbonate reservoir (Thompson et al., 2015; Goldberg et al., 2017; Barberes et al., 2024). Despite growing interest in the integration of inorganic geochemistry and organic geochemical data to assess preservation pathways, few studies have performed direct, basin-

scale comparative analyses between the Santos and Campos source rocks, particularly in terms of mineralogical and geochemical controls on organic matter accumulation and retention.

The integration of chemostratigraphic data has proven essential for interpreting organic-rich sedimentary successions, providing refined insights into depositional processes and stratigraphic correlation (Sano et al., 2013; Craigie, 2015; Craigie et al., 2016a; Craigie et al., 2016b; Remírez et al., 2022). The application of major and trace element geochemistry has enabled not only the differentiation and correlation of sedimentary layers, but also the reconstruction of paleoredox conditions associated with oceanic anoxic events in organic-rich shales (Tribovillard et al., 2006; Turgeon and Brumsack, 2006; Tribovillard et al., 2008; Negri et al., 2009; Jenkyns, 2010). These geochemical tools reveal significant lateral and vertical variations, even at fine stratigraphic scales, underscoring their relevance for high-resolution paleoenvironmental reconstructions.

The integration of mineralogical data into chemostratigraphic framework has become increasingly relevant, particularly due to the complex and variable organic matter-mineral associations (OMMA) in shales (Sebag et al., 2006; Rahman et al., 2017; Rahman et al., 2018). In the petroleum industry, whole rock geochemistry and mineralogical profiling have emerged as powerful tools for enhancing stratigraphic resolution and evaluating diagenetic and depositional controls on source rock quality (Hildred et al., 2010; Ratcliffe et al., 2010; Wright et al., 2015). Building on this approach, the present study combines integrated mineralogical (XRD) and elemental (XRF) data with organic geochemical analyses, including TOC and Rock-Eval 7S pyrolysis with sulfur speciation, to investigate mechanisms of organic matter preservation in the Jiquiá Shale. By comparing samples from three wells in the Campos Basin and one in the Santos Basin, this study assesses both lateral and regional variability in depositional environments and diagenetic pathways. This integrative analysis aims to contribute to the literature by providing a basin-scale comparison of chronostratigraphically analogous Middle Aptian lacustrine source rocks, with implications for the understanding of geochemical controls on organic matter accumulation in pre-salt petroleum systems.

2. Geological Setting

The Campos and Santos basins (Figure 1) are located along the southeastern margin of Brazil. Both are part of a series of offshore sedimentary basins that originated in the Lower Cretaceous period, resulting from the fragmentation of the supercontinent Gondwana and the subsequent expanse of the South Atlantic Ocean (Cainelli & Mohriak, 1999; Guardado et al., 2000). These sedimentary basins developed as a result of extensional tectonic activity, leading to progressive subsidence and accumulation of thick sedimentary sequences. Their stratigraphy provides information on the evolution of passive continental margins and contains some of the most prolific petroleum systems in the world (Mello et al., 1988; Mohriak et al., 1990). The chronostratigraphic attribution of the analyzed records to the pre-salt system was based on lithostratigraphic correlation with the markers established by Moreira et al. (2007) and Winter et al. (2007). Winter et al. (2007) subdivided the Campos and Santos basins into three major Supersequences: the Rift Supersequence, the Post-Rift Supersequence, and the Drift Supersequence. This identification was confirmed by stratigraphic data and composite well logs provided by ANP (National Petroleum Agency), which position the studied formations within

the Lower Cretaceous pre-salt sequence: Atafona and Coqueiros formations in the Campos Basin, and Piçarras and Itapema formations in the Santos Basin (Figure 2).

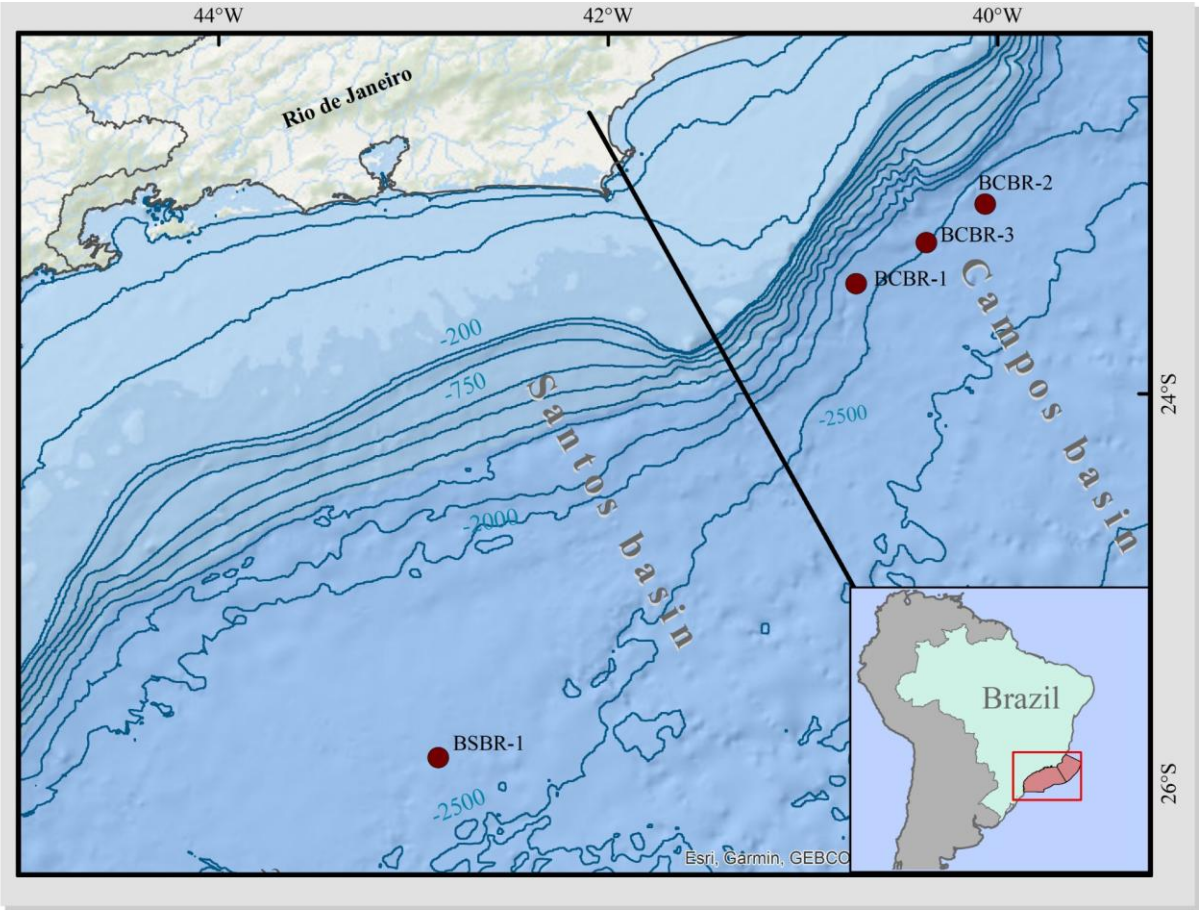

Figure 1. Map of the southeastern Brazilian margin, showing the location of the well samples in the Campos (BCBR-1, BCBR-2 and BCBR-3) and Santos (BSBR-1) basins. The bathymetric lines are shown in meters of depth.

Campos Basin

The Campos Basin covers an area of approximately 100,000 km² and is delimited to the north by the Vitória High and to the south by the Cabo Frio High, which separates it from the Santos Basin (Winter et al., 2007). Its geological evolution is subdivided into three Supersequences -- Rift, Post-Rift (transitional), and Drift -- which together define its tectono-stratigraphic framework (Dias et al., 1990; Chang et al., 1992). During the Rift Supersequence, the Lagoa Feia Group was deposited in predominantly lacustrine environments, laying the foundation for the petroleum systems currently active in the basin. Within this group, Atafona Fm. was formed by deposition in alkaline lacustrine conditions and is made up of sandstones, siltstones and shales. Evaporitic conditions during this phase led to the formation of specific minerals such as talc and stevensite (Winter et al., 2007). These mineralogical characteristics have increased the unit's potential as both source rock and reservoir rock. Overlying the Atafona Fm., the Coqueiros Fm. consists of bioclastic carbonates and shales, reflecting deposition in a dominantly lacustrine setting with intermittent marine incursions documented during biozones

OS-1010 and OS-1100 (Jiquiá Stage) based on micropaleontological evidence (Silva-Telles Jr. et al., 1994; Thompson et al., 2015). The Coqueiros Formation constitutes the main source rock of the Jiquiá Stage in the Campos Basin, corresponding to the Jiquiá Shale as defined by Winter et al. (2007). This paleoenvironment favored organic matter preservation and may have contributed to hydrocarbon generation and entrapment (Baumgarten et al., 1988; Mizuno et al., 2018).

Santos Basin

The Santos Basin is the largest sedimentary basin in Brazil, extending offshore to water depths exceeding 3,000 meters (Moreira et al., 2007) and covering an area of approximately 350,000 km². It shares a similar tectonic history to the Campos Basin, also comprising Rift, Post-Rift, and Drift Supersequences (Cainelli & Mohriak, 1999; Pereira & Feijó, 1994). During the Rift Supersequence, the volcanic activity related to the Camboriú Formation preceded the deposition of fluvial and lacustrine siliciclastic sediments. These deposits are represented by Fm. Piçarras, characterised by conglomerates, sandstones and lacustrine shales. The depositional characteristics of this unit provide insights into the formation and initial stages of rift evolution, contributing to the structural and stratigraphic architecture of the pre-salt system (Moreira et al., 2007). Overlying these units, the Itapema Fm. (Jiquiá Stage; Middle Aptian) consists of lacustrine coquinas intercalated with black shales, representing highly productive lacustrine systems, conducive to the favourable generation and storage of hydrocarbons (Moreira et al., 2007; Mizuno et al., 2018). The Itapema Formation represents the main source rock of the Santos Basin, corresponding to the Jiquiá Shale as defined by Winter et al. (2007). Recent seismic stratigraphic analyses have further refined the understanding of pre-salt architecture in the Santos Basin (Pizarro et al., 2025; Vital & Lupinacci, 2023). During the Post-Rift Supersequence, the onset of evaporitic conditions led to the formation of the Barra Velha Fm. This unit comprises microbial carbonates, stromatolites, and laminated carbonates deposited under highly alkaline lacustrine conditions influenced by hydrothermal activity. These processes promoted calcium enrichment, enhancing carbonate precipitation and contribution to reservoir development.

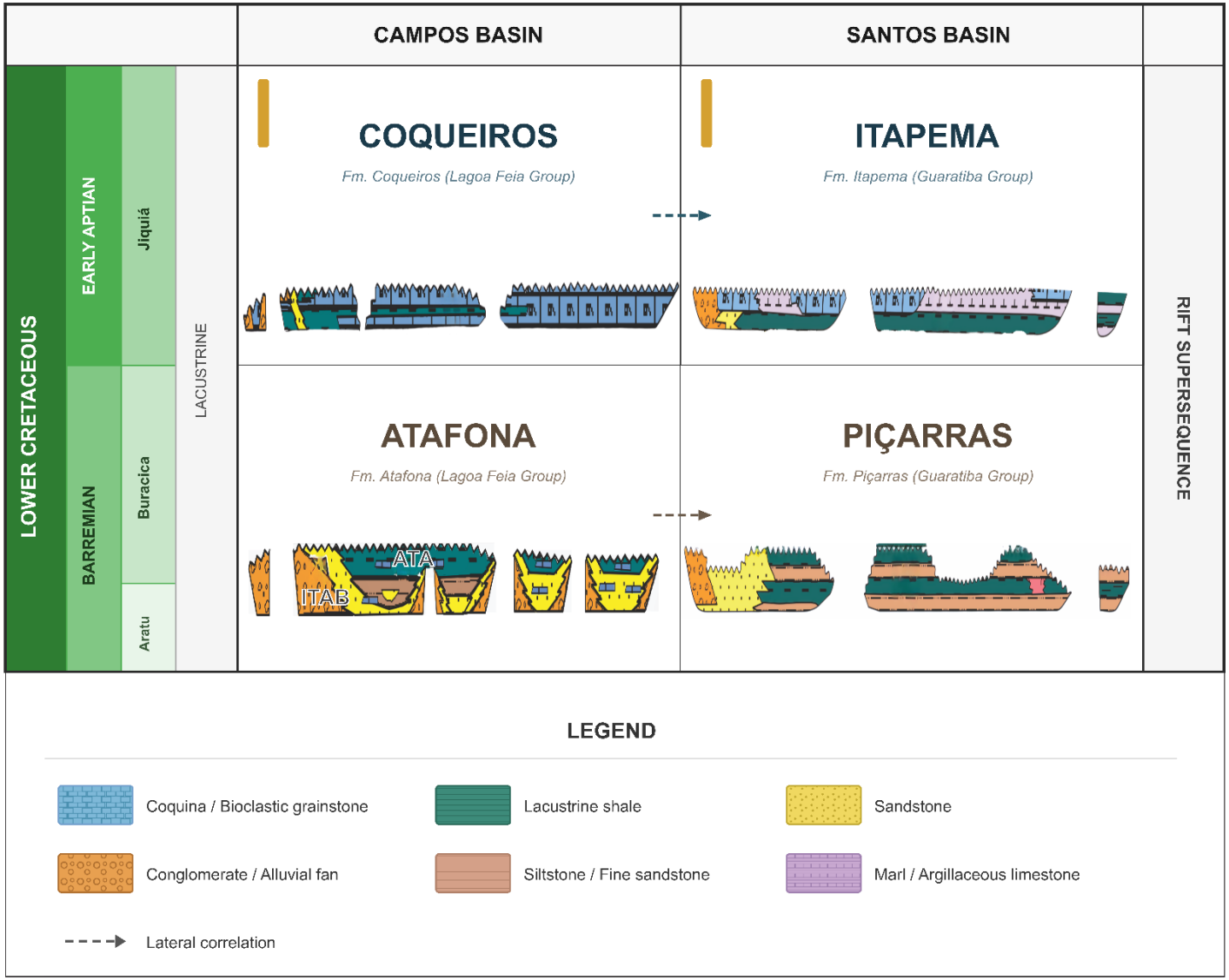

Figure 2. Comparative chronostratigraphic chart of the Campos and Santos basins during the Lower Cretaceous (Barremian to Early Aptian), showing the rift supersequence formations. In Campos Basin: Coqueiros Formation (Fm. Coqueiros, Lagoa Feia Group) and Atafona Formation (Fm. Atafona, Lagoa Feia Group). In Santos Basin: Itapema Formation (Fm. Itapema, Guaratiba Group) and Piçarras Formation (Fm. Piçarras, Guaratiba Group). The Jiquiá Stage corresponds to the Early Aptian, while the Buracica Stage corresponds to the Barremian. Dashed arrows indicate lateral correlation between equivalent units. Modified after Moreira et al. (2007) and Winter et al. (2007).

3. Materials and Methods

3.1 Sampling and sample treatment

In this study, 50 core samples were collected from four wells, distributed between the Campos and Santos basins. Three wells are located in the Campos Basin - BCBR-1 (n=14), BCBR-2 (n=7) and BCBR-3 (n=11) - and one in the Santos Basin - BSBR-1 (n=18) (Figure 1). To ensure sample integrity and minimise contamination, all containers and materials were rigorously cleaned using 10% (v/v) neutral detergent solution (Isodert, Isofar Laboratory), followed by treatment with 10% (v/v) HCl solution (P.A. 37%, Supelco®). The samples were manually sorted to remove drilling contaminants, such as metal fragments and fibres from sampling bags, and washed with 2 L of deionised water to remove drilling fluid residues. After washing, all samples were dried at 50°C for 24 hours and then pulverised in a Retsch S1 planetary ball mill (Hann, Germany).

3.2 Rock-Eval pyrolysis (RE7)

Aliquots of 50-100 mg of pulverised samples (100 mesh) were analysed using a Rock-Eval 7S instrument (Vinci Technologies). The instrument was calibrated using certified reference materials IFP 160000 and IFP 400000 standards (Institut Français du Pétrole), with three readings of the IFP 160000 standard performed for calibration. The analytical precision for TOC was ±0.12 wt% and for sulfur was ±0.02 wt%.

The analytical procedure comprised two sequential steps: pyrolysis and oxidation. For pyrolysis, the samples were heated from 100°C to 800°C in a nitrogen atmosphere. The effluents generated were separated into three streams: hydrocarbons were quantified by a flame ionisation detector (FID), while CO_2 and CO were measured by an infrared detector (IR). Reduced sulphur compounds-oxidised to SO_2 -were detected by an ultraviolet detector (UV). In the oxidation stage, the sample residue was transferred to an oxidation furnace and heated in air from 100°C to 1200°C. At 750°C, the atmosphere was changed to nitrogen to allow thermal degradation of the sulphates. CO and CO_2 emissions were monitored by the IR detector, while SO_2 was quantified directly by the UV detector. Total Organic Carbon (TOC) values were determined directly from the Rock-Eval 7S analysis, calculated as the sum of carbon released during both the pyrolysis and oxidation phases.

Rock-Eval 7S analysis provides two SO_2 profiles for sulphur species: one from pyrolysis and one from oxidation. The total sulfur content (STotal) is derived from the combination of both profiles. During the pyrolysis phase, pyritic sulphur (Pyro Fe S) and organic sulphur (SOrganic) can be differentiated and quantified separately, as they are represented by two distinct SO_2 peaks. However, in the oxidation phase, these two types of sulphur appear as a single peak, making differentiation unfeasible. Thus, the sulphate peak is identified exclusively in the oxidation phase. Total iron sulfides (TSFeS) represent the sum of pyritic sulfur and other iron-bound sulfur phases detected by the instrument.

3.3 XRD and XRF analysis

Mineralogical analyses were performed using a Bruker D2 PHASER benchtop powder diffractometer operating in Bragg-Brentano geometry. Samples were sieved to 106 μm to ensure homogeneity. Measurements were conducted using Cu-kα radiation (30 kV, 10 mA) over a 2θ range of 3° to 100°, with a step size of 0.02° and an acquisition time of 3 seconds per step. Mineral phase identification was performed using EVA software, based on the ICSD database. Quantitative phase abundances were determined using Rietveld refinement with TOPAS software, which refines crystal structure parameters and phase fractions by fitting calculated diffraction patterns to the observed data.

Major and trace elements were analyzed using an EDXRF spectrometer (Epsilon 3, Malvern Panalytical, Netherlands), equipped with a silver anode X-ray tube and 50 μm beryllium window. Measurements were conducted in air and helium atmospheres. Instrument calibration was performed using a fused reference pellet for X-ray fluorescence (FLX-C3, Fluxana, Bedburg-Hau, Germany), with all elements showing a standard deviation of less than 0.3. The operating conditions were: 50 kV tube voltage, 1 mA current, and 9 W power. Detection was achieved using a high-resolution silicon drift detector (SDD) with 135 eV resolution and 8 μm (Be) window.

Geochemical proxies were interpreted to infer paleoenvironmental conditions. Ti and Zr served as indicators of terrigenous input; Ca and Sr were associated with carbonate accumulation; Al and K reflected the presence of feldspars and clays; and Cu, Ni, and Zn were interpreted as redox-sensitive elements (Pearce & Jarvis 1992; Pearce et al. 1999; Tribovillard et al. 2006; Nance & Rowe 2015; Turner et al. 2016).

3.4 Statistical Analysis and Lithofacies Classification

Statistical comparisons between basins were performed using the Mann-Whitney U test due to the heterogeneous nature of geochemical data from different depositional environments. Correlations between geochemical parameters and TOC were evaluated using Spearman's rank correlation, with $|\rho| \geq 0.5$ considered significant. Principal component analysis (PCA) was employed to investigate the relationships and infer controls on organic matter preservation. Significant components were identified using the Kaiser criterion. All statistical procedures were performed using STATISTICA® 12.0, with a 95% confidence level ($p \leq 0.05$).

Lithofacies classification was based on a modified Pettijohn (1975) scheme using carbonate content (MinC). Samples were classified as: i. siliceous (carbonate content < 25% by weight, MinC < 3%); ii. marl (carbonate content between 25-50% by weight, MinC 3-6%); or iii. carbonate (carbonate content between 50-100% by weight, MinC 6-12%).

4. Results

The total organic carbon (TOC) content is significantly higher in the Santos Basin (5.1 ± 1.1%) than in the Campos Basin (3.1 ± 1.3%) (Mann-Whitney $U = 72.0$, $p < 0.05$) (Supplementary Table S1). Organic sulfur concentrations are also higher in Santos (0.013 ± 0.011%) than in Campos (0.009 ± 0.006%), although this difference is not statistically significant ($U = 260.0$, $p > 0.05$) (Table S1).

Mineralogical analysis reveals a clear compositional contrast between basins (Figure 3, 4, 5, 6; Table S2). Santos Basin exhibits a predominantly carbonate-rich assemblage composition (74.6% ± 10.7% total carbonates), whereas Campos Basin is more siliciclastic (38.3% ± 13.0% total carbonates) (Table S2). Calcite is the dominant carbonate phase in Santos (49.1% ± 13.6%) compared to Campos (20.5% ± 7.1%), with the difference being statistically significant ($p < 0.05$). Conversely, terrigenous minerals (quartz, K-feldspar, clay minerals) are more abundant in the Campos Basin (Figure 3).

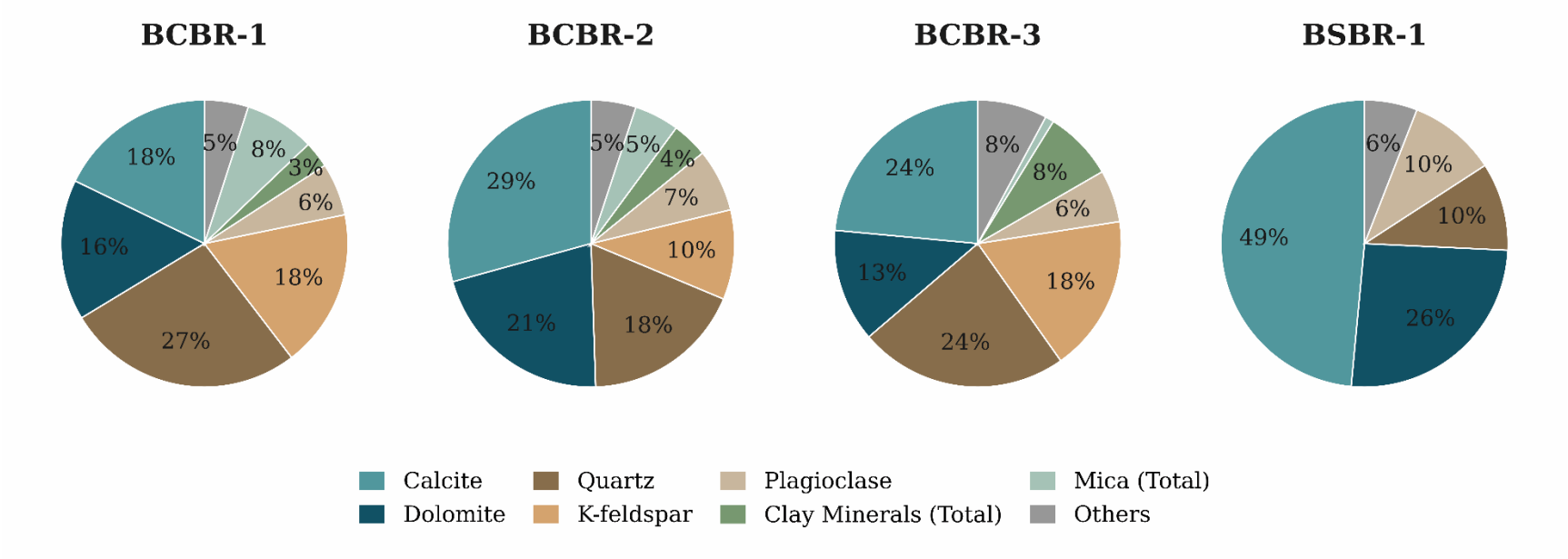

Figure 3. Average mineralogical distribution in wells BCBR-1, BCBR-2 and BCBR-3 (Campos Basin) and BSBR-1 (Santos Basin). The graphs show the compositional contrast between basins, with carbonates (calcite + dolomite) predominant in well BSBR-1 (75%) and greater siliciclastic content in Campos Basin wells.

The major element geochemistry supports these mineralogical trends (Table S1, Table S2). Santos Basin sediments contain elevated CaO (60.0% ± 9.4%) compared to Campos (31.5% ± 8.1%) ($U = 4.0$, $p < 0.05$). In contrast, terrigenous proxies such as SiO_2 (15.9% ± 6.2% in Santos vs. 38.1% ± 6.7% in Campos) and Al_2O_3 (2.7% ± 1.2% vs. 6.6% ± 2.2%) are significantly enriched in Campos Basin samples ($p < 0.05$).

Trace element patterns further emphasize these distinctions (Table S1). Santos samples show systematically lower concentrations of redox-sensitive and terrigenous-associated elements, particularly Cu (54.6 ± 22.6 ppm vs. 142.4 ± 58.5 ppm) and Rb (51.5 ± 17.8 ppm vs. 78.2 ± 14.7 ppm), with all differences being statistically significant ($p < 0.05$). However, Zn concentrations show no significant difference between basins (164.7 ± 41.8 ppm vs. 275.1 ± 280.5 ppm, $p > 0.05$).

4.1 Carbonate-Dominated System: Geochemical Patterns in Santos Basin Well (BS-BR1)

The Piçarras Formation (n=4) shows high TOC levels, with a mean of 5.1% ± 1.1%. Organic sulfur concentrations average 0.017% ± 0.008%, with values ranging from 0.007% to 0.025%, where the maximum occurs at 6018 m depth (Table S1). The mineralogy shows moderate carbonate content, with calcite at 44% ± 12% and dolomite at 16% ± 10% (Figures 3, 4; Table S2). Clay minerals (8% ± 5%) and micas (0.2% ± 0.2%) appear in deeper sections (6045-6099 m), reaching up to 12%, alongside slight quartz increases (11% ± 1%) (Table S2). The elemental composition exhibits significant siliciclastic components with SiO_2 (23% ± 5%) and Al_2O_3 (4% ± 1%), coupled with decreased CaO (52% ± 9%).

The Itapema Formation (n=14) displays high organic content with TOC averaging 5.2% ± 1.1%. The maximum TOC values (7.0%) occur at intermediate depths (5991 m) in the transition zone between the Itapema and Piçarras formations (Table S1, Figure 4). The organic sulfur concentration shows a range of 0.004-0.038% with notable enrichment in deeper sections, reaching maximum values (0.036-0.038%) at 5964-5991 m (Table S1). The mineralogy shows strong carbonate signatures with calcite (50% ± 12%) and dolomite (28% ± 6%) (Figures 3, 4; Table S2). Calcite decreases with depth from 60% to 35%, while dolomite increases from 23% to 35% (Figure 4). Plagioclase (8% ± 4%) dominates over K-feldspar (0.2% ± 0.5%) and increases with depth from 6% to 14%. Quartz remains stable (10% ± 2%), and clay minerals are notably absent. Elemental analysis reveals high CaO content (62% ± 8%), decreasing systematically with depth. SiO_2 (14% ± 5%) and Al_2O_3 (2% ± 1%) remain consistently low but increase toward the formation base. Fe_2O_3 content averages 3.6 ± 1.6%. Terrigenous oxides, including K_2O (1.8% ± 0.7%) and TiO_2 (0.5% ± 0.3%), show gradual increase with depth (Table S1, Figure 3). Trace elements show moderate Cu concentrations (51.6 ± 23.2 ppm), with slightly elevated values in the basal Itapema Formation (up to 106 ppm at 5937 m) as documented in the Cu profile of Figure 4.

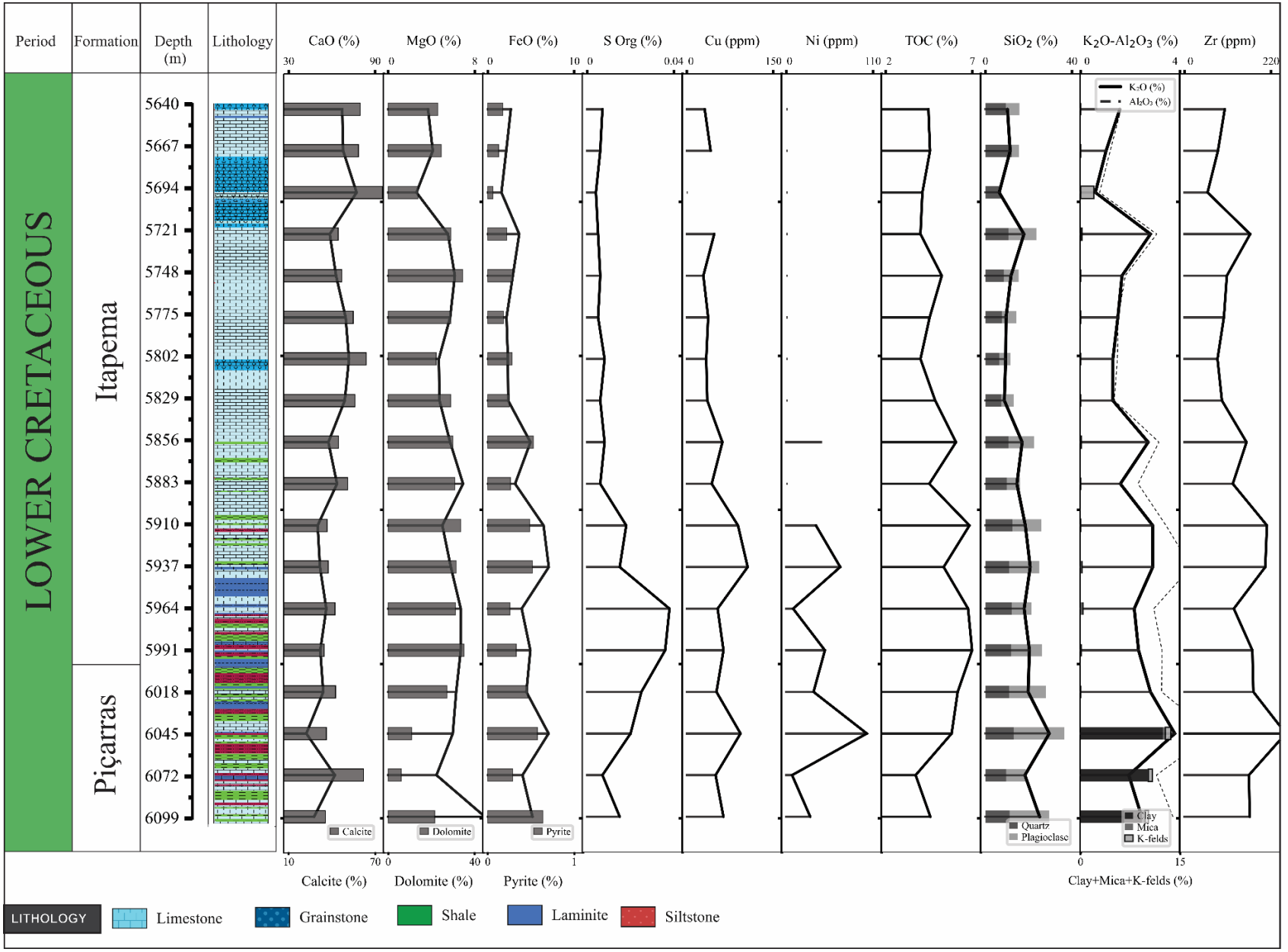

Figure 4. Stratigraphic column and geochemical-mineralogical profiles of well BS-BR1 from the Santos Basin, showing vertical variations in mineral content, major oxides, organic parameters, and trace elements across the Itapema and Piçarras formations. The lithology column displays: limestone (light blue), grainstone (dark blue), shale (green), laminite (purple), and siltstone (red).

4.2 Mixed Carbonate-Siliciclastic System: Geochemical Variability in Campos Basin Wells (BC-BR1, BC-BR2, BC-BR3)

The Atafona Formation presents lower organic content, with TOC values ranging from 1.1% to 2.8% and a global average of 1.8% ± 0.5% across wells BC-BR1 and BC-BR3 (Table S1; Figures 5, 6). Organic sulfur concentrations are consistently low, ranging from 0.001% to 0.015% with an average of 0.005% ± 0.004% (Table S1). A distinct characteristic of the Atafona Formation is its lower carbonate content compared to other studied units. Mineralogically, it shows distinct patterns between wells. In BC-BR1, calcite averages 13% ± 4% and dolomite 9% ± 3%, with abrupt variations in K-feldspar (15-26%), quartz (21-34%), and clay minerals (2-8%) as shown in the detailed stratigraphic profile of Figure 5. BC-BR3 exhibits higher calcite content (20% ± 6%) with similar dolomite levels (9% ± 6%) but shows more gradual trends and higher continental mineral content, characterized by progressive increases in K-feldspar (16% to 41%) and clay minerals (6% to 16%) (Figure 6). Figure 5 particularly illustrates the systematic increase in terrigenous components toward the base of the formation. A distinctive feature of the Atafona Formation is the exclusive presence of talc (1-2%), with rare occurrences in the transitional zone to the Coqueiros Formation. The elemental composition is characterized by elevated concentrations of terrigenous oxides, with Al_2O_3 (8.4% ± 2.5%), K_2O (3.6% ± 2.1%), and TiO_2 (1.1% ± 0.4%) significantly higher than in the Coqueiros Formation, as demonstrated in the geochemical profiles of Figures 5 and 6. Well BC-BR3 shows consistently higher concentrations (up to 2-3 times higher for K_2O) of these terrigenous oxides compared to BC-BR1, evident when comparing the K_2O profiles between Figures 5 and 6. The presence of amphiboles and pyroxenes in some Atafona samples results in elevated Na_2O (1.0% ± 0.3%) and MgO (7.2% ± 0.5%) compared to samples without these minerals. The formation shows higher concentrations of terrigenous oxides and variable Zn levels (98.6-806 ppm), with the highest concentrations occurring in well BC-BR3 as shown in Figure 6.

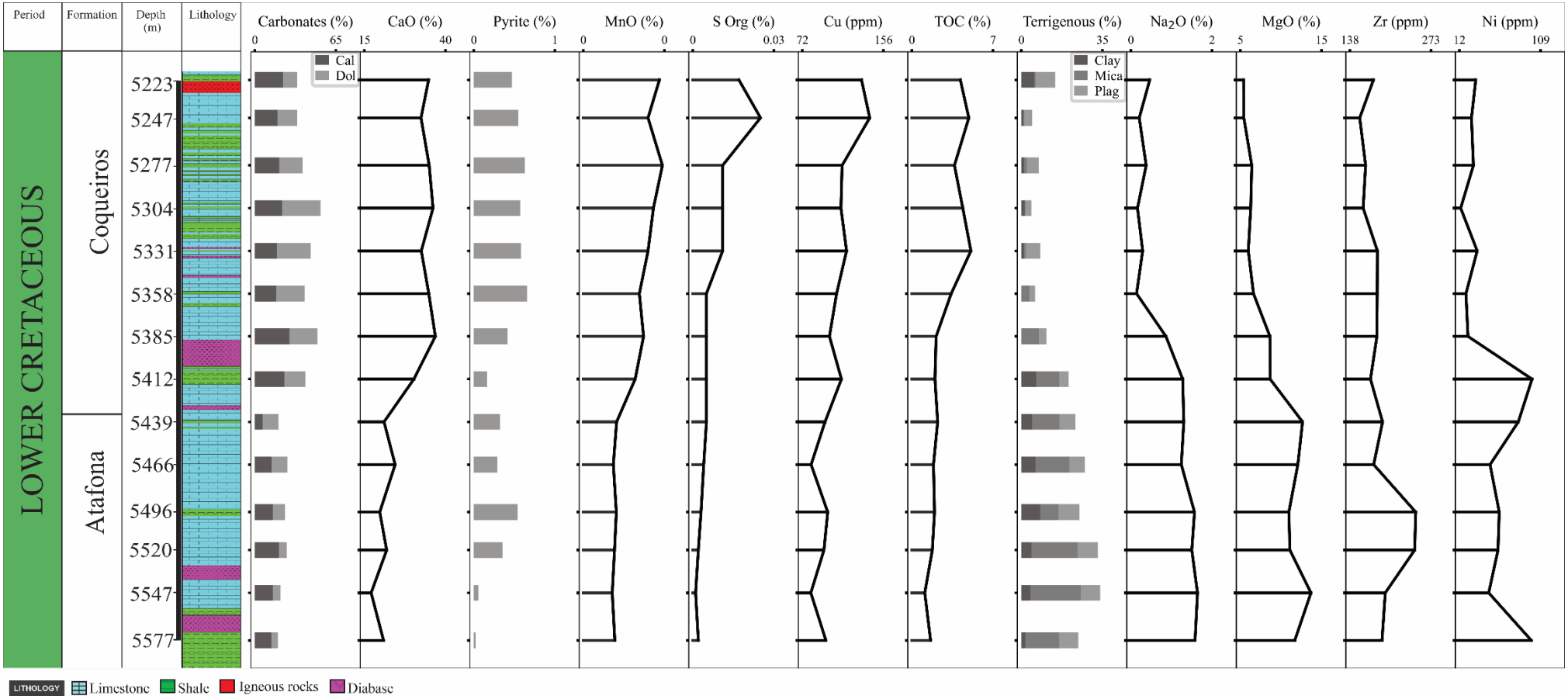

Figure 5. Stratigraphic column and geochemical-mineralogical profiles of well BC-BR1 from the Campos Basin, showing vertical variations in mineral content, major oxides, organic parameters, and trace elements across the Coqueiros and Atafona formations. The lithology column displays: limestone (light blue), shale (green), diabase (pink), and igneous rock (purple).

The Coqueiros Formation exhibits significant organic matter content with TOC values ranging from 2.0% to 5.3%, averaging 3.9% ± 1.0% across 21 samples (Table S1). The vertical distribution patterns shown in Figures 5 and 6 reveal that organic sulfur concentrations range from 0.005% to 0.019%, averaging 0.010% ± 0.004%. This distribution shows notable consistency among the analyzed wells, with BC-BR1 averaging 3.7% ± 1.2%, BC-BR2 showing 4.2% ± 0.7%, and BC-BR3 presenting 3.7% ± 0.9%. Mineralogically, it is characterized by intermediate carbonate content, with calcite (26% ± 8%, maximum 48%) and dolomite (20% ± 7%, maximum 35%) as primary constituents, notably lower than Santos Basin but higher than the Atafona Formation. It also contains substantial amounts of quartz (14-49%) and total feldspars (4.5-31.7%), with K-feldspar predominating over plagioclase. Well-specific variations are evident when comparing Figures 5 and 6, with BC-BR3 showing the highest calcite content (28% ± 10%) and BC-BR1 displaying the lowest average calcite values (21% ± 4%). The elemental composition shows considerable heterogeneity both vertically and laterally across wells. Average concentrations include CaO (36% ± 5%), SiO_2 (35% ± 5%), Al_2O_3 (6% ± 1%), K_2O (2.8% ± 0.8%), and Fe_2O_3 (7.6% ± 1.5%). Figure 5 shows that well BC-BR1 displays relatively uniform elemental distribution throughout the Coqueiros Formation. Figure 6 demonstrates that BC-BR3 exhibits the highest compositional heterogeneity, with a systematic increase in terrigenous oxides toward the Atafona Formation transition. The formation shows marked enrichment in Cu (143.4 ± 58.6 ppm), with Cu concentrations decreasing consistently with depth (5223-6382 m) as evident in the Cu profiles of Figures 5 and 6.

The transition between Atafona and Coqueiros formations, well-documented in BC-BR1 (5412-5439 m) and BC-BR3 (5444-5477 m), marks significant mineralogical changes, as shown in Figures 5 and 6. Moving upward from Atafona to Coqueiros, calcite increases from 16% ± 6% to 26% ± 8%, and dolomite shows an even more pronounced increase from 9% ± 5% to 20% ± 7%. This transition is accompanied by substantial reduction in feldspar content, decreasing from up to 54% (combining K-feldspar and plagioclase) in Atafona, while quartz maintains an average of 20%. The vertical distribution pattern shows a general increase in TOC values moving upward, particularly evident in this transitional zone in both wells.

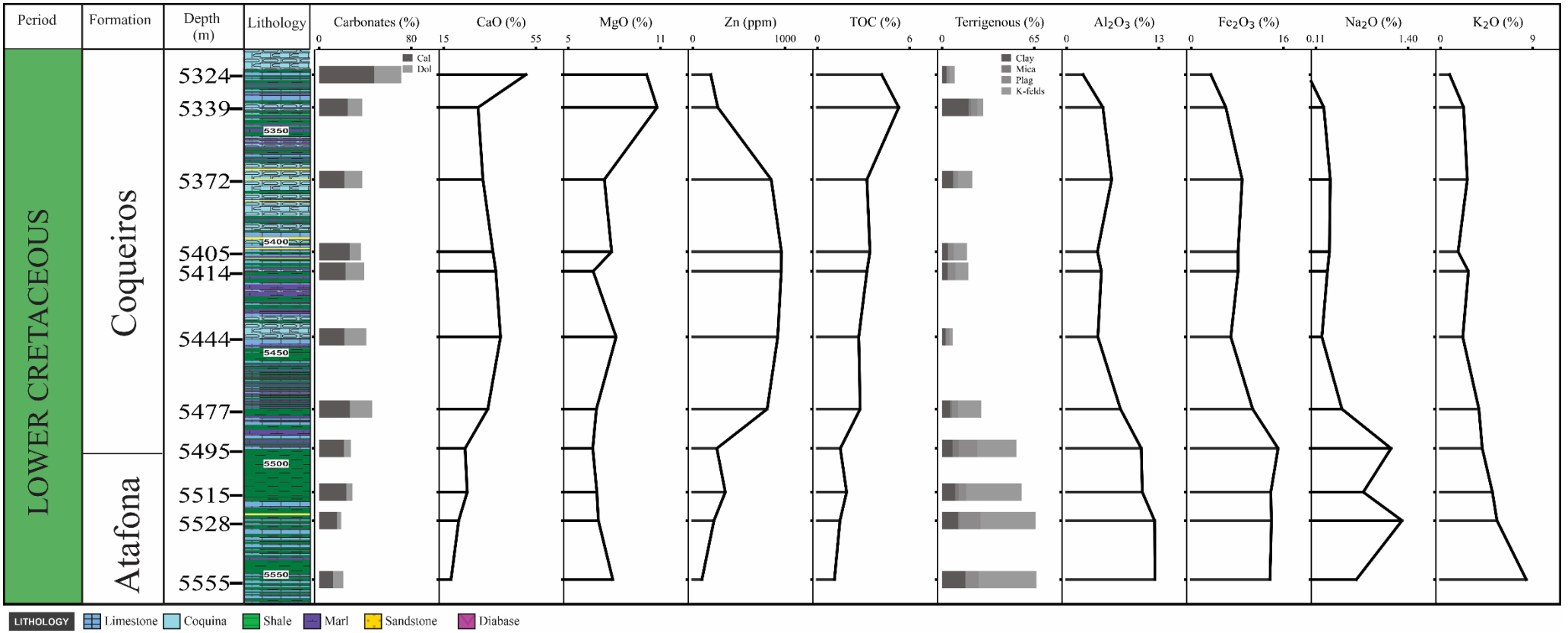

Figure 6. Stratigraphic column and geochemical-mineralogical profiles of well BC-BR3 from the Campos Basin, showing vertical variations in mineral content, major oxides, organic parameters, and trace elements across the Coqueiros and Atafona formations. The lithology column displays: limestone (blue), coquina (light blue), shale (dark green), marl (purple), sandstone (yellow), and diabase (pink).

Accessory minerals present throughout both formations include barite (0.4-19.7%), pyrite (<1-3.7%), amphibole/pyroxene (0-6%), anhydrite (0-3.5%), and halite (0-3%). The relationship between carbonate content and pyrite is notable, with low-carbonate rocks (<25%) showing higher pyrite content (0.001-0.187%, averaging ~0.05%), while high-carbonate rocks (>50%) exhibit significantly lower values (typically <0.01%), as illustrated in the pyrite profiles of Figures 5 and 6.

4.3 Inorganic sulfur speciation with RE-7S

The lithofacies classification was based on a modified Pettijohn (1975) scheme using carbonate content (MinC) as described in the methodology section. In the Santos Basin, where carbonate content (MinC = 7.8 ± 1.2%) is significantly higher than Campos Basin (MinC = 5.2 ± 2.2%), the Itapema and Piçarras formations show notably low Pyro Fe S values (0.004 ± 0.002% and 0.015 ± 0.007%, respectively) and total iron sulfide values (TSFeS: 0.008 ± 0.006% and 0.038 ± 0.016%, respectively). These low values indicate substantial analytical interference during Rock-Eval 7S pyrolysis, where reactions between pyritic sulfur and cations released during carbonate decomposition reduce signal recovery (Cohen-Sadon et al., 2022).

This analytical complexity is illustrated by the relationship between carbonate content and iron sulfide detection across both basins (Table S2; Figure 7). In the Campos Basin, a clear inverse relationship emerges between carbonate content and both iron sulfide fractions. Siliceous samples (MinC <3%, n=7), all from the Atafona Formation, exhibit the highest values for both Pyro Fe S (0.031 ± 0.064%) and total iron sulfide (TSFeS: 0.324 ± 0.327%). Marl samples (MinC 3-6%, n=14) show intermediate values (Pyro Fe S: 0.021 ± 0.039%; TSFeS: 0.229 ± 0.312%), while carbonate samples (MinC 6-12%, n=29) demonstrate the lowest concentrations (Pyro Fe S: 0.007 ± 0.008%; TSFeS: 0.071 ± 0.114%). The systematic reduction in both iron sulfide fractions with increasing carbonate content provides clear evidence of carbonate matrix interference in Rock-Eval 7S analysis, with this effect being more pronounced in the carbonate-rich Santos Basin samples, which show approximately 63% lower Pyro Fe S and 93% lower total iron sulfide values compared to equivalent lithofacies in the Campos Basin.

As shown in Figure 7, this relationship is inverse to the Sulfate/Total Sulfur ratio pattern, where samples with low carbonate content show lower ratios (~0.62 for <25% carbonates), while those with medium and high carbonate content exhibit progressive increases in this ratio (~0.87 for 25-50% and ~0.95 for >50% carbonates). Samples with the highest Sulfate S content (>3.0%) show combined barite + anhydrite + gypsum contents of up to 2.7% by XRD analysis, whereas samples with low Sulfate S (<1.0%) typically contain <2.0% total sulfate minerals. The Santos Basin samples, despite higher carbonate content, show consistently lower Sulfate S values (0.2-1.4%) and correspondingly lower sulfate mineral abundances compared to equivalent carbonate-rich samples from the Campos Basin.

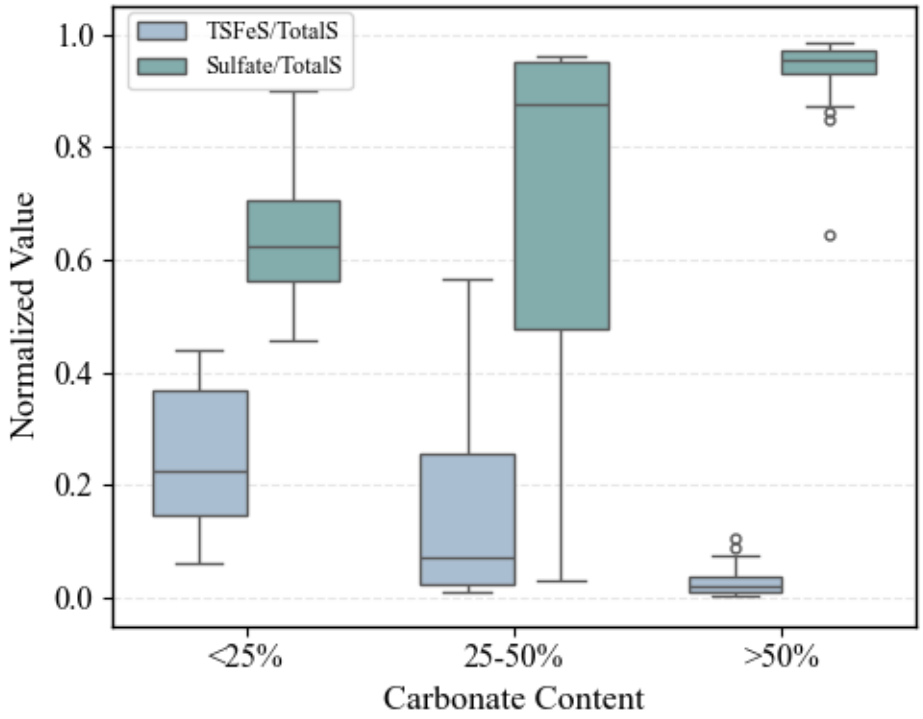

Figure 7. Relationship between carbonate content (<25%, 25-50%, >50%) and the TSFeS/Total Sulfur and Sulfate/Total Sulfur ratios. Samples with higher carbonate content show an increase in sulfate proportion, while TSFeS progressively decreases.

5. Discussion

5.1 The Organic Geochemical Pattern in the Pre-salt Interval of Santos Basin

Geochemical and mineralogical analysis of the Santos Basin reveals trends reflecting its depositional evolution and the factors controlling organic matter preservation. The basin exhibited notably high TOC concentrations, with the Itapema Formation presenting a mean value of 5.2% ± 1.1%. This TOC value is significantly higher than the 1.4% mean reported by Zuo et al. (2022), though within their documented range (0.4-7.3%). Similarly, the Piçarras Formation's mean TOC (5.1%) neared the upper limit of the range (0.7-4.8%, mean 2.1%) reported for it by the same authors. Further, the organic-rich black shales are concentrated in the more distal portions of the Santos Basin (Moreira, 2007), which is the case of well BS-BR1 (depths 5640-6099 m), as shown in Figure 1.

Geochemical analysis revealed significant correlations between major and trace elements in siliciclastic sediments. The terrigenous element suite comprising SiO_2, Al_2O_3, Fe_2O_3, K_2O, and TiO_2 showed strong positive intercorrelations ($\rho > 0.9$), with particularly strong relationships for Al_2O_3-SiO_2 ($\rho = 1.0$), Fe_2O_3-TiO_2 ($\rho = 1.0$), and Al_2O_3-K_2O ($\rho = 1.0$). The Fe_2O_3-TiO_2 correlation indicates their common source from Fe-Ti oxide minerals (Nadoll et al., 2014). These terrigenous elements show positive correlations with detrital minerals including plagioclase (Fe_2O_3: $\rho = 0.9$, TiO_2: $\rho = 0.9$) and quartz (Fe_2O_3: $\rho = 0.7$, TiO_2: $\rho = 0.7$), and negative correlations with calcite (ρ = -0.8 to -0.9), confirming their concentration in siliciclastic input. Notably, positive correlations with pyrite (Fe_2O_3: $\rho = 0.9$, TiO_2: $\rho = 0.9$)

indicate that terrigenous Fe-Ti phases provided reactive iron for authigenic sulfide formation under reducing conditions.

Mineralogical associations further support these relationships. Plagioclase shows significant correlations with K_2O ($\rho = 0.9$) and SiO_2 ($\rho = 0.9$), while mica and quartz display positive correlations with terrigenous elements ($\rho = 0.5$-0.8), suggesting varying degrees of mineral preservation during transport. Trace elements Rb and Zr exhibit significant correlations with terrigenous elements ($\rho > 0.9$), with notable Al_2O_3-Zr ($\rho = 1.0$) and K_2O-Rb ($\rho = 1.0$) relationships. Rb association with potassic minerals (illite and mica) and Zr presence reflects consistent detrital zircon input, indicating sediments derived from a predominantly felsic source area under moderate weathering conditions (Taylor & McLennan, 1985).

The positive correlation between CaO and calcite ($\rho = 0.9$), coupled with high calcite concentrations reaching 75%, reflects the dominance of carbonate sedimentation. This is particularly evident in the Itapema Formation which was previously described as containing calcirudites composed of pelecypod shell fragments (Moreira et al., 2007). This carbonate predominance is contrasted by siliciclastic phases, evidenced by strong negative correlations with silicate minerals (plagioclase, $\rho = -0.9$; quartz, $\rho = -0.8$) and their constituent elements (SiO_2, $\rho = -1.0$; Al_2O_3, $\rho = -1.0$; K_2O, $\rho = -0.9$). The terrigenous nature of the less carbonate-rich intervals is further corroborated by strong negative correlations of CaO with trace elements (Zr, $\rho = -0.9$; Rb, $\rho = -0.9$) and other major oxides (TiO_2, $\rho = -0.9$; MgO, $\rho = -0.6$).

Trace metal enrichment and reducing condition indicators show significant variations throughout the profile, with maximum expression at the basal portion of the Itapema Formation (5910-5991 m), as illustrated in Figure 4. In this interval, the association between high TOC, Cu, Zn, organic S, and pyrite suggests persistent reducing conditions. The strong positive correlations between Fe_2O_3 and pyrite ($\rho = 0.9$) and Fe_2O_3 and Cu ($\rho = 0.9$) indicate a close association between iron and sulfide phases. This relationship primarily reflects the role of terrigenous iron input as a source of reactive Fe that, under reducing conditions, undergoes reduction and subsequently precipitates as iron sulfides when H_2S is available in pore waters. This process occurs alongside organometallic complexation mechanisms, both contributing to trace metal sequestration under anoxic conditions (Tribovillard et al., 2006). The relationship between organic S and TOC shows statistically significant correlation ($\rho = 0.7$, $p < 0.05$) but considerable variability. This variability likely reflects differences in organic matter composition and reactivity rather than redox fluctuations alone, as pyrite formation is kinetically favored over organic sulfur incorporation. Notably, organic S reaches its maximum values (0.038%) at the basal Itapema Formation (5964 m), where organic sulfur is enriched relative to Pyro Fe S, suggesting variable sulfurization pathways influenced by local depositional conditions.

The PCA reinforces the described interactions between geochemical parameters, with the first two components explaining 71.5% of the total variance (Factor 1: 55.2%; Factor 2: 16.2%). The PCA biplot (Figure 8) reveals three distinct geochemical associations that correspond to key depositional processes: (1) a carbonate-dominated assemblage in the positive Factor 1 region (CaO with strong positive loading of 0.8), characteristic of the Itapema Formation; (2) a terrigenous/heavy elements suite in the negative Factor 1 region (with notably strong negative

loadings for TiO_2: -1.0, Fe_2O_3: -1.0, Zr: -0.9, and Al_2O_3: -0.9), predominant in the Piçarras Formation; and (3) an organic matter/anoxic indicators association (TOC: -0.6, organic S: -0.9, and MnO: -0.6 on Factor 2) linked to reducing conditions, particularly expressed in the basal portion of the Itapema Formation (5910-5991 m). The positioning of MgO (-0.7 on Factor 2) reflects diagenetic processes such as dolomitization or authigenic mineral formation rather than redox conditions. The clear separation of SiO_2 (-0.7, -0.3) from other silicate minerals suggests additional silicification processes beyond simple detrital input, while the opposing positions of MgO and CaO reflect different pathways of incorporation during diagenesis, with MgO likely associated with authigenic clay mineral formation.

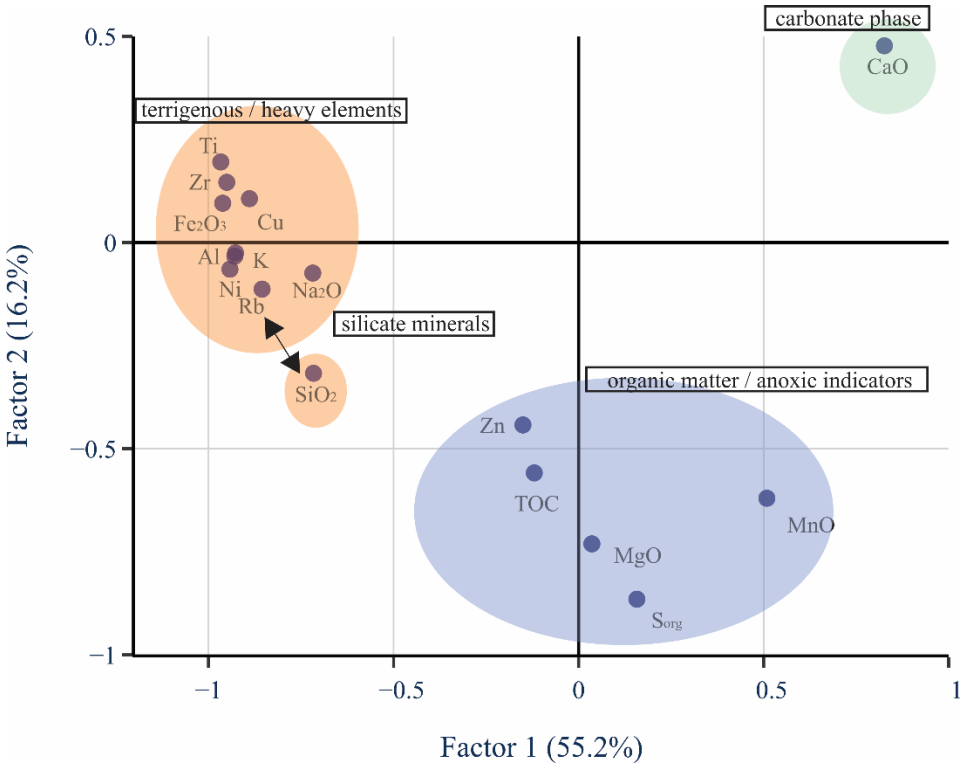

Figure 8. Principal Component Analysis biplot for Santos Basin samples showing relationships among geochemical elements and organic parameters. Factor 1 (55.2% variance) distinguishes carbonate from terrigenous elements; Factor 2 (16.2% variance) highlights organic matter and redox-sensitive elements.

Our data partially contrast with Pietzsch et al. (2018), who identified significant fluvial input during the Itapema Formation deposition, as our analyses demonstrate that the upper portion of this formation (5640-5883 m) is characterized by low detrital content, with minimal clay, mica, and K-feldspar presence as shown in Figure 4. However, we observe a notable increase in detrital material with depth, particularly in the transition zone to the Piçarras Formation (5991-6018 m) and throughout the Piçarras interval (6018-6099 m), where clay minerals and micas become significantly more abundant (up to 15%). This observation aligns with Moreira et al. (2007), who described the Piçarras Formation as consisting of alluvial fan deposits and lacustrine sandstones.

The geochemical data from our well samples reveal a moderate positive correlation between MgO and SiO_2 ($\rho = 0.62$), which indicates the likely presence of stevensite, particularly in the Piçarras Formation where elevated levels of MgO (6-9%), clay minerals, and SiO_2 coexist. This mineralogical signature is analogous to assemblages documented by Alvarenga et al. (2016) in hydrothermal volcanic systems within the Lagoa Feia Group of the Campos Basin and corroborates Winter et al.'s (2007) characterization of talc-stevensite as typical products of hydrothermal activity in alkaline volcanic lakes. The carbonate-dominated architecture with sustained anoxia documented in Santos Basin parallels highly productive alkaline lake systems such as the Eocene Green River Formation (Wyoming) and Permian Lucaogou Formation (Junggar Basin, China), where similar evaporative concentration and hydrothermal influence promoted exceptional organic preservation under evaporative, chemically stratified conditions (Carroll, 1998; Bohacs et al., 2000).

In the Itapema Formation, our analysis reveals that intervals interbedded between coquina-rich layers exhibit lower carbonate content with higher concentrations of dolomite (reaching 30-40%) and quartz, suggesting that partial dissolution of primary calcite during early diagenesis created secondary porosity, as evidenced by the inverse relationship between calcite and dolomite content (Fig. 3). This enhanced permeability facilitated Mg and Si-enriched fluid circulation and promoting dolomitization and silicification. Figure 4 demonstrates the inverse relationship between calcite and dolomite content throughout the stratigraphic column, further supporting the hypothesis of diagenetic fluid migration.

This pattern parallels observations by Pietzsch et al. (2020) in the Barra Velha Formation, where dolomite distribution appears controlled by textural heterogeneity, following Rameil's (2008) stratiform dolomitization model that emphasizes early diagenetic processes in Mg-enriched environments, with stevensite transformation potentially providing additional Mg during dolomitization as suggested by Herlinger Jr et al. (2017) and Lima and De Ros (2019).

5.2 Terrigenous Controls on Organic Matter Preservation in the Pre-salt Interval of Campos Basin

The integrated analysis of geochemical and mineralogical parameters from the Campos Basin reveals patterns that reflect its depositional evolution and diagenetic processes. The basin is characterized by a mixed carbonate-siliciclastic system with total carbonate content ranging from 45-50%.

The Atafona Formation, the basal unit, exhibits pronounced terrigenous signatures with K-feldspar content reaching 40% and clay minerals up to 16%, accompanied by elevated terrigenous oxides (Al_2O_3: 8.4% ± 2.5%, K_2O: 3.6% ± 2.1%, TiO_2: 1.1% ± 0.4%). These variations are particularly pronounced in well BC-BR3, where K_2O concentrations are 2-3 times higher than BC-BR1. The formation's low carbonate content and TOC values (1.8 ± 0.5%) reflect a predominantly siliciclastic system. Geochemical analysis demonstrates significant correlations between terrigenous elements (Al_2O_3-TiO_2: $\rho = 0.9$, Al_2O_3-Fe_2O_3: $\rho = 0.9$, Fe_2O_3-TiO_2: $\rho = 0.8$), with strong associations with K-feldspar and clay minerals ($\rho > 0.7$), indicating provenance from silicate and aluminosilicate phases. A distinctive feature is the exclusive presence of talc (1-2%), with rare occurrences in the transitional zone to the Coqueiros

Formation. The presence of amphiboles and pyroxenes in some samples results in elevated Na_2O (1.0% ± 0.3%) and MgO (7.2% ± 0.5%), while Zn levels vary widely (98.6-806 ppm), with highest concentrations in BC-BR3.

The overlying Coqueiros Formation exhibits higher organic matter content (TOC: 3.9% ± 1.0%) with remarkable consistency across wells (BC-BR1: 3.7% ± 1.2%, BC-BR2: 4.2% ± 0.7%, BC-BR3: 3.7% ± 0.9%). Organic sulfur concentrations range from 0.005% to 0.019% (mean: 0.010% ± 0.004%). The formation records a low-gradient carbonate ramp environment strongly influenced by wave action, where different sub-environments coexisted from margins to deeper portions (Carvalho et al., 2000). Mineralogically, it shows intermediate carbonate content with calcite (26% ± 8%, maximum 48%) and dolomite (20% ± 7%, maximum 35%), alongside substantial quartz (14-49%) and feldspars (4.5-31.7%). This heterogeneous nature aligns with findings from Barberes et al. (2024), who reported analogous mineral assemblages in the same fields. The elemental composition varies considerably both vertically and laterally, with average concentrations of CaO (36% ± 5%), SiO_2 (35% ± 5%), Al_2O_3 (6% ± 1%), K_2O (2.8% ± 0.8%), and Fe_2O_3 (7.6% ± 1.5%). The formation shows marked Cu enrichment (143.4 ± 58.6 ppm), with concentrations decreasing consistently with depth (5223-6382 m).

Trace metal enrichment and redox indicators reveal distinct preservation mechanisms among the studied wells. In BC-BR1, reducing conditions dominated organic matter preservation, evidenced by strong pyrite-TOC correlation ($\rho = 0.8$) and significant correlations between TOC and redox indicators (Cu: $\rho = 0.9$, organic S: $\rho = 0.9$, MnO: $\rho = 0.9$). The Cu-organic S correlation ($\rho = 0.9$) suggests initial delivery with organic matter and subsequent incorporation into sulfur-bearing phases during early diagenesis (Tribovillard et al., 2006). These parameters decrease progressively with depth (TOC: $\rho = -0.9$, organic S: $\rho = -1.0$, Cu: $\rho = -0.9$).

Conversely, BC-BR3 exhibits terrigenous control, with pyrite-Fe_2O_3 correlation ($\rho = 0.6$) and both increasing with depth ($\rho = 0.7$ and 0.8 respectively). Iron-bearing minerals correlate positively with K-feldspar (Fe_2O_3: $\rho = 0.9$; pyrite: $\rho = 0.7$), indicating terrigenous iron as the reactive source for pyrite formation. Cu shows positive correlation with Fe_2O_3 ($\rho = 0.6$), while Zn associates preferentially with quartz ($\rho = 0.8$), suggesting predominantly detrital metal sources.

BC-BR2, positioned in the deeper platform (6220-6382 m), displays distinctive magnesian carbonate signatures. Dolomite correlates with sulfur-bearing phases (S Org: $\rho = 0.7$; Pyro Fe S: $\rho = 0.6$) and evaporitic minerals (Gypsum: $\rho = 0.9$; K_2O: $\rho = 0.6$), with negative correlations with clay minerals ($\rho = -0.9$) and Al_2O_3 ($\rho = -0.5$). The carbonate assemblage is accompanied by diverse evaporites (barite, anhydrite, halite, gypsum), indicating restricted circulation with salinity variation cycles.

The Atafona-Coqueiros transition, documented in BC-BR1 (5412-5439 m) and BC-BR3 (5444-5477 m), marks significant mineralogical changes. Upward progression shows calcite increasing from 16% ± 6% to 26% ± 8%, and dolomite from 9% ± 5% to 20% ± 7%, accompanied by substantial feldspar reduction from up to 54% to average values, while quartz maintains ~20%. This transition coincides with increasing TOC values, particularly evident in both wells.

Our PCA results (Figure 9) corroborate these interpretations, with the first component (35.1% of total variance) clearly distinguishing terrigenous from carbonate elements and reflecting the primary control over compositional variability within the succession. The positive loading of TOC (0.8) with CaO (0.9) in Factor 1 reinforces that carbonate-dominated environments enhanced organic matter preservation through rapid burial and anoxic conditions typical of alkaline lacustrine systems (Kelts, 1988), as documented in organic-rich anoxic sediments (8-20% TOC) where carbonates and organic matter coexist under reducing conditions (Talbot & Kelts, 1986). The second component, accounting for 24.2% of total variance, highlights elemental associations related to redox conditions. This supports the interpretation that carbonate-rich intervals enhanced preservation of autochthonous (lacustrine algal) organic matter, while increased terrigenous input diluted the concentration of this endogenous organic matter, thereby reducing source rock potential.

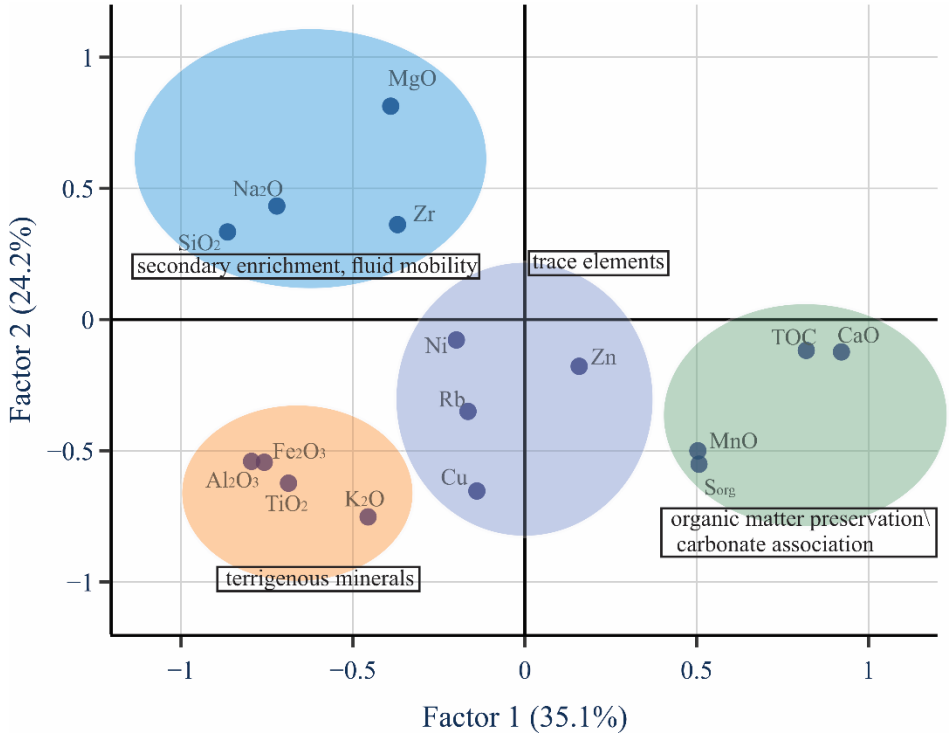

Figure 9. Principal Component Analysis biplot for Campos Basin samples. Factor 1 (35.1% variance) reflects terrigenous-carbonate opposition; Factor 2 (24.2% variance) shows redox-related elemental associations.

The isolated position of MgO in the upper quadrant of the PCA diagram (loading of 0.8 in Factor 2, Figure 9) indicates unique mechanisms of magnesium enrichment in the system. This distinct placement suggests different pathways for magnesium incorporation, potentially related to both dolomitization of carbonate phases and formation of magnesian silicate minerals, which is supported by the presence of dolomite in carbonate-rich intervals and the exclusive occurrence of talc (up to 2%) in the Atafona Formation, formed by chemical deposition processes associated with hydrothermal activity in alkaline volcanic lakes (Winter et al., 2007). The contrasting positions of trace elements (Cu, Zn, Ni) in the PCA plot (Figure 9) reinforce

their distinct incorporation pathways; Cu groups with terrigenous elements (Factor 2 loading: -0.7), unlike Zn, which shows different associations.

In well BC-BR1, reducing conditions were the dominant factor in organic matter preservation, evidenced by the progressive decrease with depth of TOC (ρ = -0.9), organic S (ρ = -1.0), and Cu (ρ = -0.9) as shown in Figure 5. In contrast, in BC-BR3, the main control was exerted by terrigenous input, resulting in exceptionally high concentrations of trace elements primarily associated with the siliciclastic fraction, as demonstrated in Figure 6.

Magnesium behavior shows distinct patterns between the studied formations. In the Atafona Formation, correlation patterns suggest complex mineral associations involving magnesian phases. The presence of talc in well BC-BR3 (up to 2%) indicates the occurrence of magnesian silicate phases formed by chemical deposition processes associated with hydrothermal activity in alkaline volcanic lakes (Winter et al., 2007). These variations in MgO distribution may represent different processes of magnesium incorporation in the units: dolomitization of carbonate phases and formation of magnesian silicates, aligning with Winter et al. (2007) observations on hydrothermal activity products in alkaline volcanic lakes.

The independent behavior of quartz in relation to other terrigenous constituents, evidenced by significant negative correlations with major terrigenous elements (Al_2O_3: ρ = -0.6; K_2O: ρ = -0.5; TiO_2: ρ = -0.6) and non-significant correlations with other indicators of continental input (K-feldspar: ρ = -0.3; micas: ρ = 0.1; Zr: ρ = 0.1), suggests additional silicification processes in the system beyond simple detrital input. The presence of calcite dissolution textures and dolomite recrystallization features in intervals with lower carbonate content indicates that partial dissolution of primary calcite created secondary porosity, subsequently filled by authigenic dolomite and quartz. This process increased effective permeability, possibly facilitating the circulation of fluids enriched in Mg and Si. These processes have also been reported in the Lagoa Feia Group (Alvarenga et al., 2016). Supporting our interpretation of diagenetic fluid migration and silicification, Barberes et al. (2024) identified heterogeneous fabric and authigenic minerals (saddle dolomite, mega-quartz) via SEM imaging.

5.3 Controls on Depositional Systems and Organic Matter Preservation

The geochemical and mineralogical patterns documented in sections 5.1 and 5.2 reveal that the pre-salt lacustrine systems of Santos and Campos basins exhibit fundamentally different depositional architectures despite their established chronostratigraphic correlation within the Jiquiá Stage (Middle Aptian; biozones NRT-008/009 to NRT-010), with main generative potential concentrated in biozone OS-1000 (Moreira et al., 2007; Penteado et al., 2024). These contrasting preservation mechanisms and depositional signatures can be understood through the interplay of stratification mechanisms, terrigenous input, and basin configuration that directly controlled organic matter preservation efficiency.

5.3.1 Stratification Mechanisms and Paleoenvironmental Framework

The preservation mechanisms and depositional signatures observed in these lacustrine systems reflect the interplay of water-column stratification, terrigenous input, and nutrient cycling operating within fundamentally anoxic environments. Both Santos and Campos basins

developed under reducing bottom-water conditions, as evidenced by their high TOC contents that classify both systems as excellent source rocks (Peters and Cassa, 1994). The difference in organic enrichment between basins reflects variations in the stability and nature of the stratification mechanism rather than fundamentally different redox states.

Although the Santos and Campos basins are geographically adjacent and experienced similar regional climatic forcing, they are structurally separated by the Cabo Frio High, which directed continental drainage into distinct catchment systems. This structural configuration, combined with the significant difference in basin size (Santos: ~350,000 km² vs. Campos: ~100,000 km²; Moreira et al., 2007; Winter et al., 2007), resulted in differential responses to regional climatic events. Different stratification regimes can develop in adjacent basins due to variations in basin geometry, hydrology, and the relationship between water supply and accommodation within each individual basin.

Santos Basin developed stable chemical stratification driven by evaporative concentration under persistently arid conditions. The occurrence of dawsonite (up to 3%) indicates highly alkaline, evaporative conditions that promoted salinity-driven density differences in the water column (Hardie and Eugster, 1970). This chemical stratification mechanism is inherently more resistant to disruption than thermal stratification, maintaining persistent bottom-water anoxia and resulting in consistently higher TOC values (5.6 ± 1.5%). The carbonate-dominated architecture (74.6% carbonates) further reflects minimal terrigenous dilution of organic matter during this stable stratification regime.

Campos Basin, while also maintaining anoxic bottom waters, relied more heavily on thermal stratification (Dean, 1981; Demaison and Moore, 1980). Thermal stratification is driven by temperature-induced density differences that are inherently weaker and more transient than salinity-driven gradients. In modern lake systems, thermoclines are seasonally eroded during cooling periods, resulting in periodic overturn that reoxygenates bottom waters (Boehrer and Schultze, 2008). The critical distinction is that freshwater input affects these mechanisms differently: in thermally stratified lakes, cooler inflowing waters can directly destabilize the temperature gradient and trigger mixing, whereas in chemically stratified lakes, freshwater input must be volumetrically sufficient to significantly dilute the dissolved solids before stratification is compromised.

Therefore, episodic humid pulses produced two simultaneous effects in Campos Basin that were attenuated in Santos Basin: (1) direct dilution of organic matter by terrigenous sediment input, and (2) destabilization of thermal stratification leading to enhanced water-column mixing and reduced preservation efficiency. The larger volume of Santos Basin provided greater buffering capacity against these perturbations, while its chemical stratification required more extreme freshwater input to be compromised. This interpretation is supported by the mineralogical evidence: Campos Basin's higher siliciclastic content (38.3% carbonates vs. 74.6% in Santos) records these differential responses to shared regional climatic forcing. The presence of talc (1--2% in the Atafona Formation) indicates distinct magnesium-rich hydrothermal processes associated with alkaline volcanic lakes under intermittent arid conditions (Winter et al., 2007), supporting the interpretation of variable rather than persistent stratification.

The stratigraphic progression observed in both basins---from more terrigenous-dominated basal units (Atafona, Piçarras) to increasingly carbonate-rich upper intervals (Coqueiros, Itapema)---suggests a regional climatic transition from more humid to increasingly arid conditions during the rift phase. This climatic evolution was modulated by the integrated effects of: (1) tectonic subsidence creating accommodation space and controlling basin connectivity; (2) volcanic activity providing alkaline waters that enhanced carbonate precipitation and created optimal conditions for microbial communities; and (3) regional climate controlling the precipitation/evaporation balance that determined the dominant stratification mechanism (Cole, 1979; Katz, 1990).

5.3.2 Scale-Dependent Preservation Controls

Multivariate statistical analysis reveals distinct preservation mechanisms operating within these lacustrine systems. Principal component analysis explains 71.5% of variance in Santos Basin and 59.3% in Campos Basin, reflecting the complex interplay of multiple controlling factors rather than a single dominant mechanism.

Both basins developed under predominantly anoxic bottom-water conditions, as evidenced by their high TOC contents (5.6 ± 1.5% in Santos and 3.1 ± 1.3% in Campos). These values classify both systems as excellent source rocks according to established criteria (Peters and Cassa, 1994), indicating that reducing conditions were maintained throughout deposition in both basins. This interpretation is consistent with observations from the conjugate Congo Basin, where Harris et al. (2004) demonstrated that redox proxies indicate reducing conditions throughout deposition of the entire synrift section. Critically, Harris et al. (2004) concluded that enhanced anoxia did not trigger deposition of the richest source rocks; instead, high rates of organic productivity and nutrient flux were the critical factors controlling organic matter enrichment.

Similarly, in the Santos and Campos basins, the difference in TOC content reflects the interplay of three key factors operating within anoxic systems:

(1) Primary productivity and nutrient availability: Santos Basin's basal Itapema Formation (5910-5991 m) reaches TOC of 7.0% coincident with elevated Cu (up to 106 ppm) and organic sulfur (0.036-0.038%), reflecting conditions where high primary productivity was sustained by favorable nutrient cycling in a chemically stratified water column. The positive correlation between $\delta^{13}C$ of organic matter and TOC observed in analogous systems (Harris et al., 2004; Gonçalves, 2002) indicates that bioproductivity exerted significant control on organic carbon enrichment in the late rift sections.

(2) Dilution by terrigenous input: Terrigenous input exhibits systematic inverse relationships with organic matter accumulation, reflecting the dilution control mechanism (Bohacs et al., 2005). This relationship is most pronounced in Campos Basin well BC-BR3, where terrigenous proxies correlate negatively with TOC. The higher siliciclastic content in Campos Basin (38.3% carbonates vs. 62.5% in Santos) indicates that episodic increases in terrigenous flux during humid climatic pulses diluted organic matter accumulation. Studies from the Congo Basin similarly demonstrate that detrital inputs degrade source rock quality by diluting autochthonous organic matter (Behar et al., 2021).

(3) Stability of water-column stratification: Santos Basin's characteristics align with conditions where chemical stratification developed readily due to closed hydrology and evaporative concentration (Hardie & Eugster, 1970), promoting sustained anoxia through density differences maintained by salinity gradients. Campos Basin, while also maintaining anoxic bottom waters, relied more heavily on thermal stratification (Dean, 1981), which is inherently more vulnerable to disruption during periods of enhanced freshwater input. This difference in stratification mechanism---rather than a fundamental difference in redox state---explains the greater variability in preservation efficiency observed in Campos Basin.

This multi-factor framework aligns with the 'production-destruction-dilution-accommodation' model proposed by Bohacs et al. (2005), which recognizes that source rock development results from the balance between organic matter supply, preservation efficiency, dilution rates, and accommodation space rather than from any single dominant control. The moderate carbonate environments (45-65%) that provide optimal preservation conditions in both basins reflect this balance: sufficient alkalinity to support high productivity without excessive carbonate precipitation that would dilute organic matter.

The relationship between extreme calcite concentrations (>70%) and reduced TOC values does not indicate inhibition of preservation despite favorable redox conditions, as originally stated. Rather, this pattern reflects simple dilution of organic matter by carbonate sediments, consistent with observations from other lacustrine systems (Tyson, 2001). Both basins maintained the anoxic conditions necessary for organic matter preservation; the difference in source rock quality reflects variations in the other controlling factors operating within these fundamentally reducing environments.

5.4 Behavior of Inorganic Sulfur Phases in Rock-Eval 7S Analysis

Pyro Fe S determined by Rock-Eval 7S pyrolysis showed moderate positive Spearman correlations with XRD-identified pyrite in both Campos ($\rho = 0.5$) and Santos ($\rho = 0.5$) basins, with similar correlations observed for XRF-determined total sulfur (Campos: $\rho = 0.6$; Santos: $\rho = 0.6$). These moderate correlations between Rock-Eval 7S Pyro Fe S and independent analytical methods demonstrate reasonable agreement while reflecting analytical limitations from carbonate matrix interference effects documented by Cohen-Sadon et al. (2022).

This interference manifests as systematic signal suppression with increasing carbonate content, as documented in section 4.3 and illustrated in Figure 7. The Santos Basin, with higher average carbonate content, exhibits strong negative Spearman correlations between Pyro Fe S and MinC ($\rho = -0.8$), total carbonates (calcite + dolomite; $\rho = -0.8$) and Ca ($\rho = -0.7$), while the Campos Basin, with lower average carbonate content than Santos, shows non-significant correlations (MinC: $\rho = 0.1$; total carbonates: $\rho = 0.1$; Ca: $\rho = 0.1$). Cohen-Sadon et al. (2022) attribute this phenomenon to reactions between pyritic sulfur and cations released during carbonate decomposition, forming secondary sulfides that reduce signal recovery by 60-95%. Importantly, this inverse relationship is not observed in XRD-determined pyrite abundances, confirming that the suppression represents a pyrolysis-specific analytical artifact rather than actual variations in pyrite content.

Sulfate sulfur quantification shows the expected systematic increase across lithofacies, consistent with sulfate mineral enrichment in carbonate-dominated environments (Vielma, 2024). XRD analysis confirms this relationship, with samples containing >3.0% Sulfate S showing combined sulfate mineral contents (barite + anhydrite + gypsum) of up to 2.7%, while samples with <1.0% Sulfate S typically contain <2.0% total sulfate minerals, as documented in section 4.3. However, quantitative interpretation requires caution due to potential analytical limitations including incomplete sulfate decomposition in calcium-rich samples and possible sulfate neoformation during analysis (Aboussou, 2018; Lamoureux-Var et al., 2019).

The contrasting correlation patterns between basins further illustrate these analytical complexities, as demonstrated in Figure 7. Santos Basin samples show strong negative Spearman correlations between Sulfate S and total carbonates (ρ = -0.8) and Ca (ρ = -0.7), suggesting matrix interference in quantification. Conversely, Campos Basin samples exhibit positive correlations with dolomite (ρ = 0.5) and weaker correlations with MinC (ρ = 0.5), potentially reflecting more natural sulfate-carbonate associations similar to those documented in other carbonate formations (Vielma et al., 2024). Despite showing lower overall Sulfate S values (0.2-1.4%) compared to equivalent carbonate-rich Campos samples, Santos Basin samples demonstrate this inverse relationship, supporting the interpretation of analytical artifacts. Therefore, while sulfate enrichment in carbonate lithofacies represents a genuine geochemical trend, its magnitude may be partially amplified by analytical artifacts inherent to Rock-Eval 7S analysis of carbonate-rich samples, as discussed by Espitalié et al. (2023).

6. Conclusions

This comprehensive geochemical and mineralogical investigation of the Jiquiá Shale from the Santos and Campos basins reveals that the Itapema and Coqueiros formations represent the primary source rocks of the Jiquiá Stage (Middle Aptian) in their respective basins, as previously identified by Winter et al. (2007). The study provides new insights into the fundamental controls governing organic matter preservation in these chronostratigraphically analogous formations. Through integration of high-resolution XRD, XRF, and Rock-Eval 7S analyses across four wells, this study establishes a framework for understanding depositional processes and preservation mechanisms in Middle Aptian lacustrine source rocks.

Despite established chronostratigraphic correlation within the Jiquiá Stage, the Santos and Campos basins exhibit markedly different depositional signatures. Santos Basin evolved as a predominantly carbonate system (74.6 ± 10.7% total carbonates) with consistently elevated TOC values (5.1 ± 1.1%), whereas Campos Basin developed as a mixed carbonate-siliciclastic system (38.3 ± 13.0% carbonates) with systematically lower and more variable organic content (3.1 ± 1.3%).

These source rocks, concentrated in the Coqueiros Formation (Campos Basin) and Itapema Formation (Santos Basin), correspond to the Jiquiá Shale units identified by Winter et al. (2007) as the primary hydrocarbon source rocks of the rift supersequence.

Both basins developed under predominantly anoxic bottom-water conditions, as evidenced by TOC values that classify both systems as excellent source rocks (Peters and Cassa, 1994). Santos Basin developed stable chemical stratification driven by evaporative concentration,

maintaining persistent anoxia, while Campos Basin relied more heavily on thermal stratification and experienced episodic increases in terrigenous input during humid climatic pulses. The difference in organic enrichment reflects variations in stratification stability and dilution intensity rather than fundamentally different redox states, with both systems maintaining the reducing conditions necessary for organic matter preservation.

Principal component analysis reveals three key, scale-dependent controls operating within fundamentally anoxic systems: (1) primary productivity and nutrient availability, particularly evident in Santos Basin's basal Itapema Formation where TOC reaches 7.0% coincident with elevated Cu and organic sulfur; (2) terrigenous dilution showing systematic inverse relationships with organic matter accumulation, most pronounced in Campos Basin where episodic siliciclastic input reduced organic matter concentrations; and (3) stratification stability, with Santos Basin's chemical stratification proving more resistant to disruption than Campos Basin's thermal stratification. Optimal preservation occurs in moderate carbonate environments (45-65%), while extreme calcite concentrations (>70%) dilute organic matter through simple sedimentary dilution rather than inhibition of preservation processes.

This study documents significant analytical challenges in applying Rock-Eval 7S methodology to carbonate-rich formations, where matrix interference effects reduce pyritic sulfur signal recovery by 60-95% as carbonate content increases. These findings have direct implications for paleoenvironmental interpretation in carbonate-dominated sequences.

The documented preservation mechanisms and stratification controls provide new insights for petroleum system modeling in analogous rift-related lacustrine sequences worldwide. However, this study represents detailed analysis of four strategically selected wells, and the observed patterns should be interpreted as representative of local depositional conditions. Future research incorporating additional wells across different structural and paleogeographic settings would validate the regional extent of these trends and refine understanding of the complex interplay between climate, tectonics, and volcanism in controlling lacustrine source rock development.

Declaration of Generative AI and AI-Assisted Technologies in the Manuscript Preparation Process

During the preparation of this work the authors used ChatGPT (https://chatgpt.com/) in order to only enhance readability and language clarity. After using this tool/service, the authors reviewed and edited the content as needed and take full responsibility for the content of the publication.

Data Availability

All geochemical and mineralogical data supporting this study are included in the supplementary tables. Raw analytical data will be made available upon reasonable request to the corresponding author.

Declaration of Competing Interest

The authors declare that they have no known competing financial interests or personal relationships that could have appeared to influence the work reported in this paper.

Acknowledgments

We would like to express our sincere gratitude to Petrobras for funding this research and scholarships that made this study possible (Petrobras/ANP Grant 2022/00150-1) and to BP Brasil for the donation of samples used in this study. Special thanks are extended to all members of the PR4 Project for their invaluable assistance with the analyses. ALSA acknowledges the financial support provided by the Brazilian funding agencies FAPERJ (E-26/201.008/2022 E-26/210.081/2023) and CNPq (grant 307658/2021-0), which were essential for the development and successful completion of this work.

References

Aboussou, A., 2018. New Rock-Eval method for pyritic and organic sulphur quantification: Application to study organic matter preservation in Jurassic sediments. Doctoral dissertation, Sorbonne Université. Available at: https://tel.archives-ouvertes.fr/tel-02947050

Alvarenga, R.S., Iacopini, D., Kuchle, J., Scherer, C.M.S., Goldberg, K., 2016. Seismic characteristics and distribution of hydrothermal vent complexes in the Cretaceous offshore rift section of the Campos Basin, offshore Brazil. Marine and Petroleum Geology 74, 12-25. https://doi.org/10.1016/j.marpetgeo.2016.03.030

ANP (Agência Nacional do Petróleo, Gás Natural e Biocombustíveis), 2025. Boletim Mensal da Produção de Petróleo e Gás Natural. Rio de Janeiro: ANP. Available at: https://www.gov.br/anp/pt-br/centrais-de-conteudo/publicacoes/boletins-anp/boletins/arquivos-bmppgn/2025/janeiro.pdf (accessed 18 June 2025).

Barberes, G.A., Marques, F.C., Almeida, D.A., Peixoto, L.P.F., Maia, L.F., Sant'Ana, A.C., Andrade, G.F.S., Izumi, C.M.S., Salgado-Campos, V., Feital, T., Oliveira, I.M.V., Venancio, I.M., 2024. Mineralogical and maturation considerations of the Coqueiros Formation (Campos Basin, Brazil): Insights from multi-technique analyses of source rocks. Geosciences 14 (11), 286. https://doi.org/10.3390/geosciences14110286

Barra, T.A., Torres, C.L., Dal Sasso, M.A., Pereira, V.B., Neto, E.V.S., Azevedo, D.A., 2021. Deconvolution of post- and pre-salt petroleum sources in southeastern offshore Brazilian basins. Organic Geochemistry 153, 104146. https://doi.org/10.1016/j.orggeochem.2020.104146

Baumgarten, C.S., Dultra, A.J.C., Scuta, M.S., Figueiredo, M.V.L., Sequeira, M.F.P.B., 1988. Coquinas da Formação Lagoa Feia, Bacia de Campos: evolução da geologia de desenvolvimento. Boletim de Geociências da Petrobras 2 (1), 27-32.

Behar, F., Lorant, F., Mazeas, L., 2021. Detrital input quantification in lacustrine petroleum systems: An example of the pre-salt source rocks from the Lower Congo Basin (Congo). The Depositional Record 7 (2), 245-274. https://doi.org/10.1002/dep2.131

Boehrer, B., Schultze, M., 2008. Stratification of lakes. Reviews of Geophysics 46, RG2005. https://doi.org/10.1029/2006RG000210

Bohacs, K.M., Carroll, A.R., Neal, J.E., Mankiewicz, P.J., 2000. Lake-basin type, source potential, and hydrocarbon character: an integrated sequence-stratigraphic-geochemical

framework. In: Gierlowski-Kordesch, E.H., Kelts, K.R. (Eds.), Lake Basins through Space and Time. AAPG Studies in Geology 46, pp. 3-34. https://doi.org/10.1306/St46706C20

Bohacs, K.M., Grabowski Jr., G.J., Carroll, A.R., Mankiewicz, P.J., Miskell-Gerhardt, K.J., Schwalbach, J.R., Wegner, M.B., Simo, J.A., 2005. Production, destruction, and dilution---the many paths to source-rock development. In: Harris, N.B. (Ed.), The Deposition of Organic-Carbon-Rich Sediments: Models, Mechanisms, and Consequences. SEPM Special Publication 82, pp. 61-101. https://doi.org/10.2110/pec.05.82.0061

Cainelli, C., Mohriak, W.U., 1999. Some remarks on the evolution of sedimentary basins along the Eastern Brazilian continental margin. Episodes 22 (3), 206-216. https://doi.org/10.18814/epiiugs/1999/v22i3/008

Carroll, A.R., 1998. Upper Permian lacustrine organic facies evolution, southern Junggar basin, NW China. Organic Geochemistry 28 (10), 649-667. https://doi.org/10.1016/S0146-6380(98)00040-0

Chang, H.K., Kowsmann, R.O., Figueiredo, A.M.F., Bender, A., 1992. Tectonics and stratigraphy of the East Brazil Rift system: an overview. Tectonophysics 213 (1-2), 97-138. https://doi.org/10.1016/0040-1951(92)90253-3

Cohen, A.S., 1989. Facies relationships and sedimentation in large rift lakes and implications for hydrocarbon exploration: Examples from Lakes Turkana and Tanganyika. Palaeogeography, Palaeoclimatology, Palaeoecology 70 (1-3), 65-80. https://doi.org/10.1016/0031-0182(89)90058-4

Cohen-Sadon, H., Amrani, A., Feinstein, S., Rosenberg, Y.O., 2022. A new empirical approach for rapid quantification of organic and pyritic sulfur in sedimentary rocks using the Rock-Eval 7S. Organic Geochemistry 166, 104350. https://doi.org/10.1016/j.orggeochem.2021.104350

Cole, R.D., 1979. Sedimentology and stratigraphy of the lacustrine deposits. In: Matter, A., Tucker, M.E. (Eds.), Modern and Ancient Lake Sediments. International Association of Sedimentologists Special Publication 2, pp. 147-164. https://doi.org/10.1002/9781444303698.ch8

Craigie, N.W., 2015. Applications of chemostratigraphy in Cretaceous sediments encountered in the North Central Rub' al-Khali Basin, Saudi Arabia. Journal of African Earth Sciences 104, 27-42. https://doi.org/10.1016/j.jafrearsci.2015.01.003

Craigie, N.W., Breuer, P., Khidir, A., 2016a. Chemostratigraphy and biostratigraphy of Devonian, Carboniferous and Permian sediments encountered in eastern Saudi Arabia: An integrated approach to reservoir correlation. Marine and Petroleum Geology 72, 156-178. https://doi.org/10.1016/j.marpetgeo.2016.01.018

Craigie, N.W., Rees, A., MacPherson, K., Berman, S., 2016b. Chemostratigraphy of the Ordovician Sarah Formation, North West Saudi Arabia: An integrated approach to reservoir correlation. Marine and Petroleum Geology 77, 1056-1080. https://doi.org/10.1016/j.marpetgeo.2016.07.009

Crossley, R., 1984. Controls of sedimentation in the Malawi Rift Valley, Central Africa. Sedimentary Geology 40 (1-3), 33-50. https://doi.org/10.1016/0037-0738(84)90039-4

de Carvalho, M.D., Praça, U.M., da Silva-Telles, A.C., 2000. Bioclastic carbonate lacustrine facies models in the Campos Basin (Lower Cretaceous), Brazil. In: Gierlowski-Kordesch, E.H., Kelts, K.R. (Eds.), Lake Basins through Space and Time. AAPG Studies in Geology 46, pp. 245-256. https://doi.org/10.1306/St46706C19

Dean, W.E., 1981. Carbonate minerals and organic matter in sediments of modern north temperate hard-water lakes. In: Ethridge, F.G., Flores, R.M. (Eds.), Recent and Ancient Nonmarine Depositional Environments. SEPM Special Publication 31, pp. 213-231. https://doi.org/10.2110/pec.81.31.0213

Demaison, G.J., Moore, G.T., 1980. Anoxic environments and oil source bed genesis. Organic Geochemistry 2 (1), 9-31. https://doi.org/10.1016/0146-6380(80)90017-0

Dias, J.L., Scarton, J.C., Esteves, F.R., Carminatti, M., Guardado, L.R., 1990. Aspectos da evolução tectono-sedimentar e a ocorrência de hidrocarbonetos na Bacia de Campos. In: Raja Gabaglia, G.P., Milani, E.J. (Eds.), Origem e Evolução de Bacias Sedimentares. Petrobras, Rio de Janeiro, pp. 333-360.

Erba, E., Duncan, R.A., Bottini, C., Tiraboschi, D., Weissert, H., Jenkyns, H.C., Malinverno, A., 2015. Environmental consequences of Ontong Java Plateau and Kerguelen Plateau volcanism. In: Neal, C.R., Sager, W.W., Sano, T., Erba, E. (Eds.), The Origin, Evolution and Environmental Impact of Oceanic Large Igneous Provinces. Geological Society of America Special Paper 511, pp. 271-303. https://doi.org/10.1130/2015.2511(14)

Espitalié, J., Lamoureux-Var, V., Bouton, N., 2023. Characterization of sulfur compounds. In: Baudin, F. (Ed.), The Rock-Eval Method: Principles and Applications. Wiley, Hoboken, pp. 125-152.

Glenn, C.R., Kelts, K., 1991. Sedimentary rhythms in lake deposits. In: Einsele, G., Ricken, W., Seilacher, A. (Eds.), Cycles and Events in Stratigraphy. Springer-Verlag, Berlin, pp. 188-221.

Goldberg, K., Kuchle, J., Scherer, C., Alvarenga, R., Ene, P.L., Armelenti, G., De Ros, L.F., 2017. Re-sedimented deposits in the rift section of the Campos Basin. Marine and Petroleum Geology 80, 412-431. https://doi.org/10.1016/j.marpetgeo.2016.11.022

Gonçalves, F.T.T., 2002. Organic and isotope geochemistry of the Early Cretaceous rift sequence in the Camamu Basin, Brazil: paleolimnological inferences and source rock models. Organic Geochemistry 33 (1), 67-80. https://doi.org/10.1016/S0146-6380(01)00136-4

Guardado, L.R., Spadini, A.R., Brandão, J.S.L., Mello, M.R., 2000. Petroleum system of the Campos Basin, Brazil. In: Mello, M.R., Katz, B.J. (Eds.), Petroleum Systems of South Atlantic Margins. AAPG Memoir 73, pp. 317-324. https://doi.org/10.1306/M73705C22

Hardie, L.A., Eugster, H.P., 1970. The evolution of closed-basin brines. Mineralogical Society of America Special Paper 3, 273-290.

Harris, N.B., Freeman, K.H., Pancost, R.D., White, T.S., Mitchell, G.D., 2004. The character and origin of lacustrine source rocks in the Lower Cretaceous synrift section, Congo Basin, west Africa. AAPG Bulletin 88 (8), 1163-1184. https://doi.org/10.1306/02260403069

Herlinger Jr., R., Zambonato, E.E., De Ros, L.F., 2017. Influence of diagenesis on the quality of Lower Cretaceous pre-salt lacustrine carbonate reservoirs from northern Campos Basin, offshore Brazil. Journal of Sedimentary Research 87 (12), 1285-1313. https://doi.org/10.2110/jsr.2017.70

Hildred, G.V., Ratcliffe, K.T., Wright, A.M., Zaitlin, B.A., Wray, D.S., 2010. Chemostratigraphic applications to low-accommodation fluvial incised-valley settings: An example from the Lower Mannville Formation of Alberta, Canada. Journal of Sedimentary Research 80 (11-12), 1032-1045. https://doi.org/10.2110/jsr.2010.089

Jenkyns, H.C., 2010. Geochemistry of oceanic anoxic events. Geochemistry, Geophysics, Geosystems 11 (3), Q03004. https://doi.org/10.1029/2009GC002788

Katz, B.J., 1990. Lacustrine Basin Exploration---Case Studies and Modern Analogues. AAPG Memoir 50, Tulsa, Oklahoma, 340 pp.

Kelts, K., 1988. Environments of deposition of lacustrine petroleum source rocks: An introduction. In: Fleet, A.J., Kelts, K., Talbot, M.R. (Eds.), Lacustrine Petroleum Source Rocks. Geological Society Special Publication 40, pp. 3-26. https://doi.org/10.1144/GSL.SP.1988.040.01.02

Lamoureux-Var, V., Espitalié, J., Pillot, D., Bouton, N., Garcia, B., Antonas, R., Aboussou, A., Wattripont, A., Ravelojaona, H., Noirez, S., Beaumont, V., 2019. Rock-Eval 7S: Technology and performance. In: 29th International Meeting on Organic Geochemistry (IMOG), Gothenburg, Sweden, 1-6 September 2019.

Likens, G.E., 1975. Primary production of inland aquatic ecosystems. In: Lieth, H., Whittaker, R.H. (Eds.), Primary Productivity of the Biosphere. Springer-Verlag, New York, pp. 185-202. https://doi.org/10.1007/978-3-642-80913-2_9

Lima, B.E.M., De Ros, L.F., 2019. Deposition, diagenetic and hydrothermal processes in the Aptian Pre-Salt lacustrine carbonate reservoirs of the northern Campos Basin, offshore Brazil. Sedimentary Geology 383, 55-81. https://doi.org/10.1016/j.sedgeo.2019.01.006

Mello, M.R., Telnaes, N., Gaglianone, P.C., Chicarelli, M.I., Brassell, S.C., Maxwell, J.R., 1988. Organic geochemical characterisation of depositional palaeoenvironments of source rocks and oils in Brazilian marginal basins. Organic Geochemistry 13 (1-3), 31-45. https://doi.org/10.1016/0146-6380(88)90023-X

Mizuno, T.A., Mizusaki, A.M.P., Lykawka, R., 2018. Facies and paleoenvironments of the Coqueiros Formation (Lower Cretaceous, Campos Basin): A high frequency stratigraphic model to support pre-salt "coquinas" reservoir development in the Brazilian continental margin. Journal of South American Earth Sciences 88, 107-117. https://doi.org/10.1016/j.jsames.2018.07.007

Mohriak, W.U., Mello, M.R., Dewey, J.F., Maxwell, J.R., 1990. Petroleum geology of the Campos Basin, offshore Brazil. In: Brooks, J. (Ed.), Classic Petroleum Provinces. Geological Society Special Publication 50, pp. 119-141. https://doi.org/10.1144/GSL.SP.1990.050.01.07

Moreira, J.L.P., Madeira, C.V., Gil, J.A., Machado, M.A.P., 2007. Bacia de Santos. Boletim de Geociências da Petrobras 15 (2), 531-549.

Nadoll, P., Angerer, T., Mauk, J.L., French, D., Walshe, J., 2014. The chemistry of hydrothermal magnetite: A review. Ore Geology Reviews 61, 1-32. https://doi.org/10.1016/j.oregeorev.2013.12.013

Nance, H.S., Rowe, H., 2015. Eustatic controls on stratigraphy, chemostratigraphy, and water mass evolution preserved in a Lower Permian mudrock succession, Delaware Basin, west Texas, USA. Interpretation 3 (1), SH11-SH25. https://doi.org/10.1190/INT-2014-0207.1

Negri, A., Ferretti, A., Wagner, T., Meyers, P.A., 2009. Organic-carbon-rich sediments through the Phanerozoic: Processes, progress, and perspectives. Palaeogeography, Palaeoclimatology, Palaeoecology 273 (3-4), 213-217. https://doi.org/10.1016/j.palaeo.2008.11.016

Nichols, G.J., 1987. Structural controls on fluvial distributary systems---the Luna system, northern Spain. In: Ethridge, F.G., Flores, R.M., Harvey, M.D. (Eds.), Recent Developments in Fluvial Sedimentology. SEPM Special Publication 39, pp. 269-277. https://doi.org/10.2110/pec.87.39.0269

Pearce, T.J., Besly, B.M., Wray, D.S., Wright, D.K., 1999. Chemostratigraphy: A method to improve interwell correlation in barren sequences---a case study using onshore Duckmantian/Stephanian sequences (West Midlands, U.K.). Sedimentary Geology 124 (1-4), 197-220. https://doi.org/10.1016/S0037-0738(98)00128-6

Pearce, T.J., Jarvis, I., 1992. Applications of geochemical data to modelling sediment dispersal patterns in distal turbidites: Late Quaternary of the Madeira Abyssal Plain. Journal of Sedimentary Petrology 62 (6), 1112-1129. https://doi.org/10.1306/D4267A64-2B26-11D7-8648000102C1865D

Penteado, H.L.B., Vieira, A.J.M., Spigolon, A.L.D., Dias, A.E.S., Araujo, C.V., Fracalossi, C.P., Caetano, C.M., Lima, C.D.F.M., Silva, C.F., Morais, E.T., Santos Neto, E.V., Lopes, J.P., Iemini, J.A., Silva, K.M.S., Araújo, L.M., Reis, M.A.A.A., Dehler, N.M., Espósito, R.O., Menezes, T.R., Pinto, V.H.G., Rocha, Y.S., 2024. Geração, migração e caracterização do petróleo do Pré-sal da Bacia de Santos. In: As grandes descobertas do Pré-sal no Atlântico Sul, Capítulo 10. Petrobras, Rio de Janeiro.

Pereira, M.J., Feijó, F.J., 1994. Bacia de Santos. Boletim de Geociências da Petrobras 8 (1), 219-234.

Peters, K.E., Cassa, M.R., 1994. Applied source rock geochemistry. In: Magoon, L.B., Dow, W.G. (Eds.), The Petroleum System---From Source to Trap. AAPG Memoir 60, pp. 93-120.

Pettijohn, F.J., 1975. Sedimentary Rocks, third edition. Harper & Row, New York, 628 pp.

Pietzsch, R., Oliveira, D.M., Tedeschi, L.R., Queiroz Neto, J.V., Figueiredo, M.F., Vazquez, J.C., de Souza, R.S., 2018. Palaeohydrology of the Lower Cretaceous pre-salt lacustrine system, from rift to post-rift phase, Santos Basin, Brazil. Palaeogeography, Palaeoclimatology, Palaeoecology 507, 60-80. https://doi.org/10.1016/j.palaeo.2018.06.043

Pietzsch, R., Tedeschi, L.R., Oliveira, D.M., dos Anjos, C.W.D., Vazquez, J.C., Figueiredo, M.F., 2020. Environmental conditions of deposition of the Lower Cretaceous lacustrine carbonates of the Barra Velha Formation, Santos Basin (Brazil), based on stable carbon and oxygen isotopes: A continental record of pCO_2 during the onset of the Oceanic Anoxic Event

1a (OAE 1a) interval? Chemical Geology 535, 119457. https://doi.org/10.1016/j.chemgeo.2019.119457

Pizarro, V.H., Perosi, F.A., Borghi, L., Fetter, M., 2025. Seismic stratigraphic analysis of the pre-salt of Berbigão, Sururu, and Atapu fields, Santos Basin, Brazil. Marine and Petroleum Geology 140, 107529. https://doi.org/10.1016/j.marpetgeo.2025.107529

Rahman, H.M., Kennedy, M., Löhr, S., Dewhurst, D.N., 2017. Clay-organic association as a control on hydrocarbon generation in shale. Organic Geochemistry 105, 42-55. https://doi.org/10.1016/j.orggeochem.2017.01.011

Rahman, H.M., Kennedy, M., Löhr, S., Dewhurst, D.N., Sherwood, N., Yang, S., Horsfield, B., 2018. The influence of shale depositional fabric on the kinetics of hydrocarbon generation through control of mineral surface contact area on clay catalysis. Geochimica et Cosmochimica Acta 220, 429-448. https://doi.org/10.1016/j.gca.2017.10.012

Rameil, N., 2008. Early diagenetic dolomitization and dedolomitization of Late Jurassic and earliest Cretaceous platform carbonates: A case study from the Jura Mountains (NW Switzerland, E France). Sedimentary Geology 212 (1-4), 70-85. https://doi.org/10.1016/j.sedgeo.2008.10.004

Ratcliffe, K.T., Wright, A.M., Montgomery, P., Palfrey, A., Vonk, A., Vermeulen, J., Barrett, M., 2010. Application of chemostratigraphy to the Mungaroo Formation, the Gorgon field, offshore northwest Australia. The APPEA Journal 50 (1), 371-385. https://doi.org/10.1071/AJ09022

Remírez, M.N., Dacal, A.G., Orzanco, J., 2022. Controls on the accumulation of Early Cretaceous organic-rich fine-grained deposits in a mixed marine siliciclastic-carbonate distal settings of the Neuquén Basin, central-western Argentina. Marine and Petroleum Geology 146, 105962. https://doi.org/10.1016/j.marpetgeo.2022.105962

Sano, J.L., Ratcliffe, K.T., Spain, D.R., 2013. Chemostratigraphy of the Haynesville Shale. In: Hammes, U., Gale, J. (Eds.), Geology of the Haynesville Gas Shale in East Texas and West Louisiana. AAPG Memoir 105, pp. 137-154. https://doi.org/10.1306/13441847M1053602

Sebag, D., Disnar, J.-R., Guillet, B., Di Giovanni, C., Verrecchia, E.P., Durand, A., 2006. Monitoring organic matter dynamics in soil profiles by "Rock-Eval pyrolysis": Bulk characterization and quantification of degradation. European Journal of Soil Science 57 (3), 344-355. https://doi.org/10.1111/j.1365-2389.2005.00745.x

Silva-Telles Jr., A.C., Viana, A.R., Mizusaki, A.M.P., Winter, W.R., 1994. Evidences of the first marine ingressions during the East Brazilian margin rift phase. Boletim de Geociências da Petrobras 8 (2-4), 263-279.

Sladen, C.P., 1994. Key elements during the search for hydrocarbons in lake systems. In: Gierlowski-Kordesch, E., Kelts, K. (Eds.), Global Geological Record of Lake Basins, Volume 1. Cambridge University Press, Cambridge, pp. 3-17.

Soreghan, M.J., Cohen, A.S., 1996. Textural and compositional variability across littoral segments of Lake Tanganyika: The effect of asymmetric basin structure on sedimentation in

large rift lakes. AAPG Bulletin 80 (3), 382-409. https://doi.org/10.1306/64ED87F0-1724-11D7-8645000102C1865D

Talbot, M.R., Kelts, K., 1986. Primary and diagenetic carbonates in the anoxic sediments of Lake Bosumtwi, Ghana. Geology 14 (11), 912-916. https://doi.org/10.1130/0091-7613(1986)14<912:PADCIT>2.0.CO;2

Taylor, S.R., McLennan, S.M., 1985. The Continental Crust: Its Composition and Evolution. Blackwell Scientific Publications, Oxford, 312 pp.

Thompson, D.L., Stilwell, J.D., Hall, M., 2015. Lacustrine carbonate reservoirs from Early Cretaceous rift lakes of Western Gondwana: Pre-Salt coquinas of Brazil and West Africa. Gondwana Research 28 (1), 26-51. https://doi.org/10.1016/j.gr.2014.12.005

Tribovillard, N., Algeo, T.J., Lyons, T., Riboulleau, A., 2006. Trace metals as paleoredox and paleoproductivity proxies: An update. Chemical Geology 232 (1-2), 12-32. https://doi.org/10.1016/j.chemgeo.2006.02.012

Tribovillard, N., Bout-Roumazeilles, V., Algeo, T., Lyons, T.W., Sionneau, T., Montero-Serrano, J.C., Baudin, F., 2008. Paleodepositional conditions in the Orca Basin as inferred from organic matter and trace metal contents. Marine Geology 254 (1-2), 62-72. https://doi.org/10.1016/j.margeo.2008.04.016

Turgeon, S., Brumsack, H.-J., 2006. Anoxic vs dysoxic events reflected in sediment geochemistry during the Cenomanian-Turonian Boundary Event (Cretaceous) in the Umbria-Marche Basin of central Italy. Chemical Geology 234 (3-4), 321-339. https://doi.org/10.1016/j.chemgeo.2006.05.008

Turner, B.W., Tréanton, J.A., Slatt, R.M., 2016. The use of chemostratigraphy to refine ambiguous sequence stratigraphic correlations in marine mudrocks. An example from the Woodford Shale, Oklahoma, USA. Journal of the Geological Society 173 (5), 854-868. https://doi.org/10.1144/jgs2015-125

Tyson, R.V., 2001. Sedimentation rate, dilution, preservation and total organic carbon: some results of a modelling study. Organic Geochemistry 32 (2), 333-339. https://doi.org/10.1016/S0146-6380(00)00161-3

Vielma, A., Curiale, J.A., Carvajal-Ortiz, H., Radović, J.R., Fu, Q., Malloy, T.B., Bissada, K.K., 2024. Paleoredox and lithofacies assessments in deepwater intervals of the Monterey Formation, Santa Maria Basin, California: Insights from organic sulfur geochemistry. International Journal of Coal Geology 294, 104606. https://doi.org/10.1016/j.coal.2024.104606

Vital, J.C.S., Lupinacci, W.M., 2023. Compartmentalization and stratigraphic-structural trapping in pre-salt carbonate reservoirs of the Santos Basin: A case study in the Iara complex. Marine and Petroleum Geology 151, 106163. https://doi.org/10.1016/j.marpetgeo.2023.106163

Winter, W.R., Jahnert, R.J., França, A.B., 2007. Bacia de Campos. Boletim de Geociências da Petrobras 15 (2), 511-529.

Wright, A.M., Ratcliffe, K.T., Zaitlin, B.A., Wray, D.S., 2015. The application of chemostratigraphic techniques to distinguish compound incised valleys in low-accommodation

incised-valley systems in a foreland-basin setting: An example from the Lower Cretaceous Mannville Group and Basal Colorado Sandstone (Colorado Group), Western Canadian Sedimentary Basin. In: Armitage, P.J., Butcher, A.R., Churchill, J.M., Csoma, A.E., Hollis, C., Lander, R.H., Omma, J.E., Worden, R.H. (Eds.), Reservoir Quality of Clastic and Carbonate Rocks: Analysis, Modelling and Prediction. Geological Society Special Publication 435, pp. 93-110. https://doi.org/10.1144/SP435.21

Zuo, G., Wang, H., Fan, G., Zhang, J., Zhang, Y., Wang, C., Zuo, Y., 2022. Geochemical characteristics and distribution of the subsalt source rocks in the Santos Basin, Brazil. ACS Omega 7 (29), 25715-25725. https://doi.org/10.1021/acsomega.2c03018

Supplementary Material

Table S1- Geochemical composition of samples from the Campos Basin (BC) and Santos Basin (BS) pre-salt sequences, showing organic and inorganic carbon content, sulfur speciation, major oxide concentrations (%), and trace element distributions (ppm) across different formations. Dash symbols (-) indicate values below detection limit or not determined.

Well	Depth (m)	Fm.[a]	TOC (%)	MinC (%)	S Org (%)	Pyro Fe S (%)	TSFeS (%)	Sulf. S (%)	Tot. S (%)	SiO_2 (%)	Al_2O_3 (%)	Fe_2O_3 (%)	MnO (%)	MgO (%)	CaO (%)	Na_2O (%)	K_2O (%)	TiO_2 (%)	Ni (ppm)	Cu (ppm)	Zn (ppm)	Rb (ppm)	Zr (ppm)
BC-BR1	5223	Coq	4.2	7.1	0.017	0.005	0.02	2.3	2.4	33.5	5.8	9.2	0.3	5.4	34.8	0.8	2.4	0.93	32	133	171	67	177
BC-BR1	5247	Coq	4.9	6.5	0.025	0.008	0.03	3.3	3.4	35.6	5.5	8.3	0.3	5.4	32.5	0.7	2.8	0.74	26	142	184	67	154
BC-BR1	5277	Coq	3.7	7.5	0.011	0.006	0.05	2.6	2.7	33.3	5.2	7.6	0.3	6.4	35.0	0.8	2.7	0.75	29	113	207	66	164
BC-BR1	5304	Coq	4.4	9.3	0.011	0.004	0.04	2.7	2.8	31.2	5.0	7.7	0.3	6.3	36.2	0.6	2.5	0.68	14	112	149	66	160
BC-BR1	5331	Coq	5.1	9.4	0.011	0.006	0.1	5.1	5.3	35.2	6.3	8.6	0.3	6.0	32.5	0.7	3.0	0.8	33	118	148	75	184
BC-BR1	5358	Coq	3.4	9.6	0.005	0.007	0.12	4.7	4.9	34.1	5.4	8.2	0.2	6.6	34.8	0.6	2.7	0.67	20	107	176	73	183
BC-BR1	5385	Coq	2.1	4.7	0.005	0.003	0.01	1.2	1.2	36.4	6.4	7.6	0.3	8.6	36.9	1.1	2.9	0.74	22	100	124	72	183
BC-BR1	5412	Coq	2.0	3.4	0.005	0.005	0.03	1.2	1.2	40.9	7.7	10.4	0.2	8.7	30.3	1.5	2.5	0.83	99	112	153	67	172
BC-BR1	5439	Ataf	2.2	3.0	0.005	0.004	0.3	0.5	1.1	46.9	6.4	9.2	0.1	12.7	21.1	1.5	1.9	0.8	82	95	160	68	192
BC-BR1	5466	Ataf	1.9	2.9	0.004	0.006	0.55	0.1	1.1	45.5	5.6	8.2	0.1	12.1	24.5	1.4	1.5	0.71	49	81	189	57	178
BC-BR1	5496	Ataf	2.0	2.9	0.003	0.006	0.06	0.8	0.9	50.0	7.1	9.2	0.1	11.0	19.7	1.7	2.6	0.88	60	98	127	88	248
BC-BR1	5520	Ataf	1.8	2.8	0.002	0.002	0.01	0.6	0.6	46.9	6.9	8.1	0.1	11.1	21.9	1.6	2.4	0.84	58	94	115	86	246
BC-BR1	5547	Ataf	1.1	2.1	0.001	0.001	0.07	0.4	0.5	51.1	6.1	7.7	0.1	13.7	17.1	1.7	1.8	0.71	47	81	99	66	197
BC-BR1	5577	Ataf	1.6	2.3	0.002	0.002	0.14	0.5	0.8	49.6	7.2	9.7	0.1	11.7	20.9	1.7	2.0	0.78	98	96	203	63	191
BC-BR2	6220	Coq	3.9	4.5	0.007	0.007	0.06	1.6	1.8	36.3	7.4	8.6	0.2	7.3	35.4	0.8	3.0	0.85	22	186	122	107	186
BC-BR2	6247	Coq	3.6	5.2	0.008	0.011	0.1	1.3	1.4	32.2	6.5	7.1	0.2	6.4	37.4	0.9	3.8	0.86	21	174	143	97	186
BC-BR2	6274	Coq	3.3	6.1	0.011	0.042	0.15	1.5	1.7	29.3	4.7	5.5	0.2	8.0	40.8	0.0	3.6	0.66	3	119	82	78	151
BC-BR2	6301	Coq	4.4	4.1	0.014	0.034	0.23	2.3	2.6	40.9	7.3	8.3	0.2	6.3	31.2	0.6	4.3	0.8	25	159	104	109	191
BC-BR2	6328	Coq	5.1	5.9	0.009	0.013	0.08	0.9	1.1	29.3	6.6	6.5	0.3	4.0	45.0	1.1	2.4	0.88	27	106	81	99	212
BC-BR2	6355	Coq	4.3	6.0	0.005	0.009	0.32	0.6	1.2	36.8	6.2	6.8	0.2	9.9	32.8	0.8	2.5	0.8	37	111	83	96	208
BC-BR2	6382	Coq	4.9	5.2	0.008	0.006	0.07	1.2	1.4	32.5	5.7	7.7	0.2	8.2	36.6	0.6	2.8	0.77	28	119	82	92	195
BC-BR3	5324	Coq	4.2	6.8	0.013	0.006	0.11	0.7	1.0	21.4	2.3	3.4	0.2	10.1	50.7	0.0	0.9	0.36	10	68	195	50	133

BC-BR3	5339	Coq	5.3	4.1	0.019	0.007	0.12	0.7	1.2	38.0	5.1	6.0	0.2	10.8	30.0	0.2	2.3	0.71	19	104	271	92	235
BC-BR3	5372	Coq	3.2	6.1	0.015	0.006	0.31	0.4	1.2	40.2	6.4	8.8	0.2	7.4	32.0	0.3	2.6	0.66	144	339	850	89	188
BC-BR3	5405	Coq	3.4	5.4	0.010	0.004	0.11	1.0	1.4	38.4	4.3	8.1	0.2	7.8	36.4	0.3	1.7	0.54	99	221	960	64	190
BC-BR3	5414	Coq	3.2	9.8	0.015	0.007	0.5	0.0	1.5	34.6	4.9	8.1	0.2	6.6	37.6	0.3	2.7	0.64	318	193	959	80	211
BC-BR3	5444	Coq	2.7	7.0	0.007	0.003	0.1	0.9	1.2	35.4	4.4	6.9	0.2	8.1	39.7	0.2	2.2	0.54	57	175	921	59	188
BC-BR3	5477	Ataf	2.8	4.7	0.013	0.012	0.1	1.4	1.6	36.1	7.6	10.7	0.2	6.8	34.2	0.5	3.8	1.12	83	172	806	81	161
BC-BR3	5495	Ataf	1.5	2.7	0.010	0.011	0.48	0.5	1.5	39.2	10.5	15.1	0.2	6.6	24.3	1.2	4.1	1.61	67	242	261	79	197
BC-BR3	5515	Ataf	1.9	3.1	0.009	0.013	0.96	0.1	1.7	39.4	10.7	13.8	0.2	6.9	25.2	0.8	5.1	1.52	55	225	352	82	167
BC-BR3	5528	Ataf	1.5	3.2	0.004	0.159	0.98	1.2	2.2	44.0	12.4	13.9	0.2	7.0	21.5	1.3	5.5	1.64	68	199	230	77	185
BC-BR3	5555	Ataf	1.1	2.6	0.015	0.187	0.96	1.4	2.4	44.1	12.4	13.7	0.2	7.9	18.2	0.7	8.4	1.66	67	164	99	92	165
BS-BR1	5640	Itap	4.5	8.6	0.007	0.005	0.01	0.3	0.3	10.2	1.6	2.7	0.1	3.7	67.1	0.6	1.6	0.39	-	31	139	44	102
BS-BR1	5667	Itap	4.6	8.5	0.006	0.005	0.01	0.3	0.3	11.4	1.2	2.1	0.2	4.1	67.8	0.3	1.0	0.26	-	41	154	35	85
BS-BR1	5694	Itap	4.1	9.5	0.004	0.002	0	0.2	0.2	6.4	0.8	1.6	0.1	2.6	77.1	0.3	0.6	0.18	-	-	182	19	59
BS-BR1	5721	Itap	4.0	7.3	0.005	0.004	0.01	0.7	0.7	17.8	3.1	3.6	0.2	5.5	58.5	0.5	2.8	0.6	-	48	190	64	167
BS-BR1	5748	Itap	5.2	8.2	0.006	0.005	0.01	0.4	0.4	11.8	1.8	2.9	0.2	6.2	62.8	0.0	1.7	0.41	-	29	216	39	108
BS-BR1	5775	Itap	4.5	8.7	0.005	0.004	0.01	0.3	0.3	9.5	1.5	2.2	0.1	5.7	69.5	0.0	1.5	0.37	-	37	132	32	100
BS-BR1	5802	Itap	4.0	9.6	0.008	0.003	0.01	0.5	0.5	9.4	1.5	2.3	0.1	4.7	71.8	0.2	1.3	0.34	-	34	132	32	84
BS-BR1	5829	Itap	4.9	9.6	0.006	0.001	0	0.5	0.5	8.8	1.4	2.4	0.1	4.7	68.9	0.0	1.3	0.35	-	36	116	35	95
BS-BR1	5856	Itap	6.1	7.6	0.008	0.004	0.01	0.6	0.6	17.0	3.1	4.9	0.1	5.7	57.5	0.2	2.7	0.82	44	62	174	62	158
BS-BR1	5883	Itap	4.5	8.6	0.006	0.005	0.01	0.3	0.3	14.5	2.3	3.2	0.1	6.9	63.5	0.4	1.6	0.35		43	129	41	123
BS-BR1	5910	Itap	6.8	6.8	0.018	0.003	0.01	0.9	1.0	18.5	3.4	6.4	0.1	5.0	50.1	0.5	2.9	1.08	38	89	220	68	210
BS-BR1	5937	Itap	5.3	6.7	0.015	0.006	0.01	0.9	0.9	20.7	4.4	7.1	0.1	5.8	51.7	0.7	2.9	1.08	69	106	214	62	205
BS-BR1	5964	Itap	6.8	7.1	0.038	0.006	0.01	0.8	0.9	17.9	2.9	3.9	0.2	6.7	56.1	0.0	2.2	0.56	9	53	245	51	126
BS-BR1	5991	Itap	7.0	6.7	0.036	0.009	0.03	1.2	1.3	20.4	3.3	4.9	0.2	6.7	51.9	0.4	2.3	0.79	49	64	184	67	173
BS-BR1	6018	Piça	6.2	6.5	0.025	0.009	0.03	1.1	1.1	19.7	3.3	4.5	0.2	6.3	54.0	0.4	2.8	0.74	35	51	119	67	175
BS-BR1	6045	Piça	5.8	5.2	0.020	0.019	0.05	1.4	1.5	29.5	5.3	7.0	0.2	6.0	42.2	0.4	3.8	1.18	102	93	158	89	258

BS-BR1	6072	Piça	3.7	7.8	0.007	0.007	0.02	0.5	0.5	18.3	3.0	4.0	0.2	4.5	62.0	0.0	1.9	0.68	7	50	94	57	164
BS-BR1	6099	Piça	4.6	6.5	0.015	0.025	0.06	1.3	1.4	25.1	3.7	5.2	0.2	8.9	47.6	0.4	2.5	0.79	30	64	165	64	166

Abbreviations: TOC = Total Organic Carbon; MinC = Mineral Carbon; S Org = Organic Sulfur; Pyro Fe S = Pyritic Sulfur; TSFeS = Total Iron Sulfides; Sulf. S = Sulfate Sulfur; Tot. S = Total Sulfur. [a]Formations: Coq = Coqueiros; Ataf = Atafona; Itap = Itapema; Piça = Piçarras.

Table S2- Mineralogical composition of samples from the Campos Basin (BC) and Santos Basin (BS) pre-salt sequences determined by X-ray diffraction (XRD). Mineral phases are listed in order of relative abundance within each sample across different formations and depths. [a]Dominant (> 50%); [b]Major (20–50%); [c]Minor (5–20%); [d]Trace (< 5%).

Well	Depth (m)	Fm[a]	Mineralogy Components
BC-BR1	5223	Coq	Calcite[b], Quartz[b], K-feldspar[b], Dolomite[c], Plagioclase[c], Clay[c], Mica[d], Barite[d], Pyrite[d], Gypsum[d]
BC-BR1	5247	Coq	Quartz[b], K-feldspar[b], Calcite[c], Dolomite[c], Plagioclase[d], Clay[d], Mica[d], Barite[d], Pyrite[d], Gypsum[d]
BC-BR1	5277	Coq	Quartz[b], K-feldspar[b], Calcite[c], Dolomite[c], Plagioclase[c], Clay[d], Mica[d], Barite[d], Pyrite[d], Gypsum[d]
BC-BR1	5304	Coq	Calcite[b], Dolomite[b], Quartz[b], K-feldspar[c], Plagioclase[d], Clay[d], Mica[d], Barite[d], Pyrite[d], Gypsum[d]
BC-BR1	5331	Coq	Dolomite[b], Quartz[b], K-feldspar[b], Calcite[c], Plagioclase[c], Clay[d], Mica[d], Barite[d], Pyrite[d], Gypsum[d], Pyroxene[d]
BC-BR1	5358	Coq	Dolomite[b], Quartz[b], Calcite[c], K-feldspar[c], Plagioclase[d], Mica[d], Barite[d], Pyrite[d], Gypsum[d], Pyroxene[d]
BC-BR1	5385	Coq	Calcite[b], Dolomite[b], Quartz[b], K-feldspar[c], Mica[c], Plagioclase[d], Clay[d], Barite[d], Pyrite[d], Gypsum[d], Pyroxene[d]
BC-BR1	5412	Coq	Calcite[b], Quartz[b], Dolomite[c], K-feldspar[c], Clay[c], Mica[c], Plagioclase[d], Barite[d], Pyrite[d], Gypsum[d], Pyroxene[d]
BC-BR1	5439	Ataf	Quartz[b], K-feldspar[b], Calcite[c], Dolomite[c], Plagioclase[c], Mica[c], Clay[d], Barite[d], Pyrite[d], Gypsum[d], Pyroxene[d], Anhydrite[d]
BC-BR1	5466	Ataf	Quartz[b], Calcite[c], Dolomite[c], K-feldspar[c], Plagioclase[c], Clay[c], Mica[c], Barite[d], Pyrite[d], Gypsum[d]
BC-BR1	5496	Ataf	Quartz[b], Calcite[c], Dolomite[c], K-feldspar[c], Plagioclase[c], Clay[c], Mica[c], Pyroxene[c], Barite[d], Pyrite[d], Gypsum[d], Anhydrite[d]
BC-BR1	5520	Ataf	Quartz[b], Calcite[c], Dolomite[c], K-feldspar[c], Plagioclase[c], Mica[c], Clay[d], Barite[d], Pyrite[d], Gypsum[d], Pyroxene[d], Anhydrite[d]
BC-BR1	5547	Ataf	Quartz[b], Mica[b], Calcite[c], Dolomite[c], K-feldspar[c], Plagioclase[c], Clay[d], Barite[d], Pyrite[d], Gypsum[d], Pyroxene[d]
BC-BR1	5577	Ataf	Quartz[b], Calcite[c], Dolomite[c], K-feldspar[c], Plagioclase[c], Mica[c], Clay[d], Barite[d], Pyrite[d], Gypsum[d], Pyroxene[d]
BC-BR2	6220	Coq	Calcite[b], Dolomite[c], Quartz[c], K-feldspar[c], Plagioclase[c], Clay[c], Mica[d], Barite[d], Pyrite[d], Gypsum[d], Halite[d]
BC-BR2	6247	Coq	Dolomite[b], Calcite[b], Quartz[c], K-feldspar[c], Plagioclase[c], Clay[d], Mica[d], Barite[d], Pyrite[d], Gypsum[d], Anhydrite[d], Halite[d]
BC-BR2	6274	Coq	Dolomite[b], Quartz[b], Calcite[c], K-feldspar[c], Plagioclase[d], Clay[d], Mica[d], Barite[d], Pyrite[d], Gypsum[d], Anhydrite[d], Halite[d]
BC-BR2	6301	Coq	Calcite[b], Dolomite[b], Quartz[b], K-feldspar[c], Barite[c], Plagioclase[d], Clay[d], Mica[d], Pyrite[d], Gypsum[d], Pyroxene[d], Anhydrite[d], Halite[d]
BC-BR2	6328	Coq	Calcite[b], Dolomite[c], Quartz[c], K-feldspar[c], Plagioclase[c], Clay[d], Mica[d], Barite[d], Pyrite[d], Gypsum[d], Anhydrite[d], Halite[d]
BC-BR2	6355	Coq	Calcite[b], Dolomite[c], Quartz[c], K-feldspar[c], Plagioclase[c], Clay[c], Mica[d], Barite[d], Pyrite[d], Gypsum[d], Anhydrite[d], Halite[d]
BC-BR2	6382	Coq	Calcite[b], Dolomite[b], Quartz[c], K-feldspar[c], Plagioclase[c], Clay[d], Mica[d], Barite[d], Pyrite[d], Gypsum[d], Anhydrite[d], Halite[d]
BC-BR3	5324	Coq	Calcite[b], Dolomite[b], Quartz[c], K-feldspar[d], Plagioclase[d], Clay[d], Mica[d], Barite[d], Pyrite[d], Gypsum[d], Anhydrite[d], Halite[d]
BC-BR3	5339	Coq	Calcite[b], Quartz[b], Dolomite[c], Clay[c], K-feldspar[d], Plagioclase[d], Mica[d], Barite[d], Pyrite[d], Gypsum[d], Anhydrite[d], Halite[d]
BC-BR3	5372	Coq	Calcite[b], Quartz[b], Dolomite[c], K-feldspar[c], Clay[c], Plagioclase[d], Mica[d], Barite[d], Pyrite[d], Gypsum[d], Anhydrite[d], Halite[d]
BC-BR3	5405	Coq	Calcite[b], Quartz[b], Dolomite[c], K-feldspar[c], Plagioclase[d], Clay[d], Mica[d], Barite[d], Pyrite[d], Gypsum[d], Anhydrite[d], Halite[d]
BC-BR3	5414	Coq	Calcite[b], Quartz[b], Dolomite[c], K-feldspar[c], Plagioclase[c], Clay[d], Mica[d], Barite[d], Pyrite[d], Gypsum[d], Anhydrite[d], Halite[d]
BC-BR3	5444	Coq	Calcite[b], Quartz[b], Dolomite[c], K-feldspar[d], Plagioclase[d], Clay[d], Mica[d], Barite[d], Pyrite[d], Gypsum[d], Pyroxene[d], Anhydrite[d], Halite[d], Talc[d]
BC-BR3	5477	Ataf	Calcite[b], Quartz[b], Dolomite[c], K-feldspar[c], Clay[c], Plagioclase[d], Mica[d], Barite[d], Pyrite[d], Gypsum[d], Anhydrite[d], Halite[d], Talc[d]
BC-BR3	5495	Ataf	Calcite[b], K-feldspar[b], Dolomite[c], Quartz[c], Plagioclase[c], Clay[c], Pyroxene[c], Mica[d], Barite[d], Pyrite[d], Gypsum[d], Anhydrite[d], Halite[d], Talc[d]

BC-BR3	5515	Ataf	Calcite[b], K-feldspar[b], Dolomite[c], Quartz[c], Plagioclase[c], Clay[c], Mica[d], Barite[d], Pyrite[d], Gypsum[d], Pyroxene[d], Anhydrite[d], Halite[d], Talc[d]
BC-BR3	5528	Ataf	K-feldspar[b], Calcite[c], Quartz[c], Plagioclase[c], Clay[c], Dolomite[d], Mica[d], Barite[d], Pyrite[d], Gypsum[d], Pyroxene[d], Anhydrite[d], Halite[d], Talc[d]
BC-BR3	5555	Ataf	K-feldspar[b], Calcite[c], Dolomite[c], Quartz[c], Plagioclase[c], Clay[c], Mica[d], Barite[d], Pyrite[d], Gypsum[d], Pyroxene[d], Anhydrite[d], Talc[d]
BS-BR1	5640	Itap	Calcite[a], Dolomite[b], Quartz[c], Plagioclase[c], Barite[d], Pyrite[d]
BS-BR1	5667	Itap	Calcite[a], Dolomite[b], Quartz[c], K-feldspar[d], Plagioclase[d], Barite[d], Pyrite[d]
BS-BR1	5694	Itap	Calcite[a], Dolomite[c], Quartz[c], K-feldspar[d], Barite[d], Pyrite[d]
BS-BR1	5721	Itap	Calcite[b], Dolomite[b], Quartz[c], Plagioclase[c], K-feldspar[d], Barite[d], Pyrite[d]
BS-BR1	5748	Itap	Calcite[b], Dolomite[b], Quartz[c], Plagioclase[c], Barite[d], Pyrite[d]
BS-BR1	5775	Itap	Calcite[a], Dolomite[b], Quartz[c], Plagioclase[c], K-feldspar[d], Barite[d], Pyrite[d]
BS-BR1	5802	Itap	Calcite[a], Dolomite[b], Quartz[c], Plagioclase[c], Barite[d], Pyrite[d]
BS-BR1	5829	Itap	Calcite[a], Dolomite[b], Quartz[c], Plagioclase[c], Barite[d], Pyrite[d], Dawsonite[d], Halite[d]
BS-BR1	5856	Itap	Calcite[b], Dolomite[b], Quartz[c], Plagioclase[c], K-feldspar[d], Barite[d], Pyrite[d], Dawsonite[d], Halite[d]
BS-BR1	5883	Itap	Calcite[a], Dolomite[b], Quartz[c], Plagioclase[c], Barite[d], Pyrite[d], Halite[d]
BS-BR1	5910	Itap	Calcite[b], Dolomite[b], Quartz[c], Plagioclase[c], K-feldspar[d], Barite[d], Pyrite[d], Dawsonite[d], Halite[d]
BS-BR1	5937	Itap	Calcite[b], Dolomite[b], Quartz[c], Plagioclase[c], Mica[d], Barite[d], Pyrite[d], Dawsonite[d], Halite[d]
BS-BR1	5964	Itap	Calcite[b], Dolomite[b], Quartz[c], Plagioclase[c], Mica[d], Barite[d], Pyrite[d], Dawsonite[d], Halite[d]
BS-BR1	5991	Itap	Calcite[b], Dolomite[b], Quartz[c], Plagioclase[c], Mica[d], Barite[d], Pyrite[d], Gypsum[d], Halite[d]
BS-BR1	6018	Piça	Calcite[b], Dolomite[b], Quartz[c], Plagioclase[c], Mica[d], Barite[d], Pyrite[d], Gypsum[d], Halite[d]
BS-BR1	6045	Piça	Calcite[b], Plagioclase[b], Dolomite[c], Quartz[c], Clay[c], K-feldspar[d], Mica[d], Barite[d], Pyrite[d], Gypsum[d], Halite[d]
BS-BR1	6072	Piça	Calcite[a], Dolomite[c], Quartz[c], Plagioclase[c], Clay[c], K-feldspar[d], Mica[d], Barite[d], Pyrite[d], Gypsum[d], Halite[d]
BS-BR1	6099	Piça	Calcite[b], Dolomite[b], Quartz[c], Plagioclase[c], Clay[c], K-feldspar[d], Mica[d], Barite[d], Pyrite[d], Gypsum[d], Halite[d]

CHAPTER 3

Controls on organic matter accumulation in pre-salt lacustrine source rocks: Geochemical evidence from the Lagoa Feia Group, Campos Basin, Brazil

Controls on organic matter accumulation in pre-salt lacustrine source rocks: Geochemical evidence from the Lagoa Feia Group, Campos Basin, Brazil

Lara de Paula Cunha Hercolano[1], Rut Díaz[2], Igor Martins Venancio[2], Manuel Moreira-Ramírez[2], Gabriel de Alemar Barberes[1], André Luiz Durante Spigolon[3], Ana Luiza Spadano Albuquerque[1]*

[1] Programa de Pós-Graduação em Dinâmica dos Oceanos e da Terra, Universidade Federal Fluminense, Niterói, 24210346, Brazil
[2] Programa de Geociências (Geoquímica), Universidade Federal Fluminense, Niterói 24020141, Brazil
[3] Centro de Pesquisas da PETROBRAS, Rio de Janeiro, RJ, Brazil

Abstract

The Lagoa Feia Group represents the main source rock interval in the pre-salt petroleum system of the Campos Basin, yet the controls on organic matter accumulation remain incompletely understood. This study presents an integrated geochemical investigation of 80 samples from eight wells, distributed along a proximal-distal paleobathymetric transect, combining Rock-Eval pyrolysis, LECO combustion, and XRF elemental analysis. Total Organic Carbon (TOC) ranges from 0.5% to 7.5% (mean 2.7%), with Type I–II kerogen (Hydrogen Index up to 779 mg HC/g TOC) indicating excellent oil-prone potential. A dual dilution model was identified in which both carbonate excess and siliciclastics can dilute organic matter, depending on the depositional context. Three-component sediment decomposition (Ricken, 1993) quantifies that carbonate dominates mineral dilution in the Macabu (67%) and Coqueiros (58%) formations, while siliciclastic material dominates in the Atafona (56%). When TOC is recalculated on a carbonate-free basis, the three formations converge to ~5–6%, indicating that organic carbon flux was broadly uniform and that the observed twofold variation in TOC is primarily controlled by differential mineral dilution. The Ca-TOC relationship inverts according to paleobathymetric position: negative in proximal and intermediate wells ($\rho = -0.6$ and -0.7), positive in distal wells ($\rho = +0.7$). Within individual formations, paleobathymetry modulates the type of dilution: Coqueiros loses carbonate distally (improving TOC), while Atafona gains siliciclastic (degrading TOC). Relative sedimentation rates derived from the decomposition indicate that the Macabu accumulated sediment at 1.8× the rate of the Atafona, yielding absolute estimates of 7–26 cm/ka comparable to modern eutrophic rift lakes. Vanadium emerges as the most robust redox proxy ($\rho = +0.8$), while Mn concentrations indicate that redox stability controls kerogen quality (HI = 562 for Mn < 0.2% vs 302 mg HC/g TOC for Mn > 0.3%). The proposed hierarchical model provides a predictive framework for source rock assessment in lacustrine pre-salt systems.

Keywords: Pre-salt; Lacustrine source rock; Organic matter preservation; Dual dilution model; Redox proxies; Campos Basin; Lagoa Feia Group; Chemostratigraphy

1. Introduction

Lacustrine rift basins rank among the most prolific settings for petroleum source rock development, hosting some of the highest-quality oil-prone kerogens known in the geological record (Katz, 1995, 2001; Bohacs et al., 2000). The Brazilian pre-salt petroleum system stands as a premier example of this depositional environment, with production currently accounting for over 70% of Brazil's oil output (ANP, 2025). The exceptional productivity of this system derives from Lower Cretaceous lacustrine source rocks deposited during the Barremian–Aptian rift phase of South Atlantic opening (Mello et al., 1988; Guardado et al., 2000). Despite the economic significance of these deposits, the geochemical controls governing organic matter accumulation and preservation in these carbonate-dominated lacustrine systems remain incompletely understood, limiting predictive capability for exploration.

The fundamental controls on organic matter enrichment in lacustrine systems have been extensively debated, with competing models emphasizing productivity, preservation, and dilution as primary factors (Pedersen and Calvert, 1990; Tyson, 2001; Bohacs et al., 2005). Traditional interpretations of carbonate-dominated lacustrine systems have emphasized carbonate dilution as the principal mechanism limiting organic carbon accumulation (Kelts, 1988; Harris et al., 2004). However, recent studies from the Congo Basin (Behar et al., 2021) demonstrated that terrigenous input from coastal rivers can equally dilute organic matter. A similar pattern was observed in Chinese rift basins (Liang et al., 2020). The interaction between these dilution mechanisms and their dependence on paleobathymetric position remains poorly understood, especially in mixed carbonate-siliciclastic systems.

Beyond dilution effects, organic matter preservation is fundamentally controlled by redox conditions at the water-sediment interface (Demaison and Moore, 1980; Tyson, 1995). Trace element proxies, particularly vanadium, nickel, and molybdenum, have been widely employed to reconstruct paleoredox conditions in ancient sediments (Tribovillard et al., 2006; Algeo and Maynard, 2008). Manganese concentration provides additional information on redox stability through the "Mn-shuttle" mechanism, whereby persistently euxinic conditions promote Mn remobilization to the water column while favoring optimal kerogen preservation (Calvert and Pedersen, 1996).

The Lagoa Feia Group in the Campos Basin represents an ideal case study to investigate these controls. This Barremian–Aptian unit comprises three principal formations: the basal Atafona Formation (Barremian), characterized by terrigenous-dominated facies; the overlying Coqueiros Formation (Lower Aptian), recording bioclastic carbonate sedimentation during the rift phase; and the Macabu Formation (Middle to Upper Aptian), representing the transitional post-rift phase with microbial carbonates (Winter et al., 2007; De Jesus and Vilela, 2023). The stratigraphic progression reflects regional tectono-climatic evolution from humid to arid conditions during the rift-to-post-rift transition (Thompson et al., 2015; Goldberg et al., 2017). Previous studies documented high TOC values and Type I–II kerogen indicative of excellent oil-prone potential

(Mello et al., 1988), and Hercolano et al. (2026) established the geochemical characteristics of distal facies, demonstrating the presence of world-class source rocks. However, spatial variability in source rock quality and the hierarchy of controls governing organic matter accumulation remain poorly understood.

This study presents an integrated geochemical investigation of 80 samples from eight wells distributed along a proximal-to-distal paleobathymetric transect, combining Rock-Eval pyrolysis, LECO combustion, and XRF elemental analysis. The specific objectives are to: (1) characterize organic geochemistry and kerogen type along the paleobathymetric gradient; (2) evaluate the relative importance of carbonate versus siliciclastic dilution in controlling TOC distribution; (3) establish trace element proxies for paleoredox conditions and their relationship to organic matter preservation; and (4) determine the stratigraphic control exerted by different formations (Macabu, Coqueiros, Atafona) on source rock quality. The results provide a hierarchical model of controls on lacustrine source rock development with implications for exploration assessment in the Brazilian pre-salt and analogous rift systems.

2. Geological Setting

The Campos Basin is located along the southeastern continental margin of Brazil, between latitudes 21°S and 24°S, encompassing an area of approximately 100,000 km² (Figure 1). The basin is bounded to the north by the Vitória High and to the south by the Cabo Frio High, which separates it from the Santos Basin (Winter et al., 2007). Its origin dates back to the Early Cretaceous, when the extensional tectonic regime associated with Gondwana breakup generated a series of asymmetric half-grabens that controlled initial sedimentation patterns (Cainelli and Mohriak, 1999; Chang et al., 1992).

The tectono-stratigraphic evolution of the basin is organized into three supersequences: Rift, Post-Rift (transitional), and Drift (Dias et al., 1990; Winter et al., 2007). The present study focuses on the Rift Supersequence and the basal portion of the Post-Rift Supersequence, which comprise the Lagoa Feia Group, deposited in a predominantly lacustrine environment during the Barremian-Aptian (Figure 1B). This group constitutes the main pre-salt petroleum system of the Campos Basin, currently responsible for a substantial portion of Brazilian oil production (ANP, 2025; Guardado et al., 2000).

The Lagoa Feia Group comprises three main formations, whose stratigraphic progression reflects the regional tectono-climatic evolution. The Atafona Formation (Buracica Stage, Barremian) represents the initial rift phase, characterized by lacustrine deposition with significant terrigenous input reflected in elevated feldspar and clay mineral contents (Winter et al., 2007). The presence of authigenic magnesian silicates indicates alkaline conditions typical of volcanically influenced rift lakes (Tosca and Wright, 2015). The Coqueiros Formation (Jiquiá Stage, Lower Aptian) records the transition to bioclastic carbonate-dominated sedimentation during the late rift phase, with deposition on a low-gradient carbonate ramp where bioclastic coquinas interbedded with

organic-rich shales (Bertani and Carozzi, 1985; Carvalho et al., 2000). These shales represent an important source rock interval, characterized by Type I kerogen with high hydrogen indices (Mello et al., 1988). The Macabu Formation (Alagoas Stage, middle to upper Aptian) represents the transitional post-rift phase, composed predominantly of stromatolites and chemically precipitated microbial laminites under alkaline lacustrine conditions (De Jesus and Vilela, 2023; Wright and Barnett, 2015).

The progression from terrigenous-dominated sedimentation in the Atafona Formation, through bioclastic carbonates in the Coqueiros Formation, to microbial carbonates in the Macabu Formation reflects the integrated effects of tectonic subsidence, volcanic activity (intensifying carbonate precipitation), and regional climate (controlling the balance between fluvial input and evaporation) (Thompson et al., 2015; Goldberg et al., 2017). Thermal stratification of the water column during periods of reduced freshwater input promoted anoxic bottom-water conditions favorable for organic matter preservation.

The eight wells analyzed in this study (BCBR-1, BCBR-3, and BCBR-5 to BCBR-10) are distributed along a proximal-distal transect within the Campos Basin, sampling different paleobathymetric environments from the proximal zone (BCBR-7, 219 m water depth) to the distal zone (BCBR-1, 2750 m) (Figure 1). This spatial and stratigraphic distribution allows evaluation of lateral variability in source rock characteristics controlled by both paleobathymetric position and stratigraphic formation. Chronostratigraphic assignment was confirmed through lithostratigraphic correlation with markers established by Winter et al. (2007) and composite well log data provided by ANP.

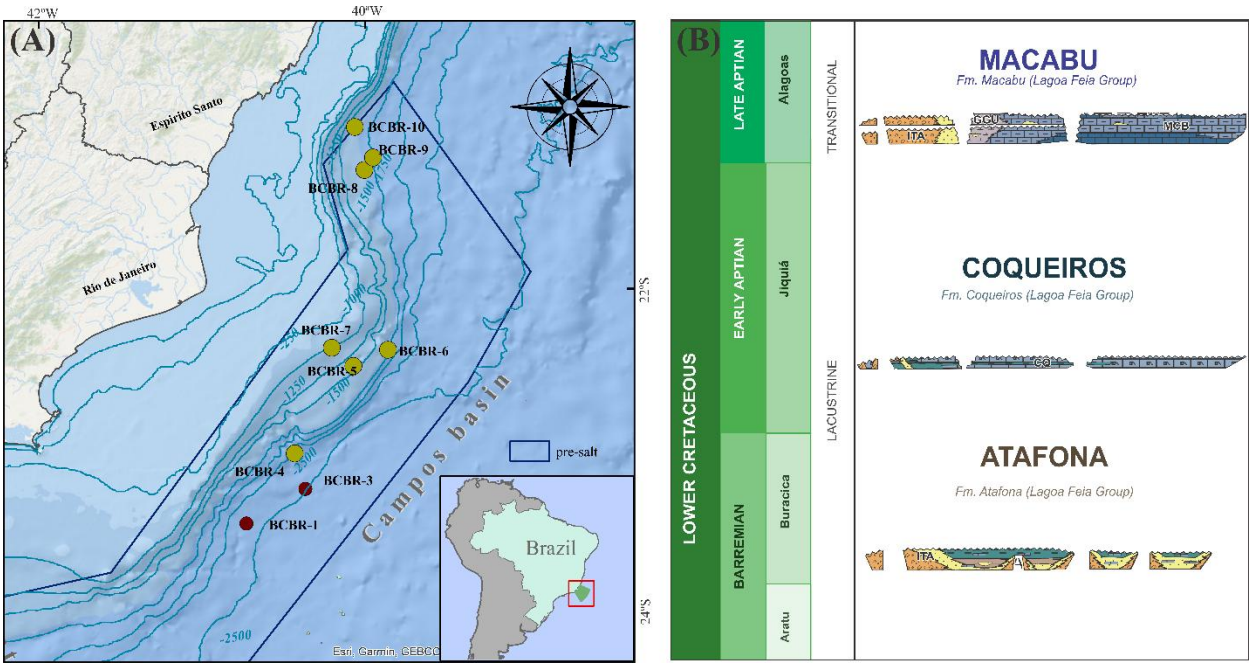

Figure 1. (A) Location map of the southeastern Brazilian margin showing the distribution of sampled wells in the Campos Basin (BCBR-1 to BCBR-10). Bathymetric contours are in meters.

(B) Chronostratigraphic chart of the Campos Basin during the Lower Cretaceous (Barremian to Aptian), showing formations of the rift and transitional post-rift supersequences. Modified from Winter et al. (2007).

3. Materials and Methods

3.1 Study area and sampling

The Campos Basin dataset comprises 81 samples from 8 wells, including 56 samples from 6 wells in the present study (BCBR-5 to BCBR-10) and 25 samples from 2 distal wells (BCBR-1, n = 14; BCBR-3, n = 11) previously published by Hercolano et al. (2026). The dataset includes 75 cuttings samples and 6 sidewall cores, the latter concentrated in wells BCBR-9 (n = 1) and BCBR-10 (n = 5). One cuttings sample from BCBR-10 was subsequently excluded due to contamination (Section 3.8), yielding a final dataset of 80 samples (74 cuttings + 6 sidewall cores). Samples are distributed among the Macabu (n = 18), Coqueiros (n = 32), and Atafona (n = 31; n = 30 after exclusion) formations, spanning a paleobathymetric transect from the proximal zone (BCBR-7, 219 m) to the distal zone (BCBR-1, 2750 m). Samples were collected from the ANP (Brazilian National Petroleum Agency) core repository facilities in Rio de Janeiro, Macaé (RJ), and Catu (BA).

3.2 Sample preparation

Sample preparation followed the protocol established by Hercolano et al. (2026). All containers and materials were rigorously cleaned using 10% (v/v) neutral detergent solution (Isodert, Isofar Laboratory), followed by treatment with 10% (v/v) HCl solution (P.A. 37%, Supelco®). Samples were manually sorted to remove drilling contaminants, such as metal fragments and fibers from sampling bags, and washed with 2 L of deionized water to remove drilling fluid residues. After washing, all samples were dried at 50°C for 24 hours and pulverized in a Retsch S1 planetary ball mill (Hann, Germany) to 100 mesh.

3.3 Rock-Eval pyrolysis

Aliquots of 50–100 mg of pulverized samples were analyzed using a Rock-Eval 7S instrument (Vinci Technologies) at HCS (Oceanus Group), Rio de Janeiro. The instrument was calibrated using certified reference materials IFP 160000 and IFP 400000 (Institut Français du Pétrole), following the procedure described by Hercolano et al. (2026). Analytical precision for TOC was ±0.12 wt%.

The analytical procedure comprised two sequential steps: pyrolysis and oxidation (Behar et al., 2001; Lafargue et al., 1998). For pyrolysis, samples were heated from 100°C to 800°C in a nitrogen atmosphere. Hydrocarbons were quantified by flame ionization detector (FID), while CO_2 and CO were measured by infrared detector (IR). In the oxidation stage, the sample residue was transferred to an oxidation furnace and heated in air from 100°C to 1200°C. TOC values were determined directly from Rock-Eval 7S analysis, calculated as the sum of carbon released during both phases.

Standard pyrolysis parameters were obtained: S1 (free hydrocarbons, mg HC/g rock), S2 (pyrolyzable hydrocarbons, mg HC/g rock), Tmax (temperature of maximum S2 generation, °C), Hydrogen Index (HI = S2/TOC × 100, mg HC/g TOC), Oxygen Index (OI = S3/TOC × 100, mg CO_2/g TOC), and Production Index (PI = S1/(S1+S2)).

3.4 TOC determination by LECO combustion

For independent validation of TOC values obtained by Rock-Eval pyrolysis, complementary analyses were performed by combustion using a LECO SC832 elemental analyzer at the Sulfur Geochemistry Laboratory (LaGEn), Fluminense Federal University (UFF). Pre-treatment for inorganic carbon removal consisted of agitating approximately 3 g of sediment in 1 mol L^{-1} HCl (Hedges and Stern, 1984), followed by washing with deionized water until pH 6. After drying, samples were ground and 100–120 mg aliquots were submitted to combustion analysis.

Comparison between methods revealed strong correlation ($\rho = 0.81$, $p < 0.001$), but LECO TOC showed more robust correlations with elemental indicators of interest: Ca ($\rho = -0.62$ vs. -0.40 for Rock-Eval) and V ($\rho = +0.8$ vs. $+0.63$). Considering that the LECO method completely eliminates the carbonate fraction before analysis, reducing analytical interferences in samples with high carbonate content (mean 61% carbonate removed during pre-treatment), LECO TOC values were adopted in subsequent statistical analyses. For wells BCBR-1 and BCBR-3 (Hercolano et al., 2026), only Rock-Eval pyrolysis data were available; TOC calculated from this method was used for these samples.

3.5 XRF analysis

Major and trace elements were analyzed using an EDXRF spectrometer (Epsilon 3, Malvern Panalytical, Netherlands), equipped with a silver anode X-ray tube and 50 μm beryllium window, at the Sedimentary Geochemistry Laboratory, Fluminense Federal University. Measurements were conducted in air and helium atmospheres. Instrument calibration was performed using a fused reference pellet for X-ray fluorescence (FLX-C3, Fluxana, Bedburg-Hau, Germany), with all elements showing standard deviation less than 0.3. Operating conditions were: 50 kV tube voltage, 1 mA current, and 9 W power. Detection was achieved using a high-resolution silicon drift detector (SDD) with 135 eV resolution and 8 μm (Be) window.

Major elements quantified include Ca, Si, Al, Fe, Mg, K, Ti, S and Mn (reported as weight percent). Trace elements analyzed include V, Ni, Cu, Zn, Zr and Sr (reported as ppm). Analytical precision, determined from replicate analyses of reference material FLX-C3, was better than 5% relative standard deviation (RSD) for major elements and 10% RSD for trace elements.

3.6 Well log data

Gamma ray (GR) logs for all studied wells were obtained from the ANP Exploration and Production Database (BDEP). GR values are reported in API units (gAPI) and were used for

lithological characterization and chemostratigraphic correlation along the paleobathymetric transect.

3.7 Geochemical proxies

Geochemical proxies were interpreted to infer paleoenvironmental conditions following established frameworks (Tribovillard et al., 2006; Algeo and Maynard, 2008). Ti and Zr served as indicators of terrigenous input; Ca and Sr were associated with carbonate accumulation; Al and K reflected the presence of feldspars and clays; and V, Ni, Cu, and Zn were interpreted as redox-sensitive elements (Hatch and Leventhal, 1992; Tribovillard et al., 2006).

The terrigenous index (TI) was calculated as the sum of Al + Si + K + Ti, representing the siliciclastic fraction of the sediment. The V/(V+Ni) ratio was calculated as a paleoredox proxy and interpreted following the classification of Hatch and Leventhal (1992): oxic (≤0.46), dysoxic (0.46–0.60), anoxic (0.60–0.84), and euxinic (>0.84). The Fe/Al ratio was used to discriminate detrital from authigenic iron (Lyons and Severmann, 2006), with values >0.5 (average crustal value) indicating authigenic Fe contribution. Enrichment factors were calculated relative to average shale values of Wedepohl (1991).

3.8 Statistical analysis

Correlations between geochemical parameters were evaluated using Spearman's rank correlation coefficient (ρ), appropriate for data that do not present normal distribution. Coefficients were interpreted following the classification: $|\rho| < 0.45$ (weak correlation), $|\rho| = 0.45–0.60$ (moderate correlation), and $|\rho| > 0.60$ (strong correlation), with statistical significance defined by $p < 0.05$. Correlation values are reported rounded to one decimal place (0.5, 0.6, 0.7, etc.).

One sample from well BCBR-10 (depth 3495 m) was excluded from statistical analyses due to evidence of contamination. This sample displays Production Index (PI = 0.22) above the 0.2 threshold established by Peters (1986) for immature rocks, combined with anomalously high S1 (21.8 mg HC/g rock), indicating probable contamination by oil-based drilling fluid or migrated hydrocarbons (Lai et al., 2024). In contrast, two sidewall cores at 3496 m from the same well exhibit exceptionally high TOC (10.9–17.7%) but normal PI values (0.05–0.06) and moderate S1 (2.8–3.8 mg HC/g rock), consistent with well-preserved Type I kerogen (HI = 694–740 mg HC/g TOC). These samples were retained as they likely represent a genuinely organic-rich horizon documenting world-class source rock potential in the Atafona Formation. The final dataset comprises 80 samples.

4. Results

4.1 Organic matter content and source rock quality

The Lagoa Feia Group contains predominantly good to excellent source rocks, with 85% of samples exceeding TOC > 1% according to the classification of Peters and Cassa (1994). TOC

ranges from 0.5% to 7.5% (mean 2.7 ± 2.4%; Table 1), with exceptional values up to 17.7% in sidewall cores from well BCBR-10. The highest typical values occur in the Atafona Formation at intermediate paleobathymetric positions. The strong correlation between S2 and TOC ($\rho = 0.9$, $p < 0.001$) confirms analytical consistency between Rock-Eval pyrolysis and LECO combustion methods, reflecting the predominantly lipid-rich nature of the preserved organic matter.

Table 1. Descriptive statistics for the Lagoa Feia Group, Campos Basin (n = 80).

Parameter	Mean	SD	Min	Max	Median
TOC (%)	2.7	2.4	0.0	17.7	2.2
S2 (mg HC/g)	12.7	10.3	0.1	63.4	10.1
Tmax (°C)	433	13	359	444	435
HI (mg HC/g TOC)	471	197	45	1083	453
OI (mg CO_2/g TOC)	45	35	6	191	35
PI	0.11	0.06	0.05	0.47	0.09

Geochemical parameters vary systematically along the paleobathymetric transect from proximal (BCBR-7, 219 m) to distal positions (BCBR-1, 2750 m; Table 2). The Macabu Formation wells illustrate distinct behavior: BCBR-5 records mean TOC of 2.5%, whereas BCBR-8 shows the lowest TOC in the dataset (0.9%) but the highest HI (779 mg HC/g TOC), indicating exceptional kerogen quality despite low quantity. This contrast reflects carbonate dilution intensity rather than paleobathymetric position.

Table 2. Mean geochemical parameters by well, ordered by paleobathymetric water depth, with formation classification.

Well	Formation	WD (m)	n	TOC (%)	HI	S2	Ca (%)	TI (%)	V (ppm)	Mn (%)
BCBR-7	Coq/Ata	219	9	2.0	360	11.6	41	11	n.d.	0.49
BCBR-5	Macabu	920	10	2.5	338	9.3	29	19	398	0.41
BCBR-10	Atafona	1222	16	4.1	493	18.2	16	29	399	0.18
BCBR-6	Coqueiros	1293	7	2.7	628	18.3	36	15	491	0.32
BCBR-8	Macabu	1374	8	0.9	779	6.5	53	7	n.d.	0.10
BCBR-9	Coqueiros	1492	5	1.3	280	6.7	30	18	198	0.25
BCBR-3*	Coq/Ata	2656	11	2.8	540	15.5	16	25	n.d.	0.15
BCBR-1*	Coq/Ata	2750	14	2.9	374	10.3	15	25	n.d.	0.17

*Wells from Hercolano et al. (2026); WD = paleobathymetric water depth; TI = Terrigenous Index (Si+Al+K+Ti); n.d. = not determined.

Organic matter distribution differs significantly among stratigraphic formations. The Macabu Formation (mean TOC 1.7 ± 1.2%, HI 534 ± 303 mg HC/g TOC) contains predominantly Type I kerogen characteristic of alkaline post-rift lacustrine environments. The Coqueiros Formation (mean TOC 2.8 ± 1.6%, HI 455 ± 162 mg HC/g TOC) shows Type I-II kerogen reflecting high algal productivity. The Atafona Formation exhibits higher mean TOC (3.1 ± 3.3%) but similar HI (452 ± 143 mg HC/g TOC), with greater scatter reflecting variable terrigenous influence. This compositional progression is consistent with humid-to-arid climatic evolution during lake system development.

4.1.1 Kerogen type and thermal maturity

The modified Van Krevelen diagram (Figure 2A) demonstrates that samples plot predominantly in the Type I and II kerogen fields, with symbol size proportional to TOC. Low OI values (mean 45 ± 35 mg CO_2/g TOC) indicate well-preserved organic matter under anoxic conditions typical of stratified lacustrine environments (Langford and Blanc-Valleron, 1990). The HI vs. Tmax diagram (Figure 2B) confirms the predominance of oil-prone kerogen, with Tmax concentrated between 430–445°C.

Data from distal wells BCBR-1 and BCBR-3 (Hercolano et al., 2026) extend the documented thermal maturity range, with Tmax reaching ~444°C at the onset of the oil generation window, while samples from the present study concentrate in the immature to early generation window. BCBR-3 exhibits mean HI of 540 mg HC/g TOC (Type I-II), whereas BCBR-1 shows HI of 374 mg HC/g TOC (Type II), demonstrating kerogen heterogeneity even at similar distal positions.

Thermal maturity indicators show 44% of samples in the immature window (Tmax < 435°C) and 56% at early oil generation (435–445°C). The mean Production Index (0.11 ± 0.06) is consistent with predominantly early maturity stage.

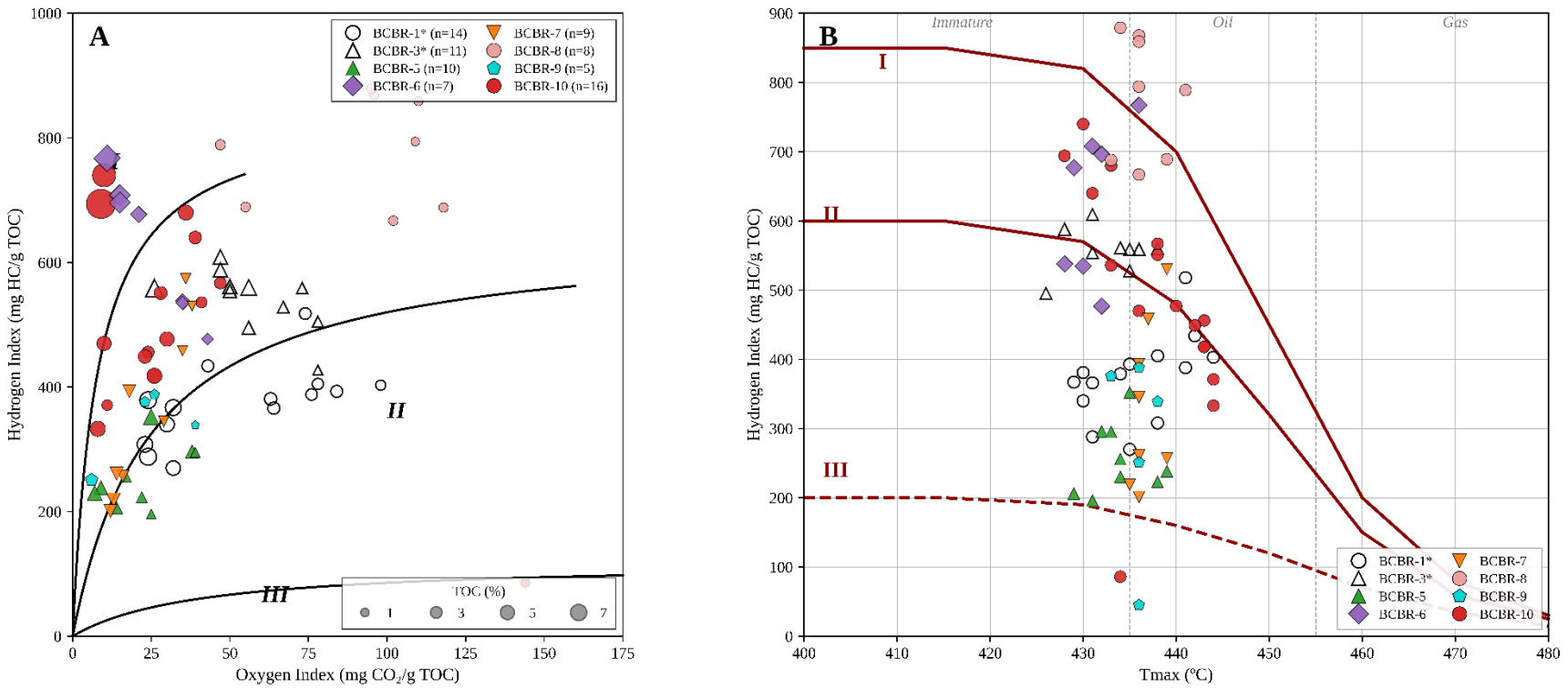

Figure 2. Kerogen type and thermal maturity of the Lagoa Feia Group, Campos Basin (n = 80). (A) Modified Van Krevelen diagram (HI vs. OI); symbol size proportional to TOC. (B) HI vs. Tmax diagram (after Espitalié et al., 1986). Wells marked with asterisks from Hercolano et al. (2026). TOC values correspond to LECO combustion, except for wells BCBR-1 and BCBR-3 (Rock-Eval TOC; Hercolano et al., 2026).

4.1.2 Sample types and analytical comparison

The final dataset comprises 74 cuttings samples (92%) and 6 sidewall cores (8%), following exclusion of one contaminated cuttings sample from BCBR-10 (see below). Comparison between analytical methods shows strong correlation for cuttings (TOC LECO vs. TOC Rock-Eval: $\rho = 0.8$, $p < 0.001$), validating analytical consistency. Sidewall cores from the Atafona Formation ($n = 5$) show higher mean TOC (5.5 ± 7.0%) compared to cuttings from the same unit (2.6 ± 1.9%), suggesting that conventional cuttings sampling may underestimate organic richness in laminated source rock intervals.

Three samples from well BCBR-10 at 3495–3496 m exhibit exceptionally high TOC (10.9–17.7%). The cuttings sample at 3495 m shows PI = 0.22 and anomalous S1 (21.8 mg HC/g), indicating probable contamination by oil-based drilling fluid (Peters, 1986; Lai et al., 2024), and was excluded from statistical analyses. In contrast, sidewall cores at 3496 m display normal PI values (0.05–0.06) and exceptional HI (694–740 mg HC/g TOC), likely representing a genuinely organic-rich horizon that documents the presence of world-class source rock intervals in the Atafona Formation.

4.2 Elemental composition

XRF analysis of 56 samples reveals a mixed carbonate-siliciclastic system with pronounced compositional heterogeneity among stratigraphic formations. Calcium dominates the major element assemblage (33 ± 14%, range 7–64%), with a strong inverse correlation with the terrigenous index (TI = Al+Si+K+Ti; $\rho = -0.93$, $p < 0.001$), confirming that the system operates between two compositional end-members.

The Ca-Sr association ($\rho = +0.71$, $p < 0.001$) indicates predominantly biogenic carbonate origin in the Coqueiros and Atafona formations. Macabu shows the highest mean Sr (0.30%), followed by Coqueiros (0.18%) and Atafona (0.16%). The elevated Sr in Macabu, combined with high Ca, is consistent with primary chemical (microbial) carbonate precipitation, while the lower Sr in Coqueiros and Atafona reflects bioclastic and mixed carbonate origins, respectively.

The Si/Al ratio, commonly used as a proxy for textural maturity and relative grain size (Calvert et al., 1996), shows negative correlation with TOC ($\rho = -0.55$, $p < 0.001$). Si/Al varies systematically among formations: Macabu shows the highest values (mean 10.8), reflecting the near-absence of clay minerals in chemical carbonate facies where Si derives primarily from diagenetic silica (chert) and siliceous precipitates rather than detrital input; Coqueiros exhibits intermediate values (mean 7.2) consistent with bioclastic carbonates with minor terrigenous clay; and Atafona shows the lowest values (mean 4.2), indicating clay-rich shales where Al-bearing detrital minerals dominate the siliciclastic fraction. The overall negative Si/Al–TOC correlation thus reflects two distinct mechanisms: in the Atafona, finer-grained clay-rich facies concentrate organic matter through mineral surface adsorption (Kennedy et al., 2002); in the Macabu, the high Si/Al paradoxically

accompanies low TOC because carbonate dilution, not grain size, controls organic matter concentration in this unit.

Zirconium correlates strongly with TI (ρ = +0.94) and Al (ρ = +0.97), confirming its utility as a proxy for detrital input associated with heavy minerals. The Zr distribution reflects compositional end-members: sandstones average 310 ppm, shales 176 ppm, and coquinas/microbial carbonates only 60 ppm.

Compositional differentiation among stratigraphic formations is pronounced (Table 3). The Macabu Formation (Ca = 40 ± 15%,TI = 13 ± 8%) represents microbial carbonate facies. The Coqueiros Formation (Ca = 37 ± 10%, TI = 14 ± 6%) represents bioclastic carbonate facies. The Atafona Formation shows inverse proportions (Ca = 20 ± 12%, TI = 27 ± 9%), dominated by shales (56%) and sandstones (26%). This distinction reflects paleoenvironmental differences: Macabu records chemical carbonate precipitation in alkaline post-rift settings; Coqueiros records high-energy bioclast accumulation; and Atafona records lower-energy deposition with greater clastic input during the early rift phase.

Table 3. Elemental composition by lithofacies in the Lagoa Feia Group, Campos Basin (n = 56).

Lithofacies	n	Ca (%)	TI (%)	Si/Al	Zr (ppm)	V (ppm)
Sandstone	9	13	28	5.4	311	477
Shale	24	30	20	6.5	176	437
Calcite mudstone	5	28	19	8.4	167	346
Coquina	15	44	11	8.9	60	214
Calcarenite	3	41	10	8.7	71	355

4.2.1 Paleobathymetric trends

Elemental composition varies systematically along the paleobathymetric transect. Manganese shows negative correlation with paleobathymetry (ρ = -0.43, $p < 0.001$), decreasing from 0.45% in proximal to 0.20% in intermediate and 0.16% in distal positions. This pattern indicates increasingly stable anoxic conditions toward deeper portions, where Mn remobilization to the water column prevents sediment accumulation. Magnesium shows the opposite trend, increasing from 4.0% proximally to 5.1% distally, reflecting more intense dolomitization at distal positions.

Iron increases distally (2.9% → 4.8% → 6.4%), indicating greater authigenic Fe (pyrite) contribution under persistent anoxic conditions. Among trace elements, zinc shows pronounced distal enrichment (324 ppm vs. 95 ppm proximally), while copper increases moderately (143 ppm vs. 93 ppm). Calcium and terrigenous index show secondary variation along the transect, being controlled primarily by stratigraphic formation.

Data from distal wells BCBR-1 and BCBR-3 (paleobathymetry > 2600 m; Hercolano et al., 2026) extend the transect to the deepest basin zone. Their composition shows SiO_2 = 37–41%, CaO =

28–32%, MgO = 7.8–9.0%, and MnO = 0.20–0.22%, with estimated TI ~25%. The elevated dolomite proportion (13–16%) corroborates Mg increase toward distal positions, while low Mn (0.15–0.17%) confirms stable anoxic conditions. Trace elements include Sr (1700–1900 ppm) and exceptionally high Zn (157–537 ppm) in BCBR-3, consistent with the distal enrichment trend.

4.2.2 Redox-sensitive elements

Redox-sensitive trace elements show significant enrichment relative to average shale (Wedepohl, 1991). Vanadium averages 390 ± 153 ppm (n = 33), representing 3.0× enrichment over the reference value (~130 ppm). Other elements also show enrichment: Cu (121 ppm, 2.7×), Cr (175 ppm, 1.9×), Zn (117 ppm, 1.2×), and Ni (84 ppm, 1.2×). The enrichment pattern V > Cu >> Cr > Zn ≈ Ni is characteristic of anoxic to euxinic environments (Tribovillard et al., 2006).

The V/(V+Ni) ratio, a widely used paleoredox proxy, averages 0.80 ± 0.17 (n = 32). According to the classification of Hatch and Leventhal (1992), 50% of samples indicate euxinic conditions (V/(V+Ni) > 0.84), 44% indicate anoxic conditions (0.60–0.84), and only 6% indicate dysoxic/oxic conditions (< 0.60). The TOC vs. V/(V+Ni) diagram (Figure 4B) illustrates the relationship between paleoredox conditions and organic matter preservation. The predominance of samples in euxinic and anoxic fields (94%), associated with higher TOC and S values, is consistent with persistent water column stratification typical of rift lakes with high productivity and restricted circulation (Katz, 1995). Vanadium shows the strongest correlation with TOC in the dataset ($\rho = +0.8$; Figure 4A), confirming its utility as a redox proxy. The single sample in the oxic field (V/(V+Ni) < 0.46) shows near-zero TOC, demonstrating the importance of reducing conditions for organic preservation.

Total sulfur shows heterogeneous distribution (mean 1.2 ± 3.1%), with anomalous values in BCBR-8 (Macabu Formation) reaching 23.6%, indicating episodes of intense sulfate-reducing activity. The Fe/Al ratio, used to discriminate detrital from authigenic Fe (Lyons and Severmann, 2006), averages 1.5 ± 0.6. Values of Fe/Al > 0.5 (average crustal value) indicate authigenic Fe contribution. Well BCBR-8 shows the highest Fe/Al ratio (3.85), suggesting intense sulfide precipitation under euxinic conditions. The strong Fe-Al correlation ($\rho = +0.91$, $p < 0.001$) in other wells indicates predominantly detrital Fe origin.

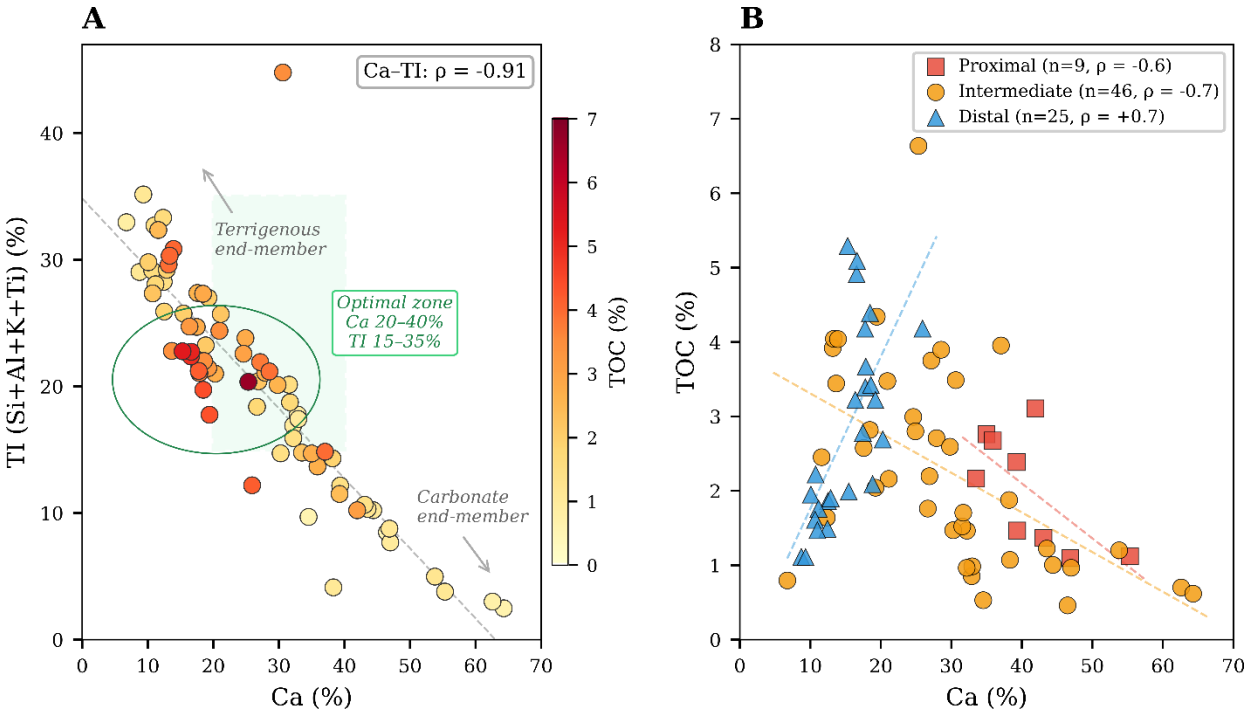

Figure 3. Dual dilution model for the Lagoa Feia Group, Campos Basin. (A) Ca (%) versus TI (Si+Al+K+Ti) (%) with TOC (%) as color scale. The dashed rectangle delineates the optimal compositional zone (Ca 20–40%, TI 15–35%) where TOC reaches maximum values (~3.5–4.1%). Three exceptional sidewall cores from BCBR-10 (TOC 10.9–17.7%) are excluded for scale clarity but included in statistical analyses. (B) Ca (%) versus TOC (%) by paleobathymetric position: proximal (n = 9, ρ = −0.6), intermediate (n = 46, ρ = −0.7), and distal (n = 25, ρ = +0.7). The sign inversion indicates that carbonate acts as a diluent in proximal–intermediate settings but co-accumulates with organic matter in distal settings (Talbot and Kelts, 1986). TOC values correspond to LECO combustion, except for wells BCBR-1 and BCBR-3 (Rock-Eval TOC; Hercolano et al., 2026).

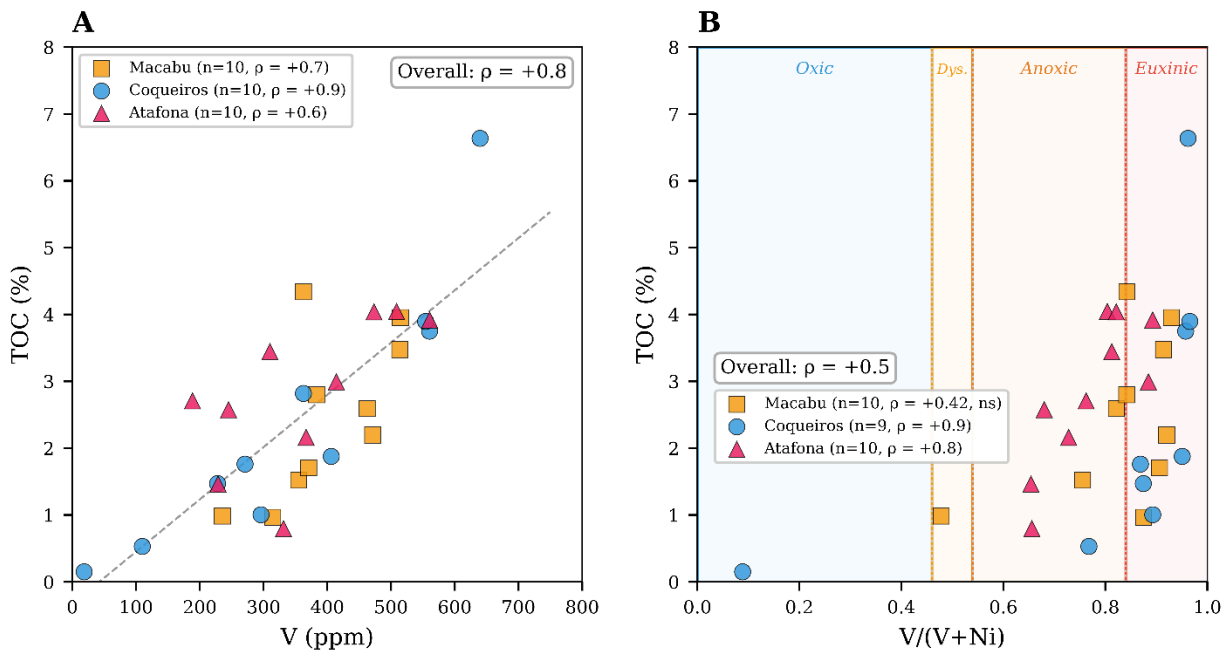

Figure 4. Redox-sensitive elemental proxies in the Lagoa Feia Group, Campos Basin (Paper 2 wells, n = 30). (A) V (ppm) versus TOC (%) by stratigraphic formation. Vanadium shows the strongest correlation with TOC in the dataset (ρ = +0.8). (B) V/(V+Ni) versus TOC (%) with redox fields after Hatch and Leventhal (1992). The majority of samples plot in the euxinic (55%) and anoxic (38%) fields. TOC values correspond to LECO combustion.

5. Discussions

5.1 Dual dilution model: carbonate and siliciclastic end-members

The integrated geochemical analysis reveals a dual dilution model controlling organic matter concentration in the Lagoa Feia Group. Unlike traditional interpretations that consider only carbonate dilution as the limiting factor in lacustrine source rocks (e.g., Bohacs et al., 2000), our data demonstrate that both carbonate excess and siliciclastic excess can dilute organic matter, depending on depositional and stratigraphic context. This bifurcated behavior aligns with observations from the Congo Basin, where Behar et al. (2021) documented that detrital input degraded source rock quality by reducing initial HI from >600 to <300 mg HC/g TOC in areas proximal to fluvial deltas.

Maximum TOC (~3.5–4.1%) occurs where carbonate (Ca ~20–40%) and siliciclastic (TI ~15–35%) components are balanced, defining an optimal compositional zone (Figure 3A). The strong anticorrelation between Ca and TI (ρ = −0.93) confirms that the system operates between two compositional end-members, consistent with the three-component mixing model of Ricken (1993) applied to organic-rich sediments. The Ca-TOC relationship varies with paleobathymetric position (Figure 3B): proximal and intermediate wells show negative correlations (ρ = −0.6 and −0.7,

respectively), while distal wells exhibit positive correlation ($\rho = +0.7$). This inversion indicates that the role of carbonate changes along the transect—acting as a diluent in proximal-intermediate positions but co-accumulating with organic matter in distal settings, where micritic carbonate and organic matter deposit together under anoxic conditions (Talbot and Kelts, 1986).

The intensity of carbonate dilution also varies by stratigraphic formation: Macabu shows the strongest negative correlation ($\rho = -0.80$), followed by Coqueiros ($\rho = -0.70$), while Atafona shows no significant Ca-TOC correlation ($\rho = -0.28$, $p = 0.13$). This hierarchy reflects fundamentally different carbonate accumulation mechanisms: chemical microbial precipitation (Macabu), bioclastic accumulation (Coqueiros), and dispersed carbonate in terrigenous matrix (Atafona), where paleobathymetric position rather than carbonate content controls organic matter accumulation. These patterns are consistent with the lake-basin type classification of Carroll and Bohacs (2001), where carbonate precipitation intensity reflects the balance between accommodation, sediment supply, and water chemistry.

Siliciclastic dilution, less commonly recognized in the literature though documented in Chinese lacustrine systems (Liang et al., 2020) and the Congo Basin (Harris et al., 2004), is demonstrated by the Atafona Formation in distal wells BCBR-1 and BCBR-3. At these positions (paleobathymetry ~2650–2750 m), elevated terrigenous index (TI = 25–37%) combined with low carbonate (Ca = 11–16%) results in TOC of only 1.6%, while the overlying Coqueiros Formation, with more balanced composition (Ca ~16%, TI ~25%), reaches TOC of 2.8–3.5%. This inversion—where Coqueiros exceeds Atafona in TOC at distal positions, contrary to the proximal pattern—demonstrates that the primary control is compositional balance, not water depth. The positive correlation between TI and TOC in proximal-intermediate wells ($\rho = +0.59$) reflects an indirect mechanism: within the TI range of 15–35%, increasing terrigenous component dilutes carbonate without diluting organic matter. Only when TI exceeds ~35% does effective siliciclastic dilution occur.

The intensity of mineral dilution can be quantified through the three-component sediment decomposition model of Ricken (1993), partitioning each sample into organic matter, carbonate, and siliciclastic fractions. Carbonate content was measured directly from the mass loss during LECO acid pre-treatment for wells BCBR-5 through BCBR-10 ($n = 55$); for wells BCBR-1 and BCBR-3, carbonate content was estimated from Ca (XRF) using a linear regression calibrated against the LECO-derived values ($CaCO_3 = 1.29 \times Ca + 18.7$, $R^2 = 0.88$, $\rho = 0.95$, $n = 55$). Organic matter was estimated from TOC using a kerogen conversion factor of 1.25, appropriate for Type I–II kerogen (Tyson, 1995), and the siliciclastic fraction was obtained by difference. The resulting three-component analysis ($n = 80$; Supplementary Figure 1, Panel A) reveals that carbonate constitutes the dominant mineral component in the Macabu ($67 \pm 17\%$) and Coqueiros ($58 \pm 17\%$) formations, accounting for 69% and 60% of total mineral dilution, respectively. In contrast, the Atafona Formation is dominated by siliciclastic material ($56 \pm 18\%$), which represents 58% of mineral dilution, while carbonate is reduced to $40 \pm 18\%$. This compositional shift from carbonate-

dominated to siliciclastic-dominated dilution across the three formations quantitatively confirms the dual dilution mechanism.

When TOC is recalculated on a carbonate-free basis, the three formations converge toward a narrower range: 6.1% (Macabu), 6.2% (Coqueiros), and 5.1% (Atafona) (Supplementary Figure 1, Panel B). This convergence indicates that organic carbon flux to the sediment was broadly uniform across the Lagoa Feia lake system, and that the observed twofold variation in measured TOC (1.7% to 3.1%) is primarily an artifact of differential mineral dilution. Critically, while organic supply was similar, the dilution intensity was not: the Macabu Formation contains 67% $CaCO_3$ compared to 58% in the Coqueiros, reflecting the greater efficiency of chemical microbial precipitation as a carbonate factory relative to bioclastic accumulation. This distinction is captured by relative sedimentation rates derived from the organic matter fraction ($SR_{rel} \propto 1/OM\%$; Ricken, 1993): the Macabu accumulated sediment at 1.8× the rate of the Atafona and 1.6× the rate of the Coqueiros, which quantifies how the carbonate factory type—not merely carbonate content—modulates dilution intensity. The stronger Ca–TOC anticorrelation in Macabu ($\rho = -0.80$) compared to Coqueiros ($\rho = -0.70$) is thus a direct consequence of higher carbonate production rates in the microbial system. The lower carbonate-free TOC in Atafona (5.1%) reflects a different mechanism: in this formation, siliciclastic material constitutes the dominant mineral component (56%), and its dilution effect persists even after carbonate removal from the calculation. This is particularly evident in distal wells BCBR-1 and BCBR-3, where the siliciclastic fraction exceeds 65% and carbonate-free TOC drops to only 2.5%. The fact that removing carbonate does not restore Atafona TOC to values comparable with Macabu and Coqueiros (~6%) provides direct quantitative evidence that siliciclastic dilution operates as the primary control on organic matter concentration in this formation, as predicted by the dual dilution model.

At the well scale, the contrast in relative sedimentation rates is more pronounced: BCBR-8 (Macabu) shows a rate 3.6× higher than the Atafona, consistent with intense chemical carbonate precipitation driving extreme dilution (Ca = 53%, TOC = 0.9%). These rates require no chronostratigraphic constraints, being derived directly from the three-component decomposition. Calibrating against typical lacustrine productivity values (100–200 $gC/m^2/a$; Kelts, 1988; Müller and Suess, 1979) yields absolute sedimentation rates of 7–26 cm/ka, broadly comparable to values reported for modern eutrophic rift lakes such as Lake Tanganyika and the Cariaco Basin (Kelts, 1988; Thunell et al., 2000).

The three-component decomposition also reveals how paleobathymetric position modulates the type of mineral dilution within each formation (Supplementary Table 1). In the Coqueiros Formation, the carbonate fraction decreases systematically from 76% in proximal wells to 42% in distal wells (WD vs $CaCO_3$: $\rho = -0.78$, $p < 0.001$), while the carbonate-free TOC remains constant (~6.3–6.9%; WD vs TOC_{cf}: $\rho = +0.03$, not significant). This pattern indicates that the increase in observed TOC from proximal (1.6%) to distal (3.6%) Coqueiros is entirely driven by the progressive reduction in carbonate dilution toward deeper settings, where high-energy coquina facies give way to calcareous shales. In contrast, the Atafona Formation shows the opposite

behavior: carbonate-free TOC decreases strongly from 7.5% in proximal to 2.5% in distal positions (WD vs TOC_{cf}: $\rho = -0.73$, $p < 0.001$), as the siliciclastic fraction increases from 30% to 65%. This divergence demonstrates that paleobathymetric position controls which dilution mechanism predominates—carbonate in proximal–intermediate settings, siliciclastic in distal settings—while the stratigraphic formation determines the intensity of each mechanism. The two axes of variation operate independently: Coqueiros responds to paleobathymetry by losing carbonate (improving TOC), while Atafona responds by gaining siliciclastic (degrading TOC).

The Si/Al ratio was adopted as a proxy for relative grain size because it reflects the mineralogical contrast between the two dominant siliciclastic components: Si is hosted primarily in detrital quartz (silt-sized grains) and secondarily in diagenetic phases, whereas Al resides almost exclusively in aluminosilicate clay minerals (Calvert et al., 1996; Craigie, 2018). In siliciclastic-dominated settings, higher Si/Al indicates coarser, quartz-rich sediments and lower values indicate clay-rich, fine-grained facies. The negative Si/Al–TOC correlation ($\rho = -0.55$) is consistent with enhanced organic matter preservation in finer-grained sediments, where lower permeability limits oxidant diffusion and greater mineral surface area promotes organo-mineral adsorption (Kennedy et al., 2002). However, in the Macabu Formation, the elevated Si/Al (mean 10.8) does not indicate coarse grain size but rather reflects the near-absence of clay minerals in chemical carbonate facies, where Si derives from diagenetic silica (chert) rather than detrital input—a distinction that must be considered when applying this ratio across mixed lithologies. The Zr distribution across lithofacies (sandstones: 310 ppm; shales: 176 ppm; coquinas: 60 ppm) confirms the utility of this element as a detrital input proxy associated with heavy minerals, following the approach of Craigie (2018) for chemostratigraphic correlation.

5.2 Paleoredox conditions and organic matter preservation

The high TOC values documented in this study (mean 2.7%, maximum 17.7%) require fundamentally anoxic bottom-water conditions for preservation, as demonstrated by multiple converging lines of evidence. This interpretation aligns with observations from the conjugate Congo Basin, where Harris et al. (2004) concluded that redox proxies indicate reducing conditions throughout deposition of the entire synrift section. Critically, Harris et al. (2004) demonstrated that enhanced anoxia did not trigger deposition of the richest source rocks—instead, the stability of anoxic conditions and the balance between organic supply and dilution determined final source rock quality.

Vanadium emerges as the most robust redox proxy in this dataset, showing the strongest correlation with TOC among all analyzed elements ($\rho = +0.8$). This result is consistent with patterns described by Algeo and Maynard (2004) in black shales, where V exhibited strong euxinic affinity with large enrichment factors, reflecting its mobilization from Fe-Mn oxyhydroxides under reducing conditions and incorporation into organo-metallic complexes or sulfides (Tribovillard et al., 2006). The enrichment pattern V > Cu >> Cr > Zn ≈ Ni, with V averaging 3.0× average shale values (Wedepohl, 1991), is characteristic of anoxic to euxinic environments.

The normalization of V by Ni exploits the contrasting redox behavior of these two elements. Vanadium is preferentially sequestered under strongly reducing conditions through incorporation into organic complexes, clay minerals, and authigenic sulfides, whereas Ni is enriched across a broader redox range—primarily via complexation with organic ligands and incorporation into sulfide phases even under moderately reducing conditions (Tribovillard et al., 2006). The V/(V+Ni) ratio thus amplifies the redox gradient signal while minimizing the effect of variable terrigenous dilution on absolute trace metal concentrations. This normalization is particularly suitable for carbonate-siliciclastic mixed systems such as the Lagoa Feia Group, where large variations in detrital input (TI = 7–37%) would otherwise obscure absolute concentration trends. The ratio also benefits from a well-established calibration framework (Hatch and Leventhal, 1992), which provides quantitative thresholds for distinguishing oxic, dysoxic, anoxic, and euxinic depositional environments.

The V/(V+Ni) ratio indicates predominantly euxinic (50%) to anoxic (44%) conditions, with only 6% of samples in the dysoxic/oxic field (Figure 4B). The contrast between BCBR-6 (V/(V+Ni) = 0.95, HI = 628 mg HC/g TOC) and BCBR-9 (V/(V+Ni) = 0.65, HI = 280 mg HC/g TOC) illustrates a fundamental principle: the stability of anoxic conditions, rather than their mere presence, determines final source rock quality. This observation supports the conclusions of Pedersen and Calvert (1990), who argued that in high-productivity systems, preservation efficiency becomes secondary to organic matter supply and dilution.

Total sulfur was included as a complementary redox indicator in Figure 4B because it records a fundamentally different aspect of redox chemistry than trace metal proxies. While V/(V+Ni) reflects the degree of water-column oxygen depletion, total sulfur records the intensity of bacterial sulfate reduction (BSR)—the dominant anaerobic degradation pathway in euxinic lacustrine environments (Berner, 1984). Elevated S values indicate authigenic sulfide precipitation (primarily pyrite), which requires the simultaneous availability of reactive iron, dissolved sulfate, and organic matter as electron donor. The co-variation of high S with high TOC and elevated V/(V+Ni) in the dataset provides convergent evidence for persistent euxinic conditions, strengthening the paleoredox interpretation beyond what any single proxy could achieve.

However, well BCBR-8 (Macabu Formation) demonstrates that favorable redox conditions are necessary but not sufficient for high TOC. Despite evidence of intense euxinia (S up to 23.6%, Fe/Al = 3.85, Mn = 0.10%), this well shows the lowest TOC in the dataset (0.9%) due to extreme carbonate dilution (Ca = 53%). This pattern is consistent with the modeling of Tyson (2001), who demonstrated that at elevated sedimentation rates, dilution emerges as the dominant control over TOC regardless of oxygen conditions. Notably, the exceptionally high HI (779 mg HC/g TOC) confirms that the preserved kerogen possesses exceptional quality—it is quantity, not quality, that limits generative potential. This decoupling between TOC and HI has important implications for source rock assessment: intervals with apparently poor organic richness may still contain high-quality kerogen capable of generating hydrocarbons.

Manganese provides additional control on kerogen quality through the Mn-shuttle mechanism (Calvert and Pedersen, 1996). The negative correlation between Mn and HI ($\rho = -0.50$) reflects redox dynamics at the water-sediment interface: under oxic conditions, Mn oxyhydroxides precipitate and catalyze oxidative degradation of organic matter; under persistent anoxic conditions, Mn is remobilized to the water column, favoring preservation. Our data quantify this control: samples with Mn < 0.2% average HI of 562 mg HC/g TOC (n = 22), while samples with Mn > 0.3% average only 302 mg HC/g TOC (n = 17)—a difference approaching 50%. Makeen et al. (2015) documented analogous patterns in the Muglad Basin, where suboxic-anoxic conditions resulted in HI > 400 mg HC/g TOC versus < 400 in more oxygenated sections.

5.3 Stratigraphic controls: formation-specific behavior

The three formations of the Lagoa Feia Group exhibit distinct geochemical behaviors reflecting their different depositional origins, consistent with the lake-basin type framework of Bohacs et al. (2000) and the production-destruction-dilution model subsequently refined by the same authors (Bohacs et al., 2005).

Macabu Formation — Deposited during the post-rift (SAG) phase, this unit consists of chemical precipitates (stromatolites and microbial laminites) controlled by alkaline lacustrine water geochemistry (Wright and Barnett, 2015; Tosca and Wright, 2015). The strongest Ca-TOC correlation in the dataset ($\rho = -0.80$) reflects the efficiency of chemical carbonate precipitation as a diluent. Wells BCBR-5 and BCBR-8 illustrate internal variability: BCBR-5 (Ca = 29%, GR = 103 gAPI) reaches TOC = 2.5%, while BCBR-8 (Ca = 53%, GR = 34 gAPI) shows only 0.9% (Figure 5A). This contrast indicates that carbonate precipitation intensity—not paleobathymetric position—is the dominant control. Macabu intervals with lower carbonate purity represent more favorable exploration targets. The elevated Sr (0.30%) with strong positive Ca correlation ($\rho = +0.66$) indicates primary carbonate origin, distinguishing these chemical precipitates from bioclastic carbonates.

Coqueiros Formation — This unit shows systematic facies transition along the paleobathymetric transect. In proximal-intermediate positions (< 1500 m), high-energy coquina facies exert strong dilution control (ρ Ca-TOC $= -0.71$), resulting in TOC of 1.3–2.7% despite elevated HI (280–628 mg HC/g TOC). In distal positions (> 2000 m), the transition to more argillaceous calcareous shales (GR increases from ~47 to ~82 gAPI) weakens the Ca-TOC correlation ($\rho = -0.24$, not significant), and TOC reaches maximum values of 2.8–3.5%. In this lower-energy context, micritic carbonate co-accumulates with organic matter rather than acting as a diluent. The boxplots (Figure 5B) confirm this pattern: Coqueiros Formation TOC increases progressively toward distal wells. This facies-dependent behavior has direct analogs in the Green River Formation, where Carroll and Bohacs (2001) documented maximum organic enrichment in laminated profundal mudstones rather than in carbonate-dominated intervals.

Atafona Formation — This unit shows no significant Ca-TOC correlation at formation scale ($\rho = -0.28$, $p = 0.13$), but reveals a spatially dependent pattern (Table 4). In proximal positions (BCBR-7), carbonate dilution predominates (Ca = 36%) and elevated Mn (0.74%) results in the lowest HI in the dataset (278 mg HC/g TOC). In intermediate positions (BCBR-10), favorable compositional balance (TI = 29%, Ca = 16%) allows redox proxies (V: $\rho = +0.79$; S: $\rho = +0.74$) to control preservation, yielding the highest TOC in the dataset (4.1%). Sidewall cores from this formation show higher TOC than cuttings (5.5% vs. 2.7%), suggesting that conventional sampling may underestimate organic richness in laminated intervals. In distal positions, the dilution mechanism inverts: the TI-TOC correlation becomes negative ($\rho = -0.41$), indicating that intensified terrigenous input during the early rift phase (TI = 29%) diluted organic matter despite favorable redox conditions (Mn = 0.13%).

Table 4. Geochemical statistics for the Atafona Formation by paleobathymetric position. HI in mg HC/g TOC; GR in gAPI. Bold values indicate optimal configuration.

Position	Well(s)	n	TOC (%)	HI	Ca (%)	TI (%)	GR	Mn (%)
Proximal	BCBR-7	4	2.5	278	36	14	65	0.74
Intermediate	BCBR-10	16	4.1	493	16	29	85	0.18
Distal	BCBR-1, BCBR-3	10	1.6	455	11	29	60	0.13

The dual dilution model therefore operates asymmetrically among formations. In Macabu and proximal Coqueiros, dilution is primarily carbonate-driven. In distal Atafona, dilution is primarily siliciclastic-driven. Consequently, optimal source rock development varies spatially: Coqueiros reaches maximum in distal settings, while Atafona reaches maximum in intermediate positions (Figure 6).

5.4 Integrated model and exploration implications

The synthesis of observed patterns reveals a hierarchy of controls on source rock quality in the Lagoa Feia Group (Figure 6). This multi-factor framework aligns with the production-destruction-dilution-accommodation model proposed by Bohacs et al. (2005), which recognizes that source rock development results from the balance between organic matter supply, preservation efficiency, dilution rates, and accommodation space rather than from any single dominant control.

Primary control — Stratigraphic formation: The depositional unit determines the predominant carbonate type and, consequently, carbonate dilution intensity—most intense in Macabu (microbial precipitation), moderate in Coqueiros (bioclastic accumulation), and attenuated in Atafona (dispersed carbonate). This stratigraphic control operates independently of paleobathymetry and reflects fundamental differences in lake chemistry and carbonate factory type (sensu Wright, 2012).

Secondary control — Paleobathymetric position: Water depth modulates the primary control differently in each formation. In Coqueiros, distal positions favor source rock development due to facies transition from coquina to calcareous shales. In Atafona, intermediate positions are optimal due to favorable compositional balance. In Macabu, carbonate precipitation intensity overrides paleobathymetric effects.

Tertiary control — Redox conditions: Expressed by V > 400 ppm and Mn < 0.2%, redox conditions become determinant only where compositional dilution is minimized. This finding supports the conclusion of Harris et al. (2004) that enhanced anoxia does not trigger deposition of the richest source rocks—productivity and dilution exert primary control, with anoxia serving as a necessary but not sufficient condition.

This hierarchical model explains the contrasts observed in the dataset. BCBR-10 (intermediate Atafona) achieves the highest TOC (4.1%) through the combination of favorable compositional balance (Ca = 16%, TI = 29%) and stable anoxic conditions (Mn = 0.18%). Distal wells BCBR-1 and BCBR-3 show elevated TOC in Coqueiros (2.8–3.5%) but reduced TOC in Atafona (1.6%), demonstrating the inversion of dilution mechanism between formations. BCBR-8 represents the unfavorable extreme: despite intense euxinic conditions, extreme carbonate dilution (Ca = 53%) limits TOC to 0.9%, although exceptional kerogen quality (HI = 779 mg HC/g TOC) is preserved.

Prospect evaluation in the Lagoa Feia Group should integrate stratigraphic formation, paleobathymetric position, compositional balance, and redox proxies. Based on our dataset, intervals with Ca = 20–40%, TI = 15–35%, V > 400 ppm, Mn < 0.2%, and gamma ray response of 60–120 gAPI (indicating mixed lithology) represent the highest probability targets. The Atafona Formation at intermediate paleobathymetric positions and the Coqueiros Formation at distal positions emerge as the most favorable exploration targets.

The documented organic richness—maximum TOC of 4.1% and mean HI of 471 mg HC/g TOC—is comparable to world-class lacustrine source rocks, including Lakes Tanganyika and Kivu (Talbot, 1988), the Green River Formation (Carroll and Bohacs, 2001), and Congo Basin analogs (Harris et al., 2004; Behar et al., 2021). These values confirm the Lagoa Feia Group as a first-order petroleum system with excellent source rock potential where depositional conditions achieved optimal balance between organic supply, preservation, and dilution. The Lagoa Feia Group shares fundamental characteristics with age-equivalent source rocks on the conjugate African margin, including the Bucomazi Formation in the Congo Basin and the Melania Formation in Gabon, where similar dual dilution controls have been documented. The carbonate-siliciclastic mixing and formation-specific behavior observed in Campos Basin likely reflect regional climatic and tectonic controls operating across the nascent South Atlantic rift system during the Barremian-Aptian.

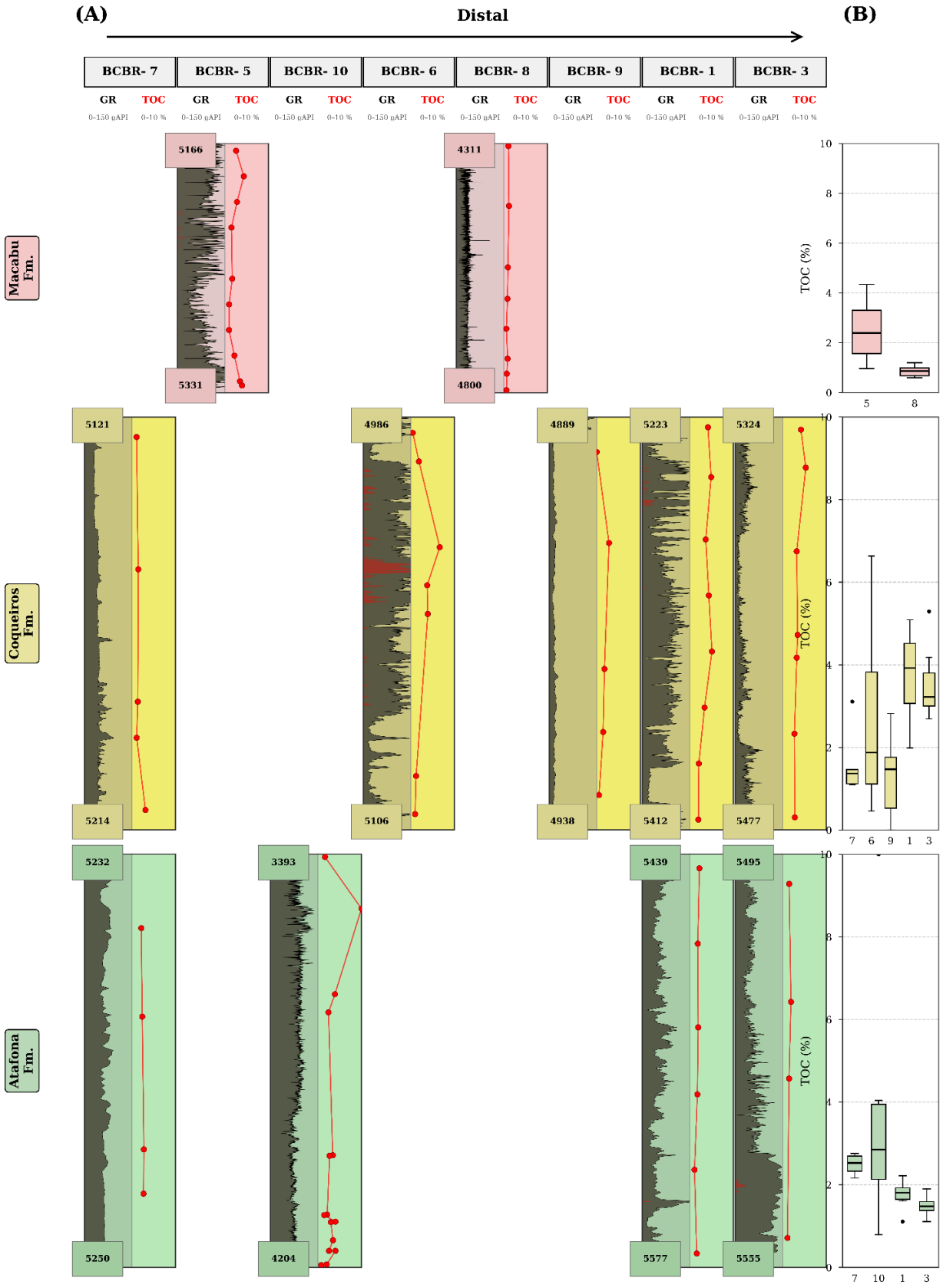

Figure 5. Chemostratigraphic correlation of the Lagoa Feia Group along the paleobathymetric gradient, Campos Basin. (A) Gamma ray (GR, 0–150 gAPI) and TOC (0–10%) profiles for the eight studied wells, organized from proximal (BCBR-7) to distal (BCBR-3) position. (B) TOC boxplots by well for each formation. TOC values correspond to LECO combustion, except for wells BCBR-1 and BCBR-3 (Rock-Eval TOC; Hercolano et al., 2026).

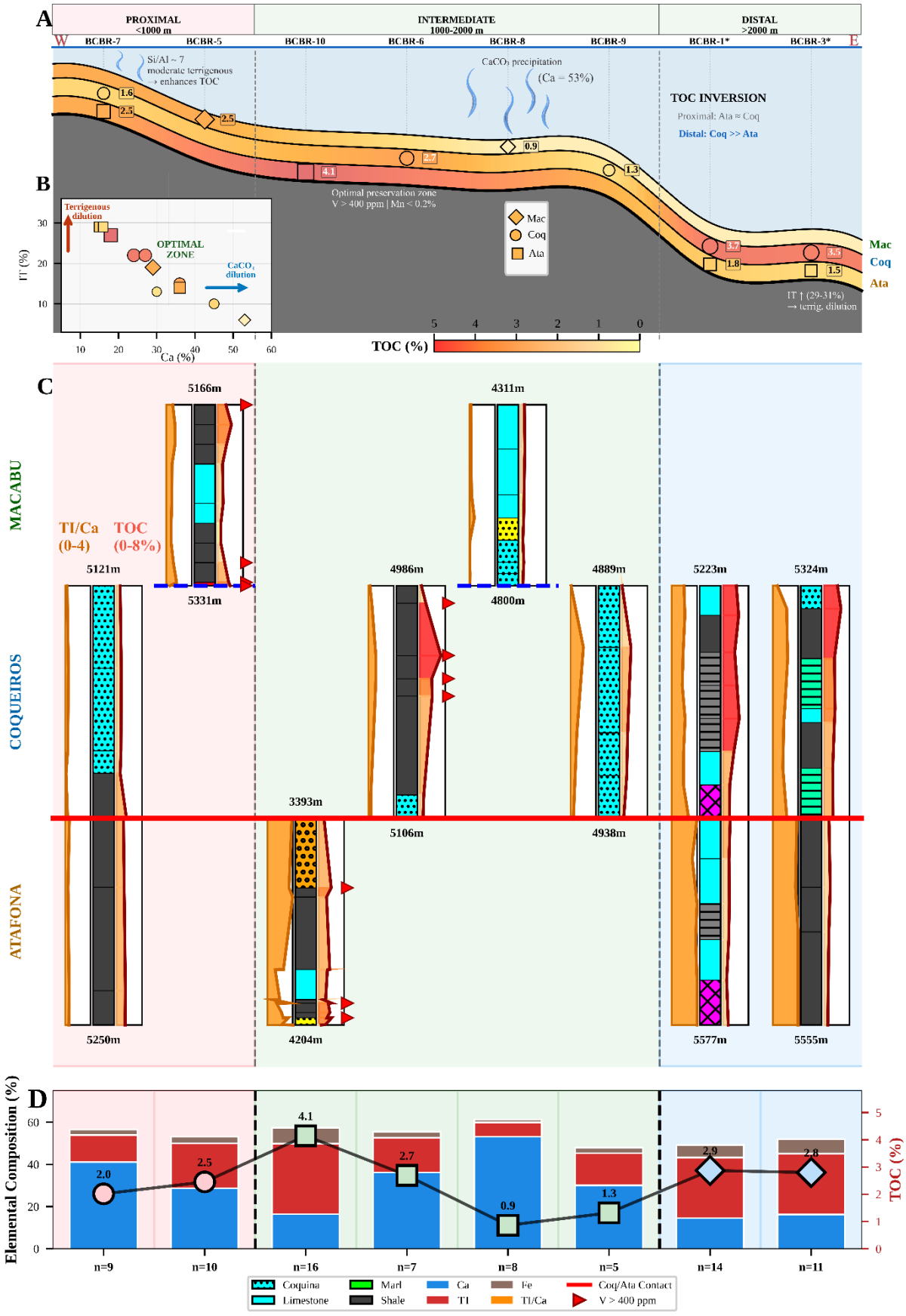

Figure 6. Integrated depositional and geochemical model for the Lagoa Feia Group. (A) TOC distribution by formation. (B) TI–Ca diagram with compositional end-members. (C) Lithological columns (red arrows: V > 400 ppm). (D) Mean Ca, TI, and TOC by well. *Hercolano et al. (2026).

6. Conclusions

The integration of Rock-Eval pyrolysis, LECO combustion, and XRF elemental analysis data from 80 samples across eight wells of the Lagoa Feia Group reveals that organic matter accumulation in pre-salt lacustrine source rocks is controlled by the interaction between sedimentary dilution, paleobathymetric position, and redox stability. Total Organic Carbon ranges from 0.5% to 7.5% (mean 2.7%), with Type I–II kerogen (HI up to 779 mg HC/g TOC) confirming excellent oil-prone potential.

The principal finding is a dual dilution model where both carbonate and siliciclastics can dilute organic matter, with intensity modulated by stratigraphic context and paleobathymetric position. Three-component sediment decomposition (Ricken, 1993) quantifies that carbonate dominates mineral dilution in the Macabu (67% $CaCO_3$) and Coqueiros (58%) formations, while siliciclastic material is the primary diluent in the Atafona (56%). When TOC is recalculated on a carbonate-free basis, the three formations converge toward ~5–6%, demonstrating that organic carbon flux was broadly uniform across the lake system and that the observed variation in TOC is primarily an artifact of mineral dilution intensity. The Macabu Formation accumulated sediment at 1.8× the rate of the Atafona (relative sedimentation rate derived from the decomposition), reflecting the greater efficiency of microbial carbonate precipitation as a diluent. Absolute sedimentation rates of 7–26 cm/ka are comparable to modern eutrophic rift lakes.

Paleobathymetric position modulates the type of dilution within each formation. In the Coqueiros Formation, the carbonate fraction decreases from 76% (proximal) to 42% (distal), while carbonate-free TOC remains constant (~6%), indicating that the increase in observed TOC toward distal positions is entirely driven by reduced carbonate dilution. In the Atafona Formation, the opposite occurs: the siliciclastic fraction increases from 30% (proximal) to 65% (distal), causing carbonate-free TOC to decrease from 7.5% to 2.5%. The Atafona achieves optimal source rock development at intermediate positions (BCBR-10, TOC = 4.1%), where compositional balance and stable anoxic conditions combine. Maximum TOC values (~3.5–4.1%) occur in zones of intermediate compositional balance (Ca ~20–40%, TI ~15–35%).

Vanadium emerges as the most robust redox proxy ($\rho = +0.8$ with TOC), while V/(V+Ni) ratios indicate predominantly euxinic to anoxic conditions. Manganese concentrations provide a sensitive indicator of redox stability: samples with Mn < 0.2% display mean HI of 562 mg HC/g TOC versus 302 mg HC/g TOC for Mn > 0.3%, demonstrating that kerogen quality is controlled by the stability of anoxic conditions rather than their mere presence.

The proposed hierarchical model — integrating stratigraphic control, compositional balance, paleobathymetric position, and redox stability — provides predictive criteria for exploration: intervals with Ca = 20–40%, TI = 15–35%, V > 400 ppm, and Mn < 0.2% represent the highest probability targets. The Lagoa Feia Group displays TOC and HI values comparable to the best global lacustrine analogs, including the Congo Basin and Chinese rift basins, confirming its status as a world-class source rock.

References

Algeo, T.J., Maynard, J.B., 2004. Trace-element behavior and redox facies in core shales of Upper Pennsylvanian Kansas-type cyclothems. Chemical Geology 206, 289–318. https://doi.org/10.1016/j.chemgeo.2003.12.009

Algeo, T.J., Maynard, J.B., 2008. Trace-metal covariation as a guide to water-mass conditions in ancient anoxic marine environments. Geosphere 4, 872–887. https://doi.org/10.1130/GES00174.1

ANP, 2025. Anuário Estatístico Brasileiro do Petróleo, Gás Natural e Biocombustíveis 2025. Agência Nacional do Petróleo, Gás Natural e Biocombustíveis, Rio de Janeiro.

Behar, F., Beaumont, V., De B. Penteado, H.L., 2001. Rock-Eval 6 technology: performances and developments. Oil & Gas Science and Technology 56, 111–134. https://doi.org/10.2516/ogst:2001013

Behar, F., Lorant, F., Mazeas, L., 2021. Detrital input quantification in lacustrine petroleum systems: An example of the pre-salt source rocks from the Lower Congo Basin (Congo). The Depositional Record 7, 245–274. https://doi.org/10.1002/dep2.131

Berner, R.A., 1984. Sedimentary pyrite formation: An update. Geochimica et Cosmochimica Acta 48, 605–615. https://doi.org/10.1016/0016-7037(84)90089-9

Bertani, R.T., Carozzi, A.V., 1985. Lagoa Feia Formation (Lower Cretaceous), Campos Basin, offshore Brazil: rift valley stage lacustrine carbonate reservoirs – II. Journal of Petroleum Geology 8, 199–220. https://doi.org/10.1111/j.1747-5457.1985.tb00269.x

Bohacs, K.M., Carroll, A.R., Neal, J.E., 2005. Lessons from large lake systems—Thresholds, nonlinearity, and strange attractors. In: Chan, M.A., Archer, A.W. (Eds.), Extreme Depositional Environments: Mega End Members in Geologic Time. Geological Society of America Special Paper 370, pp. 75–90.

Bohacs, K.M., Carroll, A.R., Neal, J.E., Mankiewicz, P.J., 2000. Lake-basin type, source potential, and hydrocarbon character: an integrated sequence-stratigraphic-geochemical framework. In: Gierlowski-Kordesch, E.H., Kelts, K.R. (Eds.), Lake Basins through Space and Time. AAPG Studies in Geology 46, pp. 3–34.

Cainelli, C., Mohriak, W.U., 1999. Some remarks on the evolution of sedimentary basins along the Eastern Brazilian continental margin. Episodes 22, 206–216.

Calvert, S.E., Bustin, R.M., Ingall, E.D., 1996. Influence of water column anoxia and sediment supply on the burial and preservation of organic carbon in marine shales. Geochimica et Cosmochimica Acta 60, 1577–1593. https://doi.org/10.1016/0016-7037(96)00041-5

Calvert, S.E., Pedersen, T.F., 1996. Sedimentary geochemistry of manganese: implications for the environment of formation of manganiferous black shales. Economic Geology 91, 36–47. https://doi.org/10.2113/gsecongeo.91.1.36

Carroll, A.R., Bohacs, K.M., 2001. Lake-type controls on petroleum source rock potential in nonmarine basins. AAPG Bulletin 85, 1033–1053. https://doi.org/10.1306/8626CA23-173B-11D7-8645000102C1865D

Carvalho, M.D., Praça, U.M., Silva-Telles, A.C., Jahnert, R.J., Dias, J.L., 2000. Bioclastic carbonate lacustrine facies models in the Campos Basin (Lower Cretaceous), Brazil. In: Gierlowski-Kordesch, E.H., Kelts, K.R. (Eds.), Lake Basins through Space and Time. AAPG Studies in Geology 46, pp. 245–256.

Chang, H.K., Kowsmann, R.O., Figueiredo, A.M.F., Bender, A.A., 1992. Tectonics and stratigraphy of the East Brazil Rift system: an overview. Tectonophysics 213, 97–138. https://doi.org/10.1016/0040-1951(92)90253-3

Craigie, N.W., 2018. Principles of Elemental Chemostratigraphy: A Practical User Guide. Springer, Cham, 189 pp. https://doi.org/10.1007/978-3-319-71216-1

De Jesus, R.F., Vilela, C.G., 2023. Campos basin review on the geology and its oil and natural gas exploration. Latin American Journal of Energy Research 10, 1–12. https://doi.org/10.21712/lajer.2023.v10.n1.p1-12

Demaison, G.J., Moore, G.T., 1980. Anoxic environments and oil source bed genesis. AAPG Bulletin 64, 1179–1209. https://doi.org/10.1306/2F919898-16CE-11D7-8645000102C1865D

Dias, J.L., Sad, A.R.E., Fontana, R.L., Feijó, F.J., 1990. Bacia de Campos. Boletim de Geociências da Petrobras 8, 215–234.

Espitalié, J., Deroo, G., Marquis, F., 1986. La pyrolyse Rock-Eval et ses applications. Troisième partie. Revue de l'Institut Français du Pétrole 41, 73–89. https://doi.org/10.2516/ogst:1986003

Goldberg, K., Kuchle, J., Scherer, C., Alvarenga, R., Ene, P.L., Armelenti, G., De Ros, L.F., 2017. Re-sedimented deposits in the rift section of the Campos Basin. Marine and Petroleum Geology 80, 412–431. https://doi.org/10.1016/j.marpetgeo.2016.12.011

Guardado, L.R., Spadini, A.R., Brandão, J.S.L., Mello, M.R., 2000. Petroleum system of the Campos Basin, Brazil. In: Mello, M.R., Katz, B.J. (Eds.), Petroleum Systems of South Atlantic Margins. AAPG Memoir 73, pp. 317–324.

Harris, N.B., Freeman, K.H., Pancost, R.D., White, T.S., Mitchell, G.D., 2004. The character and origin of lacustrine source rocks in the Lower Cretaceous synrift section, Congo Basin, west Africa. AAPG Bulletin 88, 1163–1184. https://doi.org/10.1306/02260403069

Hatch, J.R., Leventhal, J.S., 1992. Relationship between inferred redox potential of the depositional environment and geochemistry of the Upper Pennsylvanian (Missourian) Stark Shale Member of the Dennis Limestone, Wabaunsee County, Kansas, U.S.A. Chemical Geology 99, 65–82. https://doi.org/10.1016/0009-2541(92)90031-Y

Hedges, J.I., Stern, J.H., 1984. Carbon and nitrogen determination of carbonate-containing solids. Limnology and Oceanography 29, 657–663. https://doi.org/10.4319/lo.1984.29.3.0657

Hercolano, L.P.C., Lima Sobrinho, R., Díaz, R., Carreira, V.R., Barberes, G.A., Venancio, I.M., Moreira-Ramírez, M., Salgado-Campos, V.M.J., Chede, B.S., Freire, A.F.M., Spigolon, A.L.D., Albuquerque, A.L.S., 2026. Geochemical and mineralogical controls on organic matter preservation in Lower Cretaceous pre-salt lacustrine systems (Jiquiá Shale): A comparative study of Santos and Campos basins, Brazil. Marine and Petroleum Geology. https://doi.org/10.1016/j.marger.2026.207733

Katz, B.J., 1995. Factors controlling the development of lacustrine petroleum source rocks—an update. In: Huc, A.-Y. (Ed.), Paleogeography, Paleoclimate, and Source Rocks. AAPG Studies in Geology 40, pp. 61–79.

Katz, B.J., 2001. Lacustrine basin hydrocarbon exploration—current thoughts. Journal of Paleolimnology 26, 161–179. https://doi.org/10.1023/A:1011139232105

Kelts, K., 1988. Environments of deposition of lacustrine petroleum source rocks: an introduction. In: Fleet, A.J., Kelts, K., Talbot, M.R. (Eds.), Lacustrine Petroleum Source Rocks. Geological Society Special Publication 40, pp. 3–26. https://doi.org/10.1144/GSL.SP.1988.040.01.02

Kennedy, M.J., Pevear, D.R., Hill, R.J., 2002. Mineral surface control of organic carbon in black shale. Science 295, 657–660. https://doi.org/10.1126/science.1066611

Lafargue, E., Marquis, F., Pillot, D., 1998. Rock-Eval 6 applications in hydrocarbon exploration, production, and soil contamination studies. Oil & Gas Science and Technology 53, 421–437. https://doi.org/10.2516/ogst:1998036

Lai, J., Wang, G., Fan, Q., et al., 2024. Towards the scientific interpretation of geophysical well logs: typical misunderstandings and countermeasures. Surveys in Geophysics 44, 463–494. https://doi.org/10.1007/s10712-022-09767-0

Langford, F.F., Blanc-Valleron, M.-M., 1990. Interpreting Rock-Eval pyrolysis data using graphs of pyrolizable hydrocarbons vs. total organic carbon. AAPG Bulletin 74, 799–804. https://doi.org/10.1306/0C9B238F-1710-11D7-8645000102C1865D

Liang, H., Xu, G., Xu, F., Yu, Q., Liang, J., Wang, D., 2020. Paleoenvironmental evolution and organic matter accumulation in an oxygen-enriched lacustrine basin: A case study from the Laizhou Bay Sag, southern Bohai Sea (China). International Journal of Coal Geology 217, 103318. https://doi.org/10.1016/j.coal.2019.103318

Lyons, T.W., Severmann, S., 2006. A critical look at iron paleoredox proxies: New insights from modern euxinic marine basins. Geochimica et Cosmochimica Acta 70, 5698–5722. https://doi.org/10.1016/j.gca.2006.08.021

Makeen, Y.M., Abdullah, W.H., Hakimi, M.H., 2015. The origin, type and preservation of organic matter of the Barremian–Aptian organic-rich shales in the Muglad Basin, Southern Sudan, and their relation to paleoenvironmental and paleoclimate conditions. Marine and Petroleum Geology 65, 187–197. https://doi.org/10.1016/j.marpetgeo.2015.03.022

Mello, M.R., Gaglianone, P.C., Brassell, S.C., Maxwell, J.R., 1988. Geochemical and biological marker assessment of depositional environments using Brazilian offshore oils. Marine and Petroleum Geology 5, 205–223. https://doi.org/10.1016/0264-8172(88)90002-5

Müller, P.J., Suess, E., 1979. Productivity, sedimentation rate, and sedimentary organic matter in the oceans—I. Organic carbon preservation. Deep-Sea Research Part A 26, 1347–1362. https://doi.org/10.1016/0198-0149(79)90003-7

Pedersen, T.F., Calvert, S.E., 1990. Anoxia vs. productivity: what controls the formation of organic-carbon-rich sediments and sedimentary rocks? AAPG Bulletin 74, 454–466. https://doi.org/10.1306/0C9B232B-1710-11D7-8645000102C1865D

Peters, K.E., 1986. Guidelines for evaluating petroleum source rock using programmed pyrolysis. AAPG Bulletin 70, 318–329. https://doi.org/10.1306/94885688-1704-11D7-8645000102C1865D

Peters, K.E., Cassa, M.R., 1994. Applied source rock geochemistry. In: Magoon, L.B., Dow, W.G. (Eds.), The Petroleum System—From Source to Trap. AAPG Memoir 60, pp. 93–120.

Ricken, W., 1993. Sedimentation as a Three-Component System: Organic Carbon, Carbonate, Noncarbonate. Lecture Notes in Earth Sciences, vol. 51. Springer-Verlag, Berlin, 211 pp. https://doi.org/10.1007/BFb0117861

Talbot, M.R., 1988. The origins of lacustrine oil source rocks: evidence from the lakes of tropical Africa. In: Fleet, A.J., Kelts, K., Talbot, M.R. (Eds.), Lacustrine Petroleum Source Rocks. Geological Society Special Publication 40, pp. 29–43. https://doi.org/10.1144/GSL.SP.1988.040.01.03

Talbot, M.R., Kelts, K., 1986. Primary and diagenetic carbonates in the anoxic sediments of Lake Bosumtwi, Ghana. Geology 14, 912–916. https://doi.org/10.1130/0091-7613(1986)14<912:PADCIT>2.0.CO;2

Thompson, D.L., Stilwell, J.D., Hall, M., 2015. Lacustrine carbonate reservoirs from Early Cretaceous rift lakes of Western Gondwana: Pre-Salt coquinas of Brazil and West Africa. Gondwana Research 28, 26–51. https://doi.org/10.1016/j.gr.2014.12.005

Thunell, R.C., Varela, R., Llano, M., Collister, J., Muller-Karger, F., Bohrer, R., 2000. Organic carbon fluxes, degradation, and accumulation in an anoxic basin: Sediment trap results from the Cariaco Basin. Limnology and Oceanography 45, 300–308. https://doi.org/10.4319/lo.2000.45.2.0300

Tosca, N.J., Wright, V.P., 2015. Diagenetic pathways linked to labile Mg-clays in lacustrine carbonate reservoirs: a model for the origin of secondary porosity in the Cretaceous pre-salt Barra Velha Formation, offshore Brazil. Geological Society, London, Special Publications 435, 33–49. https://doi.org/10.1144/SP435.1

Tribovillard, N., Algeo, T.J., Lyons, T., Riboulleau, A., 2006. Trace metals as paleoredox and paleoproductivity proxies: An update. Chemical Geology 232, 12–32. https://doi.org/10.1016/j.chemgeo.2006.02.012

Tyson, R.V., 1995. Sedimentary Organic Matter: Organic Facies and Palynofacies. Chapman & Hall, London, 615 pp.

Tyson, R.V., 2001. Sedimentation rate, dilution, preservation and total organic carbon: some results of a modelling study. Organic Geochemistry 32, 333–339. https://doi.org/10.1016/S0146-6380(00)00170-X

Wedepohl, K.H., 1991. The composition of the upper earth's crust and the natural cycles of selected metals. Metals in natural raw materials. Natural Resources. In: Merian, E. (Ed.), Metals and Their Compounds in the Environment. VCH, Weinheim, pp. 3–17.

Winter, W.R., Jahnert, R.J., França, A.B., 2007. Bacia de Campos. Boletim de Geociências da Petrobras 15, 511–529.

Wright, V.P., 2012. Lacustrine carbonates in rift settings: the interaction of volcanic and microbial processes on carbonate deposition. In: Garland, J., Neilson, J.E., Laubach, S.E., Whidden, K.J. (Eds.), Advances in Carbonate Exploration and Reservoir Analysis. Geological Society, London, Special Publications 370, pp. 39–47. https://doi.org/10.1144/SP370.2

Wright, V.P., Barnett, A.J., 2015. An abiotic model for the development of textures in some South Atlantic early Cretaceous lacustrine carbonates. Geological Society, London, Special Publications 418, 209–219. https://doi.org/10.1144/SP418.3

Supplementary Material

Supplementary Figure 1. Quantification of mineral dilution in the Lagoa Feia Group, Campos Basin (n = 80). (A) Three-component sediment decomposition (Ricken, 1993) by formation, showing the relative proportions of $CaCO_3$ (measured by LECO acid pre-treatment for BCBR-5 to BCBR-10; estimated from Ca XRF regression for BCBR-1 and BCBR-3), siliciclastic material (by difference), and organic matter (OM = TOC × 1.25; Tyson, 1995). TOC formation means indicated above each bar. (B) Comparison of observed TOC and carbonate-free TOC (= TOC/(100 − $CaCO_3$) × 100) by formation. Gray band highlights the convergence zone (~5–6%) after removal of carbonate dilution; the lower value for Atafona reflects that siliciclastic dilution is the primary control in this formation. TOC values correspond to LECO combustion, except for wells BCBR-1 and BCBR-3 (Rock-Eval TOC; Hercolano et al., 2026).

Supplementary Table 1. Three-component sediment decomposition and relative sedimentation rates for the Lagoa Feia Group, Campos Basin (n = 80).

(a) By formation

Formation	n	n (est.)	TOC (%)	OM (%)	$CaCO_3$ (%)	Silicl. (%)	Carb. dilut. (%)	TOC carb.-free (%)	SR_{rel}
Macabu	18	0	1.7	2.2	67	31	69	6.1	1.8×
Coqueiros	32	15	2.8	3.4	58	39	60	6.2	1.1×
Atafona	30	10	3.1	3.9	40	56	42	5.1	1.0×

(b) By formation × paleobathymetric position

Formation	Position	n	TOC (%)	$CaCO_3$ (%)	Silicl. (%)	CDI (%)	TOC carb.-free (%)
Macabu	Intermediate	18	1.7	67	31	68	6.1
Coqueiros	Proximal	5	1.6	76	22	77	6.9
Coqueiros	Intermediate	12	2.1	69	28	71	5.7
Coqueiros	Distal	15	3.6	42	53	44	6.3
Atafona	Proximal	4	2.5	67	30	69	7.5
Atafona	Intermediate	16	4.1	38	57	39	6.1
Atafona	Distal	10	1.6	33	65	34	2.5

Three-component compositional decomposition of the Lagoa Feia Group source rocks: (a) by formation; (b) by formation × paleobathymetric position. $CaCO_3$ was estimated from Ca (XRF) using a linear regression ($CaCO_3$ = 1.29 × Ca + 18.7, R^2 = 0.88, calibrated against LECO-derived values, n = 55); n(est.) indicates the number of samples relying on this estimate. Organic matter (OM) = TOC × 1.25 (Tyson, 1995); siliciclastic fraction = 100 − $CaCO_3$ − OM. CDI (Carbonate Dominance Index) = $CaCO_3$/($CaCO_3$ + siliciclastic) × 100. TOC carb.-free = TOC/(100 − $CaCO_3$) × 100. SR_rel = relative sedimentation rate (∝ 1/OM%; Ricken, 1993), normalized to the Atafona Formation (e.g., 1.8× = 1.8 times faster). Paleobathymetric positions: Proximal (219 m), Intermediate (920–1492 m), Distal (2656–2750 m).

GENERAL CONCLUSIONS

This thesis investigated the geochemical controls on organic matter accumulation and preservation in Brazilian pre-salt lacustrine source rocks, integrating Rock-Eval pyrolysis, LECO combustion, XRD, and XRF data. The second study analyzed 80 samples from eight wells in the Campos Basin (BCBR-1, BCBR-3, and BCBR-5 through BCBR-10), while the first study conducted an inter-basin comparison with 50 samples from four wells (BCBR-1, BCBR-2, BCBR-3, and BSBR-1), of which two wells (BCBR-1 and BCBR-3) are shared between the studies. The combination of an inter-basin comparative analysis (Chapter 2) with an intra-basin investigation along a paleobathymetric transect (Chapter 3) enabled the construction of a multi-scale framework for understanding the factors governing source rock quality in Lower Cretaceous lacustrine rift systems.

The first study (Hercolano et al., in press) established that the Santos and Campos basins, despite their chronostratigraphic correlation within the Jiquiá Stage, developed markedly distinct depositional architectures. The Santos Basin evolved as a predominantly carbonate system (74.6 ± 10.7% total carbonates) with consistently high TOC values (5.1 ± 1.1%), while the Campos Basin developed as a mixed carbonate-siliciclastic system (38.3 ± 13.0% carbonates) with systematically lower and more variable organic contents (3.1 ± 1.3%). Principal component analysis identified three key controls acting within fundamentally anoxic systems: (1) primary productivity and nutrient availability; (2) terrigenous dilution; and (3) stratification stability, with the chemical stratification of the Santos Basin proving more resistant to disruption than the thermal stratification of the Campos Basin.

The second study expanded the spatial coverage in the Campos Basin, analyzing 80 samples from eight wells. The main finding is a dual dilution model in which both carbonate excess and siliciclastics can dilute organic matter, with intensity modulated by stratigraphic and paleobathymetric context. The three formations of the Lagoa Feia Group exhibit distinct Ca-TOC correlations: Macabu ($\rho = -0.80$), Coqueiros ($\rho = -0.70$), and Atafona ($\rho = -0.46$). The Ca-TOC relationship inverts according to paleobathymetric position: negative in proximal and intermediate wells, positive in distal wells ($\rho = +0.60$). Maximum TOC values (~3.5–4.1%) occur in zones of intermediate compositional balance (Ca ~20–40%, TI ~15–35%).

The integration of both studies enabled the validation of trace element proxies for paleoredox reconstruction in carbonate lacustrine systems. Vanadium emerged as the most robust redox proxy, with a TOC correlation of $\rho = +0.76$ in the Campos Basin. V concentrations > 400 ppm indicate euxinic conditions favorable to organic matter preservation, while Mn concentrations < 0.2% reflect redox stability associated with better kerogen quality (HI = 562 vs. 302 mg HC/g TOC for Mn > 0.3%). These formation-calibrated thresholds offer greater predictive power than the universally applied traditional thresholds.

The resulting hierarchical model organizes the controls on source rock quality into three levels. The primary control is the stratigraphic formation, which determines the predominant carbonate type and dilution intensity — most intense in Macabu (microbial precipitation), moderate in Coqueiros (bioclastic accumulation), and attenuated in Atafona (dispersed carbonate). The secondary control is the paleobathymetric position, which modulates the primary control differently in each formation. The tertiary control corresponds to redox conditions, which

become determinant only where compositional dilution is minimized. This hierarchical framework aligns with the production-destruction-dilution-accommodation model proposed by Bohacs et al. (2005).

From an exploration perspective, the results of this thesis demonstrate that stratigraphic classification alone is insufficient for source rock quality prediction. The integration of depositional facies indicators and redox proxies is essential for a robust predictive assessment. The formation-specific calibrations constitute applicable tools for evaluating pre-salt petroleum systems and analogous lacustrine rift systems in conjugate South Atlantic margins.

The inter-basin comparison conducted in the first study revealed that the Santos Basin presents consistently higher TOC values than the Campos Basin, associated with more stable chemical stratification and lower terrigenous dilution. However, this analysis was based on a single well in the Santos Basin (BSBR-1), limiting the assessment of spatial variability in that basin. Future work should expand the investigation of the Santos Basin at a scale equivalent to that conducted for Campos in the second study, incorporating multiple wells distributed along paleobathymetric transects. This expansion will allow evaluation of whether the dual dilution model and the hierarchy of controls identified in the Campos Basin are transferable to the Santos Basin, or whether the carbonate predominance of that basin imposes a fundamentally different dilution dynamic.

Beyond the expansion to the Santos Basin, future perspectives include: (i) trace element analysis by ICP-MS to enhance analytical sensitivity in quantifying redox and productivity proxies at concentrations below conventional XRF detection limits; (ii) application of artificial intelligence models for continuous TOC prediction from well log and XRF data; (iii) comparison with African conjugate margins to test the applicability of the hierarchical model in different structural and paleogeographic contexts of the South Atlantic rift system; and (iv) investigation of reservoir-scale controls, evaluating how the source rock variability documented in this thesis translates into petroleum charge heterogeneity in pre-salt carbonate reservoirs.

In summary, this thesis demonstrates that organic matter accumulation in pre-salt lacustrine source rocks is controlled by the interaction between sedimentary dilution, paleobathymetric position, and redox stability. The integrated framework proposed herein, validated with 80 samples from eight wells in the Campos Basin and expanded through inter-basin comparison with the Santos Basin, provides a conceptual basis and quantitative tools for the assessment of lacustrine rift petroleum systems, with direct applications in the exploration of the Brazilian pre-salt and analogous systems worldwide.

GENERAL REFERENCES

ALGEO, T. J.; MAYNARD, J. B. Trace-metal covariation as a guide to water-mass conditions in ancient anoxic marine environments. **Geosphere**, v. 4, p. 872–887, 2008.

AGÊNCIA NACIONAL DO PETRÓLEO, GÁS NATURAL E BIOCOMBUSTÍVEIS. **Boletim da Produção de Petróleo e Gás Natural**. Brasília: ANP, 2025.

BARRA, T. S. *et al.* Pre-salt lacustrine source rocks of the Santos Basin, offshore Brazil. **Marine and Petroleum Geology**, v. 127, 104958, 2021.

BEHAR, F. *et al.* Organic geochemistry of the Congo Basin pre-salt source rocks. **Organic Geochemistry**, v. 156, 104241, 2021.

BERTANI, R. T.; CAROZZI, A. V. Lagoa Feia Formation (Lower Cretaceous), Campos Basin, offshore Brazil: rift valley stage lacustrine carbonate reservoirs – I. **Journal of Petroleum Geology**, v. 8, p. 37–58, 1985.

BOHACS, K. M. *et al.* Lake-basin type, source potential, and hydrocarbon character. *In*: GIERLOWSKI-KORDESCH, E. H.; KELTS, K. R. (ed.). **Lake Basins through Space and Time**. Tulsa: AAPG, 2000. p. 3–34. (AAPG Studies in Geology, 46).

BOHACS, K. M.; CARROLL, A. R.; NEAL, J. E. Lessons from large lake systems. **Geological Society of America Special Paper**, v. 370, p. 75–90, 2005.

CAINELLI, C.; MOHRIAK, W. U. Some remarks on the evolution of sedimentary basins along the eastern Brazilian continental margin. **Episodes**, v. 22, p. 206–216, 1999.

CALVERT, S. E.; PEDERSEN, T. F. Sedimentary geochemistry of manganese. **Economic Geology**, v. 91, p. 36–47, 1996.

CHAN, S. A. *et al.* Total organic carbon (TOC) quantification using artificial neural networks. **Journal of Petroleum Science and Engineering**, v. 208, 109302, 2022.

CHANG, H. K. *et al.* Tectonics and stratigraphy of the East Brazil Rift system. **Tectonophysics**, v. 213, p. 97–138, 1992.

CRAIGIE, N. W. Applications of chemostratigraphy in Cretaceous sediments, Saudi Arabia. **Journal of African Earth Sciences**, v. 104, p. 27–42, 2015.

CRAIGIE, N. W. Chemostratigraphy and biostratigraphy of Devonian–Permian sediments, Eastern Saudi Arabia. **Marine and Petroleum Geology**, v. 72, p. 392–411, 2016.

DE JESUS, A.; VILELA, P. C. Campos basin: review on the geology. **Latin American Journal of Energy Research**, v. 10, p. 1–12, 2023.

DEMAISON, G. J.; MOORE, G. T. Anoxic environments and oil source bed genesis. **AAPG Bulletin**, v. 64, p. 1179–1209, 1980.

DIAS, J. L. *et al.* Aspectos da evolução tectono-sedimentar da Bacia de Campos. *In*: RAJA GABAGLIA, G. P.; MILANI, E. J. (ed.). **Origem e Evolução de Bacias Sedimentares**. Rio de Janeiro: Petrobras, 1990. p. 333–360.

GLENN, C. R.; KELTS, K. Sedimentary rhythms in lake deposits. *In*: EINSELE, G. *et al.* (ed.). **Cycles and Events in Stratigraphy**. Berlin: Springer-Verlag, 1991. p. 188–221.

GUARDADO, L. R. *et al.* Petroleum geology of the Campos Basin, Brazil. *In*: **AAPG Memoir**, v. 73, p. 317–324, 2000.

HARRIS, N. B. *et al.* The character and origin of lacustrine source rocks, Congo Basin. **AAPG Bulletin**, v. 88, p. 1163–1184, 2004.

HERCOLANO, L. P. C. *et al.* Geochemical and mineralogical controls on organic matter preservation in Lower Cretaceous pre-salt lacustrine systems (Jiquiá Shale). **Marine and Petroleum Geology**, *in press*, 2026.

HILDRED, G. V. *et al.* Chemostratigraphic applications to low-permeability gas reservoirs. **AAPG Bulletin**, v. 94, p. 1803–1828, 2010.

KATZ, B. J. Factors controlling lacustrine petroleum source rocks. *In*: **AAPG Studies in Geology**, v. 40, p. 61–79, 1995.

KATZ, B. J. Lacustrine basin hydrocarbon exploration. **Journal of Paleolimnology**, v. 26, p. 161–179, 2001.

KELTS, K. Environments of deposition of lacustrine petroleum source rocks. *In*: **Geological Society Special Publication**, v. 40, p. 3–26, 1988.

LIANG, H. *et al.* Paleoenvironmental evolution and organic matter accumulation in lacustrine basins. **International Journal of Coal Geology**, v. 217, 103318, 2020.

MELLO, M. R. *et al.* Geochemical and biological marker assessment using Brazilian offshore oils. **Marine and Petroleum Geology**, v. 5, p. 205–223, 1988.

MOREIRA, J. L. P. *et al.* Bacia de Santos. **Boletim de Geociências da Petrobras**, v. 15, p. 531–549, 2007.

MORFORD, J. L.; EMERSON, S. The geochemistry of redox sensitive trace metals. **Geochimica et Cosmochimica Acta**, v. 63, p. 1735–1750, 1999.

PEDERSEN, T. F.; CALVERT, S. E. Anoxia vs. productivity: what controls the formation of organic-carbon-rich sediments and sedimentary rocks? **AAPG Bulletin**, v. 74, p. 454–466, 1990.

PENTEADO, H. L. B. *et al.* Santos Basin pre-salt petroleum system assessment. **Marine and Petroleum Geology**, v. 160, 106646, 2024.

PEREIRA, M. J.; FEIJÓ, F. J. Bacia de Santos. **Boletim de Geociências da Petrobras**, v. 8, p. 219–234, 1994.

RATCLIFFE, K. T. *et al.* Chemostratigraphy: a refined tool for stratigraphic correlation. **AAPG Bulletin**, v. 94, p. 1693–1722, 2010.

RICKEN, W. **Sedimentation as a Three-Component System**. Berlin: Springer-Verlag, 1993. 211 p. (Lecture Notes in Earth Sciences, 51).

SCHALLER, H. Estratigrafia da Bacia de Campos. In: CONGRESSO BRASILEIRO DE GEOLOGIA, 27., 1973, Aracaju. **Anais** [...]. Aracaju: SBG, 1973. v. 3, p. 247–258.

SOREGHAN, M. J.; COHEN, A. S. Textural and compositional variability in Lake Tanganyika. **AAPG Bulletin**, v. 80, p. 382–409, 1996.

TALBOT, M. R. The origins of lacustrine oil source rocks. *In*: **Geological Society Special Publication**, v. 40, p. 29–43, 1988.

TRIBOVILLARD, N. *et al.* Trace metals as paleoredox and paleoproductivity proxies. **Chemical Geology**, v. 232, p. 12–32, 2006.

TYSON, R. V. **Sedimentary Organic Matter**. London: Chapman & Hall, 1995. 615 p.

TYSON, R. V. Sedimentation rate, dilution, preservation and total organic carbon. **Organic Geochemistry**, v. 32, p. 333–339, 2001.

WINTER, W. R. *et al.* Bacia de Campos. **Boletim de Geociências da Petrobras**, v. 15, p. 511–529, 2007.